HYDRIDE FORMATION IN TITANIUM ALUMINII

By

ARBIND KUMAR

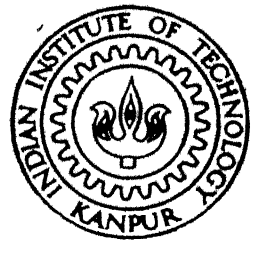

Department of Materials and Metallurgical Engineering

INDIAN INSTITUTE OF TECHNOLOGY KANPUR

OCTOBER, 1996

HYDRIDE FORMATION IN TITANIUM ALUMINIDES

A Thesis submitted
in partial fulfillment of the
requirements for the degree of
MASTER OF TECHNOLOGY
by

ARBIND KUMAR

To the

DEPARTMENT OF MATERIALS AND METALLURGICAL ENGINEER
INDIAN INSTITUTE OF TECHNOLOGY, KANPUR

October 1996.

DEDICATED TO MY PARENTS

CERTIFICATE

This is to certify that the work on performed in this thesis entitled "Hydride Formation in Titanium Aluminides" has been carried out by Mr. Arbind Kumar under my supervision and that it has not been submitted elsewhere for a degree.

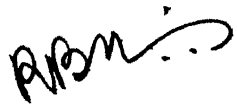

(R. Balasubramaniam)
Assistant Professor
Department of Materials and Metallurgical Engineering
Indian Institute of Technology, Kanpur 208016

ACKNOWLEDGEMENTS

I wish to express my gratitude and indebtedness to my supervisor Dr. R. Balasubramaniam for his inspiration, encouragement and guidance throughout my thesis work. The freedom that I enjoyed at his hands has given me confidence to do what I think is right and I thank him for this.

I specially thank Dr. M. N. Mungole for his technical guidance and help. I would also like to acknowledge Mr. P.K. Pal and Mr. K.P. Mukherjee for their assistance in my experimental work. The wonderful moments that I shared with Mr. C. Thakur, Dr. S. K. Choudhary, Dr. T. K. Roy and Mr. K. S. Rao will always be cherished. I thank all those who made my stay at Kanpur a memorable one.

Finally, I would also like to acknowledge the financial support for this thesis work provided by the Indian National Science Academy.

Arbind Kumar

(Arbind Kumar)

CONTENTS

LIST OF TABLES

LIST OF FIGURES

CHAPTER 1

INTRODUCTION

1.1 INTERMETALLICS

Metals and alloys have the general characteristics of good ductility, relatively high strength, stiffness and shock resistance. They are easily shaped, machined and joined. Due to these properties, they can be used for many purposes such as structural parts in load bearing applications. Almost all metals have medium to high density, except for a few light metals like Al, Mg, Be, Ti etc. The relatively high density is not a big problem for ground based application but a big disadvantage as far as aerospace applications are concerned. One of the basic requirements for candidate aerospace materials is a low weight/strength ratio.

There are many intermediate structures formed when mixing two elements that are not fully soluble in each other (i.e., those that do not obey Hume-Rothery's rule for extensive solid solubility). The intermediate structures formed at fixed composition and having a fixed crystal structure different from either of the parent elements are called intermetallic compounds. Some examples of intermetallic compounds are Fe_3Al, FeAl, Ti_3Al, TiAl, Fe_3C etc. The intermetallic compounds generally have very high melting points, relatively high strengths, low weight (especially those in which one of the components is Al, which are called aluminides) and low room temperature ductility. The poor room temperature ductility is one of the main hindrance in the commercial use of the intermetallic compounds.

1.1.1 Ti_3Al BASED INTERMETALLICS

Titanium alloys were developed in the early 1950s for aerospace applications, in which their high strength/density ratio was attractive. Ti is referred to by various names like the wonder metal, glamour metal etc. Research and development on Ti and its alloys have greatly increased due to their potential applications

in space exploration applications, the development of supersonic planes and the growing interest in oceanography. When Al is alloyed to Ti to create stoichiometric compositions of Ti_3Al and TiAl, these intermetallics are called titanium aluminides.

Titanium exist in two allotropic forms : (i) α-Ti having the HCP crystal structure at room temperature which is stable up to 882°C, and (ii) β-Ti having the BCC crystal structure which is stable between 882°C and 1670°C (melting point). Al when added to Ti as an alpha stabilizer, i.e. Al raises the α-β transformation temperature and promotes the stability of α-Ti to higher temperatures [1]. This makes Al an important alloying element for Ti alloys, as the α Ti alloys have higher strengths.

The binary phase diagram for Ti-Al system is shown in Figure 1. As the percentage of Al in Ti-Al alloy increases, several phases are encountered such as α-Ti, Ti_3Al (also called as α_2), TiAl (also referred to as γ) and $TiAl_3$. The Ti_3Al intermetallic exits at room temperature for Al concentrations between 22 and 35 atomic %. It is also called α_2 Ti alloy. It has an ordered DO_{19} crystal structure below the critical ordering temperature (T_c) of 1118°C [2]. At temperatures above T_c, β Ti_3Al is stable as can be seen in the phase diagram in Figure 1. β Ti_3Al is an ordered phase having the BCC crystal structure (called as B2). α_2 Ti_3Al has a higher strength, higher resistance to hydrogen diffusion through it but lower ductility than β Ti_3Al [3]. The DO_{19} ordered crystal structure of α_2 Ti_3Al is presented in Figure 2.

1.1.2 EFFECT OF NIOBIUM ON Ti_3Al

Ti_3Al based intermetallics as well as other Ti aluminides are currently receiving much attention because of their high specific strength and ductility at higher temperature but the low temperature brittleness of this type of alloy is a major obstacle to its application. This low temperature poor ductility is basically due to limited number of slip systems in the ordered α_2 phase [4] and also due to environmental effects [5]. Hydrogen embrittlement has been postulated to be one of the main causes for low room temperature ductility [6]. The high temperature β phase is more ductile and it can accommodate higher amounts of hydrogen

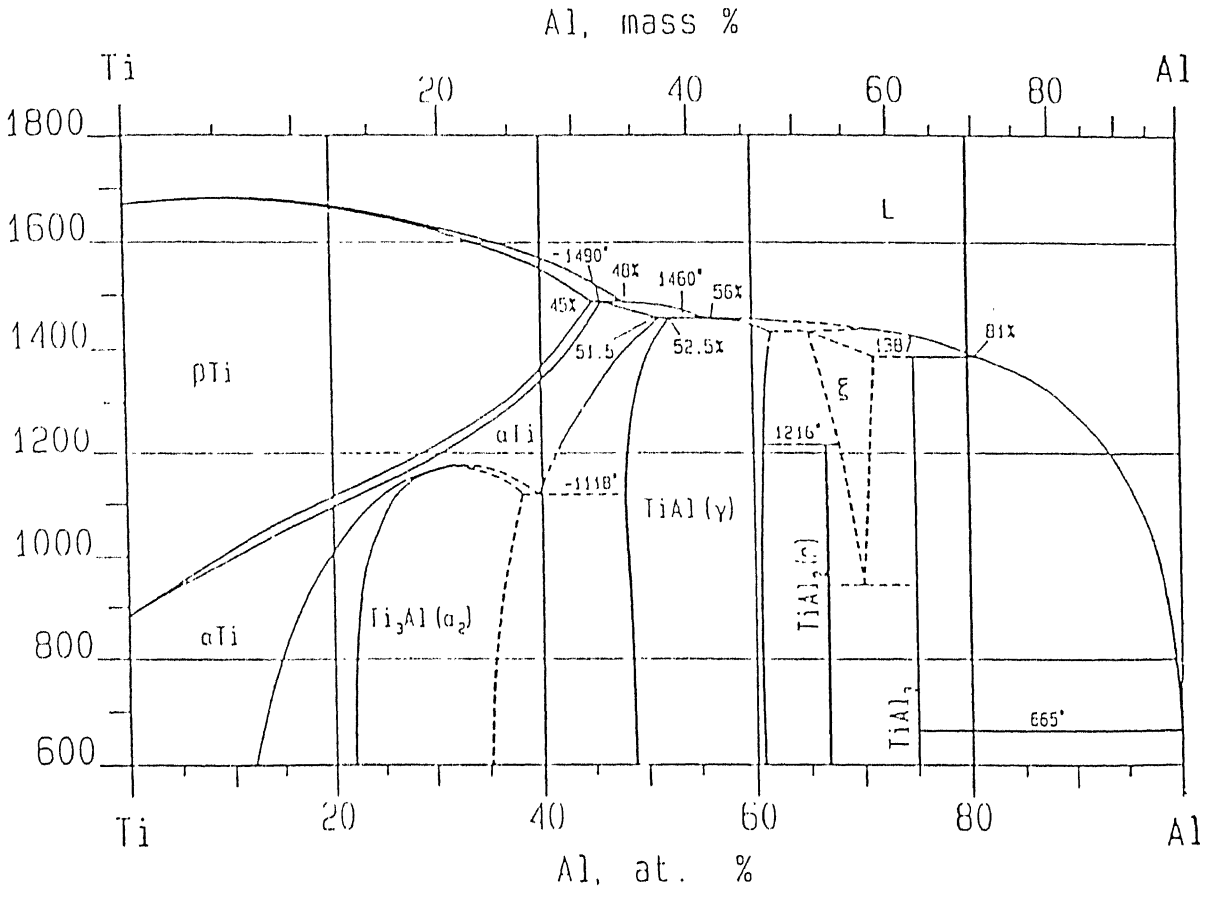

Fig 1 Binary phase diagram of the Ti-Al system.

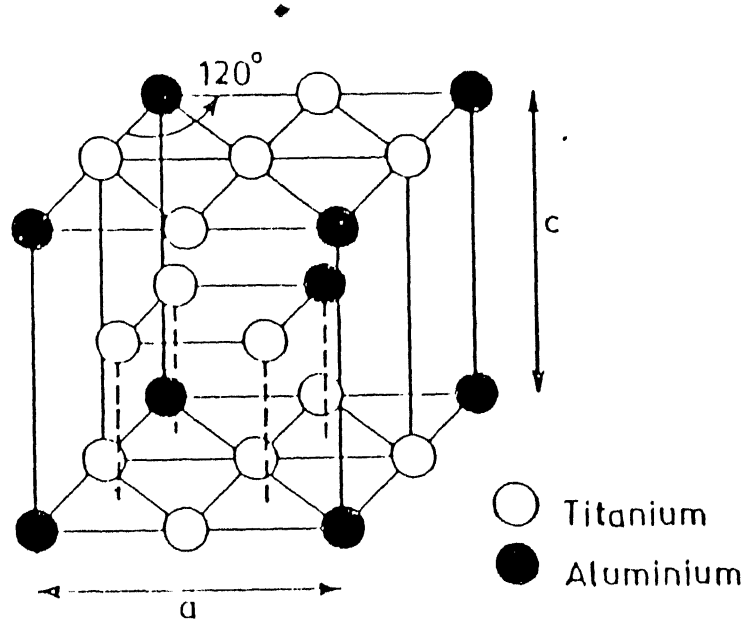

Fig 2 Ordered hexagonal DO_{19} structure of Ti_3Al.

[3] as compared to α_2 phase of titanium aluminides. So the room temperature ductility can be significantly improved by alloying the addition of elements which (partially or completely) stabilize the β phase. Some of the β stabilizing elements in the case of Ti are Nb, Mo and V, of which the most preferred is Nb [7] because it increases nonbasal slip activity in Ti_3Al [8]. Their addition to Ti aluminides result in a microstructure with a higher amount of retained beta phase [7,9,10]. However, the addition of β stabilizing elements in the alloy is limited so as not to alter the basic features of the intermetallics. Nb increases the non-basal slip activity in β Ti_3Al and so increases ductility [8,11] and it is one of the important alloying addition to Ti_3Al based intermetallics to provide enhanced ductilities.

Figure 3 provides the Ti_3Al+Nb pseudo binary phase diagram [12]. The high temperature Ti-Al-Nb cubic β phase (BCC Ordered B2) transforms at low temperature to an ordered closed packed hexagonal DO_{19} phase (Ti_3Al-type) when the amount of Nb is low and to an orthorhombic O phase with Ti_2AlNb stoichiometry at higher Nb contents (from about 11 onwards) [7]. Figure 4 shows the crystal structure of the O phase [12]. The orthorhombic phase has higher a strength and hardness than the α_2 phase due to ordering of atoms [11-13]. The O phase appears at Nb levels exceeding 12 atom % for Al contents of 24 to 25 atom %. Substitution of Ti by Nb increases the number of slip systems. Nb may partly be replaced by other elements for strength improvement (e.g. V, Mo, Ta), creep resistance (e.g. Mo), and oxidation resistance (e.g. Ta, Mo) [14]. Properties of various Ti_3Al-based titanium aluminides is presented in Table 1 [15].

1.2 OBJECTIVE OF STUDY

The primary objective of the study is to understand hydride formation in titanium aluminides, as Ti and Nb are very strong hydride formers. Hydrogen is to be introduced into the intermetallics by electrochemical cathodic charging. The effect of Nb content on the hydride formation characteristics is to be investigated, specifically the hydriding behavior of α_2 phase in Ti-24Al-20Nb intermetallic and that of the O phase in Ti-24Al-27Nb

Table 1

Room temperature properties and elevated creep rupture life of some Ti_3Al-based intermetallics with various microstructures controlled by thermomechanical processing [15].

Alloys	Micro-structure*	YS (MPa)	UTS (MPa)	El %	K_{IC} (MPa$\sqrt{m}$)	Creep rupture**
Ti-25Al	E	538	538	0.3	--	--
Ti-24Al-11Nb	W	787	824	0.7	--	44.7
	FW	761	967	4.8	--	--
Ti-24Al-14Nb	W	831	977	2.1	--	59.5
TI-25AL-10Nb-3V-1Mo	W	825	1042	2.2	13.5	360
	FW+P	942	1097	2.7	--	--
Ti-24.5Al-17Nb	W	952	1010	5.8	28.3	62
Ti-25Al-17Nb-1Mo	FW	989	1133	3.4	20.9	476

* E - equiaxed α_2 grain; W - widmanstatten; FW - fine widmanstatten; P - primary α_2 grain.

** Time to rupture in hour at 923K and 380 MPa.

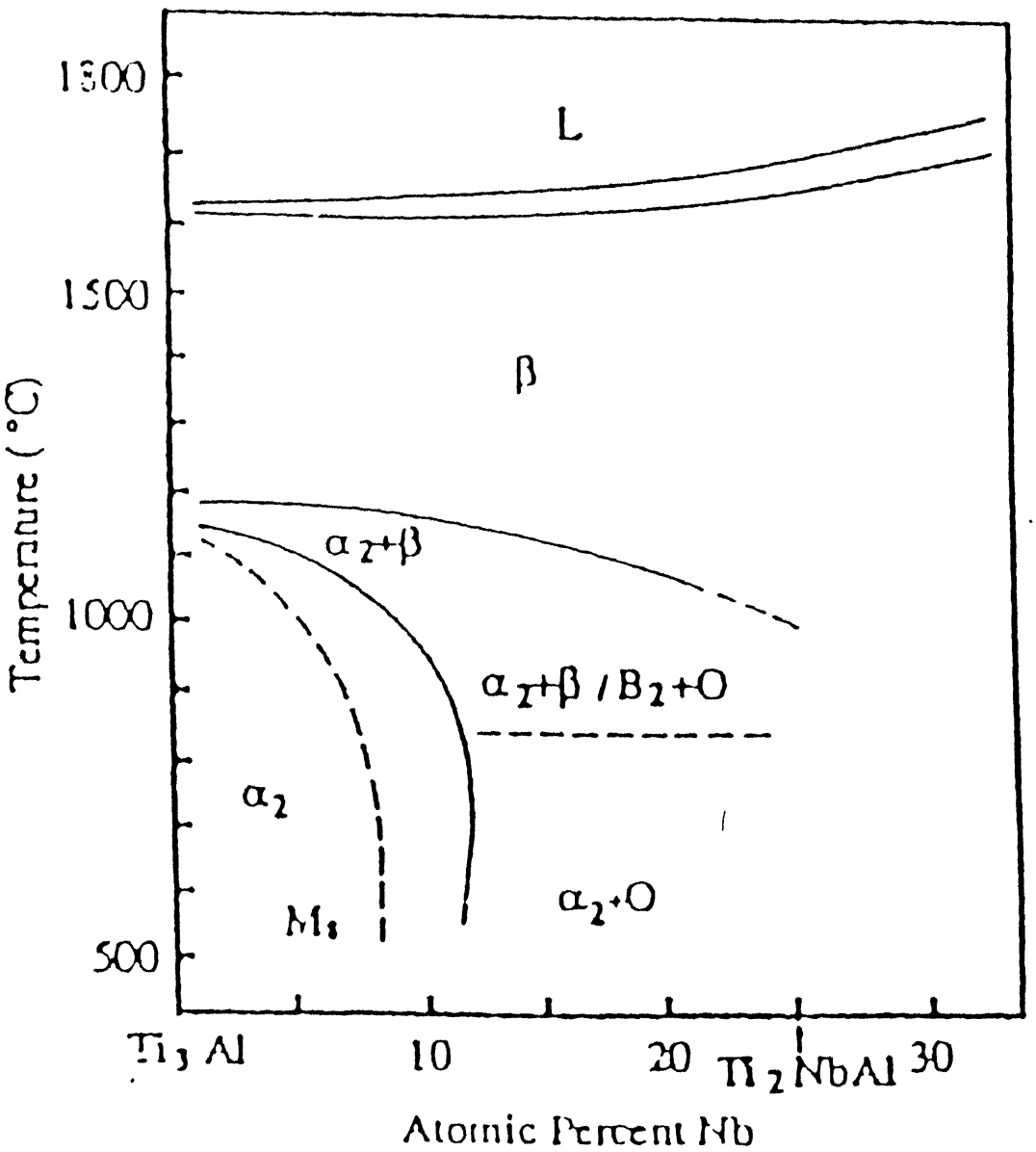

Fig 3 Ti_3Al-Nb pseudo binary phase diagram [12].

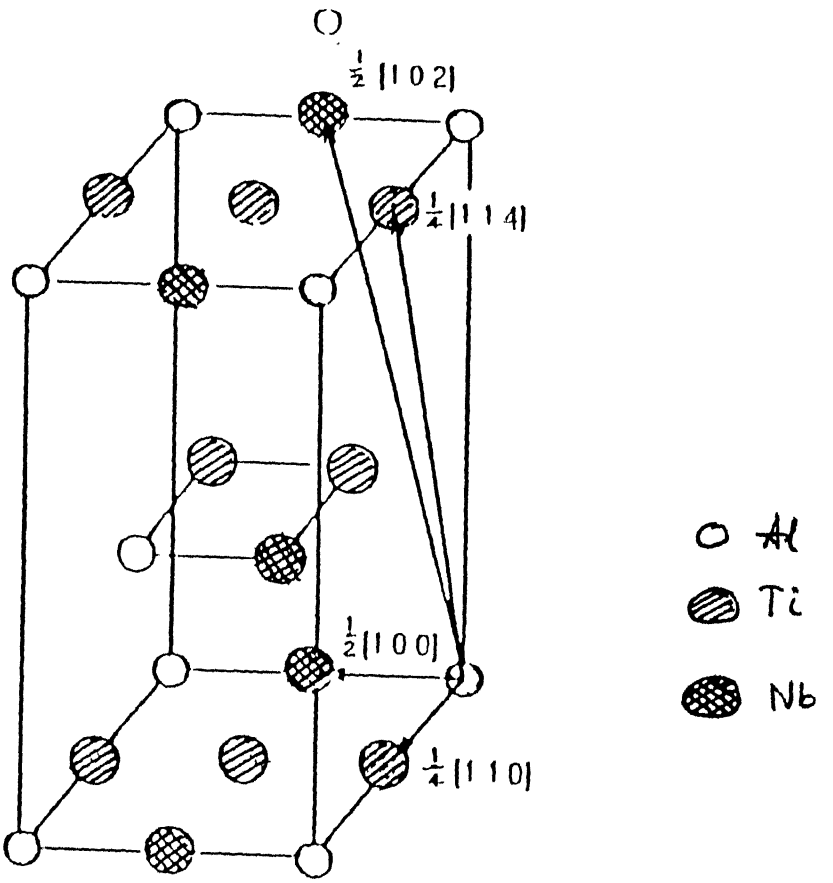

Fig 4 Crystal structure of O phase [12].

intermetallic. There are no published reports on the formation of hydrides in the O phase and this is the first study to attempt this. Hydride formation is planned to be characterized by hardness measurements, X-ray diffraction (XRD), optical and scanning electron microscopy. Stability of the hydrides is to be addressed by high temperature baking experiments after cathodic charging. The secondary aim of the thesis is to understand the role of surface oxides on hydride formation and also understand the oxidation process at high temperature and its effect on the hydride formation. The diffusivity of oxygen is calculated from hardness profiles in the intermetallics exposed to high temperatures.

1.3 PLAN OF WORK

The work in the thesis is to be performed in the following stages. Two intermetallics of compositions Ti-24Al-20Nb and Ti-24Al-27Nb would be charged electrochemically with hydrogen and the effect of hydrogen on the material would be followed by microhardness profiling. The effect of heat treatment and alloy composition are to be studied. Hydride formation is to be characterized by XRD and microscopy in addition to microhardness profiling. The high temperature oxidation characterization is also to be addressed by performing isothermal oxidation experiments at 1273 K. The diffusivity of oxygen at 1273 K is calculated from subscale microhardness profiles.

CHAPTER 2

LITERATURE REVIEW

2.1 GENERAL INTRODUCTION

Alloys based on the compound Ti_3Al have received sufficient attention to show that they may be legitimate candidate materials of construction for aerospace system [16]. Of particular interest are both the engines and airframe of a hydrogen burning propulsion system [17]. Since such alloy contain Ti, with its propensity to interact with hydrogen, it is important to have a clear picture of the effects of hydrogen on the properties and microstructure of these aluminide intermetallics. As the original interest in this material has been for high performance aircraft engines which typically operate under oxidizing condition, there has been little efforts expended in studying the effects of oxygen on titanium aluminides.

On the basis of pioneering studies [18], it is now well established that the low temperature phase of pure titanium, α-Ti has a relatively low solid solubility for hydrogen and precipitates a hydride when the solubility limit is reached. This hydride, the γ phase in the Ti-H system, was originally designated as TiH_2 but in more recent literature [19,20] has been designated as TiH, a better description of its typical stoichiometry, although the limiting composition of γ phase stoichiometry is indeed TiH_2. In the case of Ti_3Al intermetallics, which is designated α_2 in the titanium-aluminum system, hydrides are also reported to form [21] and same is true for α_2 Ti_3Al intermetallic [22]. However, the quantitative description of hydride formation conditions is still largely an open question, and only limited data on the solubility of hydrogen in this compound are available for Ti-24Al-11Nb [21] and α_2 Ti_3Al [22,23]. In the initial sections of this chapter, a review of the research on hydride formation in Ti, Al, Nb and Ti_3Al+Nb intermetallics is presented. The effect of temperature on hydrogen evolution and hydride stability would also be addressed.

The microstructure plays an important role as regards tolerance towards hydrogen. Some microstructures are very resistant to hydrogen damage whereas others are very susceptible [5,6]. Therefore, the role of microstrcture on the hydrogen effects is also addressed in this chapter. It has also been well known that hydrogen is a β stabilizer and therefore, it can be used as a temporary alloying addition in order to stabilize the β phase at high temperatures [24-27]. This would aid processing due to ease of hot working. Later the hydrogen can be removed by vacuum annealing. The stabilization of β by hydrogen and its role as a temporary alloying addition are also discussed in this chapter.

At higher temperatures, oxidation of the intermetallics would also have to be considered in addition to hydrogen evolution and therefore, a critical review of the literature on oxide formation and characteristics of scale formed after oxidation in Ti_3Al+Nb intermetallics is also presented. The effect of Nb on the oxidation behavior of titanium aluminides is briefly discussed.

2.2 HYDRIDE FORMATION IN Ti, Nb AND Al

Hydrogen is the most important element amongst the interstitial elements. It's small size is not much larger than the naturally occurring interstices in the several transition metal lattices and these can usually accommodate the hydrogen atom or ion to an extensive degree with less strain on the metal lattice than for say N or O [28]. In the transition metal hydrides, the H atom can be absorbed in the metal lattice to variable extents and at variable interstices, implying wide homogeneity ranges and a high mobility between parent lattice vacancies [29]. Hydrogen can be loaded into materials by two ways: electrochemical cathodic charging and hydrogen gas charging. As it enters through the pure metal lattice such as that in group IV and V, the H atoms tend to cause lattice expansion and distortion up to a high compositional limit. Once the solid solubility of hydrogen is exceeded in these materials, hydrides form in the matrix. Sometimes with temperature, ordering effects and phase transformation become gradual in Ti-H systems [30].

The concept of "stoichiometry" also becomes ill-defined when the transition metal hydrides are addressed. The stability of the given hydrides and their saturation contents depend strongly on pressure and temperature [28]. A difference however, is that, whereas the truly interstitial character holds good only for the lower oxides and solid solution and soon departs from metallic bonding to ionic or covalent oxides, all transition metal hydrides, up to the highest are interstitial compounds even though the character of bond may be variable and sometimes controversial [31].

The Ti-H system has been studied by many workers [23] and the constitutional diagram of Ti-H system is shown in Figure 5 [23]. The BCC β-Ti form is stabilized by hydrogen. The HCP α-Ti lattice is expanded by H atom. There is a rapid decrease in solubility of H with decreasing temperature after the eutectoid temperature, from about 8% H at 300^{o}C to 0.1% H at room temperature [30]. At higher hydrogen concentrations, an eutectoid decomposition reaction of the type β --> α-Ti + hydride occurs in the Ti-H system. The hydride posses an extensive homogeneity range between approximately TiH and TiH_2 but varying of course with temperature and pressure [23]. The hydride is FCC with considerable structural distortion. The hydride has a FCC unit cell with respect to titanium atoms and hydrogen atoms are distributed randomly over the tetrahedral interstitial sites (the CaF_2 type structure). At the stoichiometric composition of TiH_2, the hydride (δ) has the lattice parameter of 0.4404 nm [20]. Increasing the hydrogen content within the hydride phase with temperature is accompanied by an eventual filling of the octahedral holes in the CaF_2 lattice. For high hydrogen concentrations near the limiting composition TiH_2, the hydride transforms into a tetragonal structure ($c/a<1$) at lower temperatures [32,33], which has been referred to as δ. Table 2 summarizes some characteristics of the Ti-H and Nb-H system. It should be noted that the TiH_{1+x} hydride solid solution is present when the concentration of hydrogen is very high, but when the concentration of hydrogen is low then the precipitation of a f.c.t hydride takes place (with a = 0.421 nm and c = 0.460 nm) with four Ti atoms at the fcc translation sites

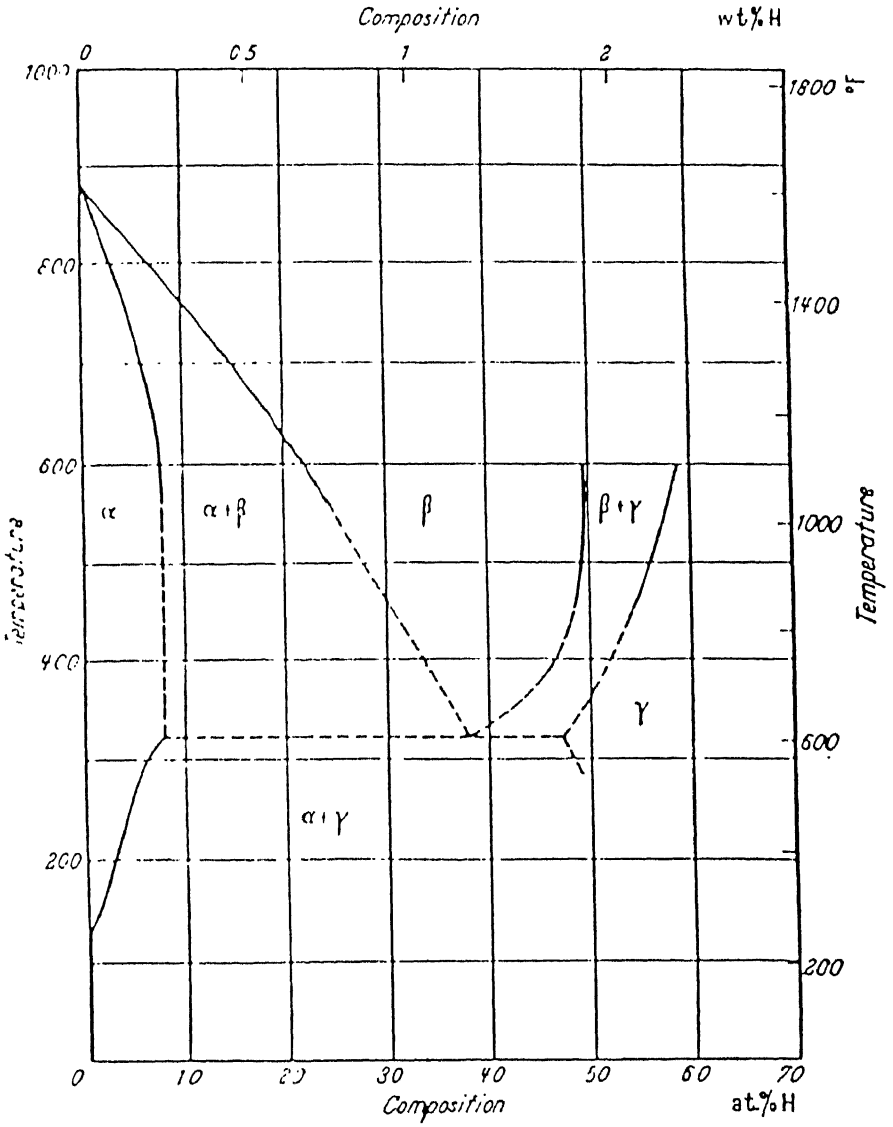

Fig 5 Constitutional diagram of the Ti-H system [28].

Table 2

Properties of Ti-H and Nb-H System.

Metal	Primary Sol. for H	Hydrides	Crystal Structure	Physical Properties	Remarks
Ti Group-iv	H stabilizer β - Ti, lattice expansion in α & β.	TiH / TiH_2.	FCC : defect CaF_2 type	Density varying from 3.78 to 4.40, TiH_2-Antiferromagnetic ordering	H atoms in tetragonal holes, TiH-TiH_2 disappear above 600°C.
Nb group-v	5% at low temperatures but supersaturation is possible, lattice expansion by H.	$NbH_{0.7-0.9}$ NbH_2-phase is reported.	FCO may be regarded as deformed BCC or FCC, low temperature ordering.	----------	Metastable high temperature NbH phase.

and the H atoms located at 1/4,1/4,3/4; 3/4,3/4,1/4; 1/4,1/4,1/4 and 3/4,3/4,3/4 [19,20]. The γ and δ forms of Ti hydride are shown in Figure 6. As the concentration of hydrogen in α-Ti increases, the relative abundance of the γ hydride with respect to the δ hydride comes down [20]. The preference to form this TiH hydride at low hydrogen contents is due to the lower volume misfit on precipitation of γ hydride (15%) compared to that of the δ hydride (22%). Two modes of precipitation were observed for the γ TiH hydride in the α matrix [19]. The habit planes are $\{01\bar{1}0\}$ prism planes for one type and near $\{02\bar{2}5\}$ pyramidal planes for the other type. The orientation relationship between the hydride and matrix are provided by Numakura and Koiwa [19]. They also noted that the precipitation sequence of hydrides is similar to that observed in the Zr-H system. An implication of the Ti-H phase relations is the facility of hydride precipitation from the α-phase. This occurs upon aging in mostly accicular form and coherently with the α-matrix. The hydride is particularly prone to precipitation in the zone of strain, whatever the origin.

Nb takes H into limited solution at room temperature with lattice expansion. A hexagonal hydride Nb_2H had first been proposed by Hagg and reported as rhombohedral [31]. An observation which ought to be revised in modern light, however, is of a FCC hydride NbH probably orthorhombic. Brauer and Hermann found BCC and BC rhombohedral NbH solid solution to equilibrate [34]. In the later, the distortion is only slight (near cubic edge, a= 3.44 Å, $\alpha = \beta = 90^{\circ}$, $\gamma = 89.4^{\circ}$). This phase is sometimes stated as face centered orthorhombic but it is same with a = 4.83, b = 4.89, c = 3.44 Å at $NbH_{0.89}$. The hydride that forms of composition NbH is termed β. At higher hydrogen contents, the monohydride can transform to a dihydride δ having the CaF_2 structure. Both the β and δ hydrides of Nb exist over a wide range of composition indicative of the low defect formation energies in these structures. It has also been reported that at lower temperatures, the β hydride transforms to a series of ordered structures by the ordering of hydrogen atoms on different subsets of interstitial sites. The hydrides that form in the Nb system have been reviewed

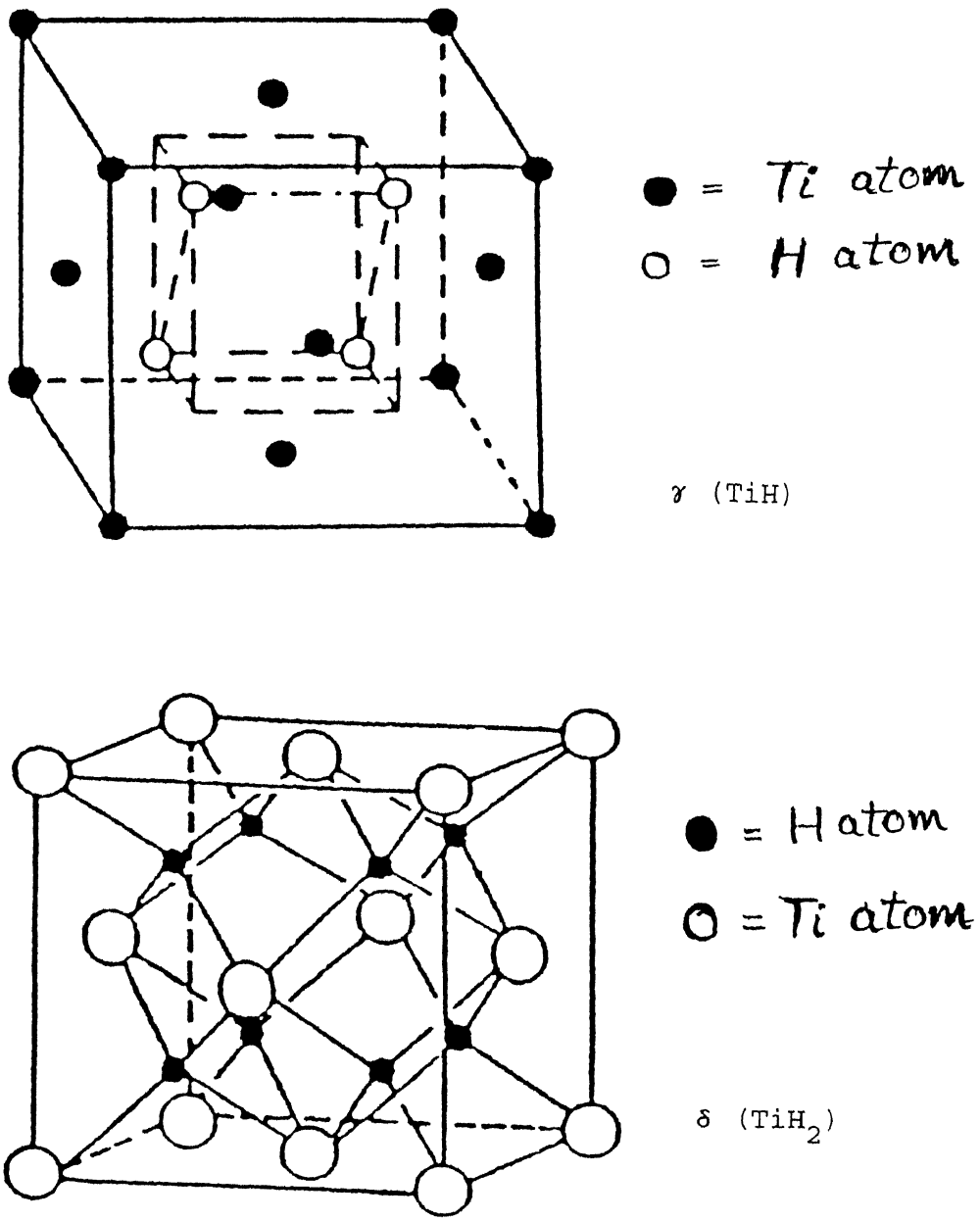

Fig 6 Structure of the γ (TiH) and δ (TiH_2) hydrides.

critically by Balasubramaniam [35].

There have been reports about the formation of AlH_3 in Al [36] but its presence has not been reported in Ti-Al or Ti-Al-Nb systems.

2.3 HYDROGEN IN Ti_3Al+Nb INTERMETALLICS

Titanium aluminides can be heat treated to obtain a wide variety of microstructures. Moreover, there are precipitation of several phases in the Ti-Al-Nb system (like to α_2, ω, O and β phases) [9]. In view of this, the hydrogen behavior in titanium aluminides can be complicating. While revering to the general topic of hydrogen behavior, it should be borne in mind that hydrogen can exist in solid solution as well as precipitate out as hydrides. Therefore, these two aspects have to be discussed separately.

2.3.1. HYDROGEN SOLUTION BEHAVIOR

The hydrogen solution behavior in the stoichiometic Ti_3Al was first studied by Rudman et al. [22,23]. Hydrogen absorption/desorption isotherms were determined in Ti_3Al at 50^{o}C intervals from 350 to 800^{o}C [23]. Typical data obtained by Rudman et al [23] is provided in Figure 7. Titanium absorbs hydrogen exothermically as evidenced by the increased pressure required to attain a given concentration as the temperature is increased. Large deviations were noted from ideal Sievert's law behavior. They analyzed the solubility results on the basis of a simple thermodynamic model and based on the analysis determined that the number of interstitial sites available to H per metal atom was 0.25 unlike 2 in the case of pure α-Ti. Moreover, the partial molar enthalpy and partial molal excess entropy on hydrogen solution in Ti_3Al was similar to that reported for α-Ti. Therefore, the dominant role of Al in Ti_3Al was summarized by them to be blocking of the interstitial sites from hydrogen occupancy, leaving essentially unchanged the H-Ti interactions in the occupied sites. The site blocking results in a higher hydrogen dissociation pressure in Ti_3Al than in α-Ti which they calculated

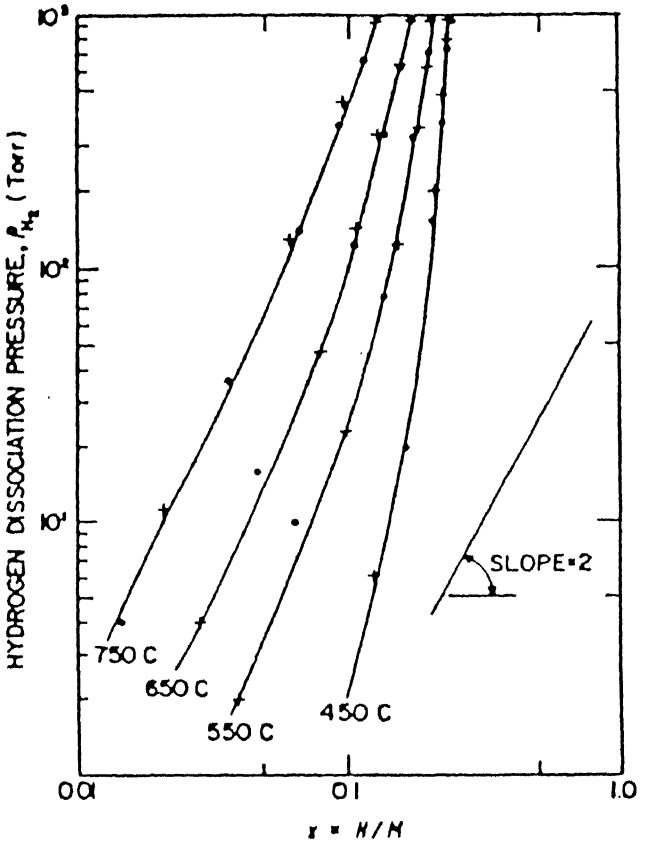

Fig 7 Typical hydrogen absorption/desorption isotherms for hydrogen in Ti_3Al [23].

to be given by the factor:

$$p_{H_2}(Ti_3Al) \; / \; p_{H_2}(\alpha\text{-}Ti) = [\; (2-x)/(0.25-x) \;]^2$$

where x is the interstitial site per metal atom (=0.25 for Ti_3Al). In the limit of $x \rightarrow 0$, this ratio is 64/1 which increases to infinity as $x \rightarrow 0.25$. They were not able to identify the sites of hydrogen occupancy as the available sites are strongly dependent on the degree of order. In a later paper, Rudman et al [22], have shown that at lower temperatures, hydrogen leads to the precipitation of ternary hydrides and the solid solubility is low.

Chu et al [21] also measured the dissolution of hydrogen in essentially α_2 phase (Ti-24Al-11Nb) as a function of temperature and hydrogen pressure. The terminal solubility of hydrogen in the α_2 phase matrix increases with temperature (Figure 8), while the overall solubility decreases with increasing temperature in the high-temperature region (Figure 9). The terminal solubility curve was obtained from two different methods (P vs 1/T and $(P)^{1/2}$ vs C_H plots). The equation for the terminal solubility as a function of temperature, at 1 atm pressure, is given by:

$$C_H \text{ (at \%)} = 6.8 \times 10^3 \exp(-5750/T)$$

and

$$C_A/(2 - C_A) = 57 \exp(-6200/T)$$

where C_A is the atomic ratio and T and exponential constants are in K. It should be noticed that the solubility of hydrogen at room temperature according to the above equation should be very low about 0.2 ppm (atomic). This indicates that all charged hydrogen should be precipitated as hydride on cooling to ambient temperature. A similar situation persists also in the case of α-Ti [19]. The equation for the overall uptake of hydrogen in the α_2 phase is given by:

$$C_H \text{ (at \%)} = 2.67 \; (P_{H_2})^{1/2} \exp(2650\ T)$$

where T is in K and the unit of P is Pa. Therefore, the α_2 phase is an exothermic occluder for hydrogen as the overall solubility

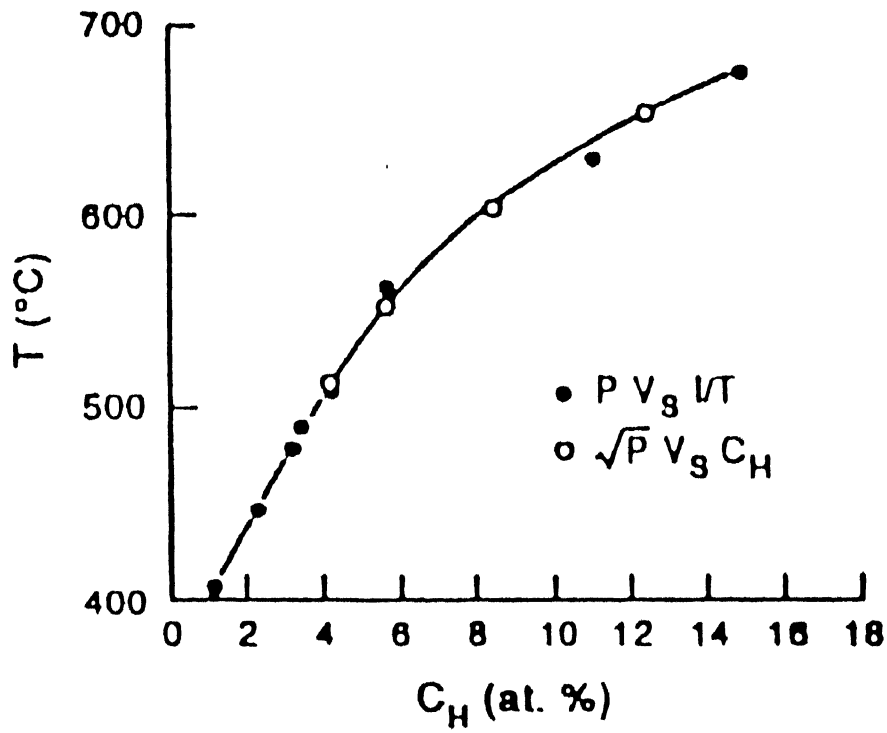

Fig 8 Terminal solubility of hydrogen in the α_2 phase in equilibrium with the hydride phase, i.e the solvus for the hydride in α_2 phase for Ti-24Al-11Nb [21].

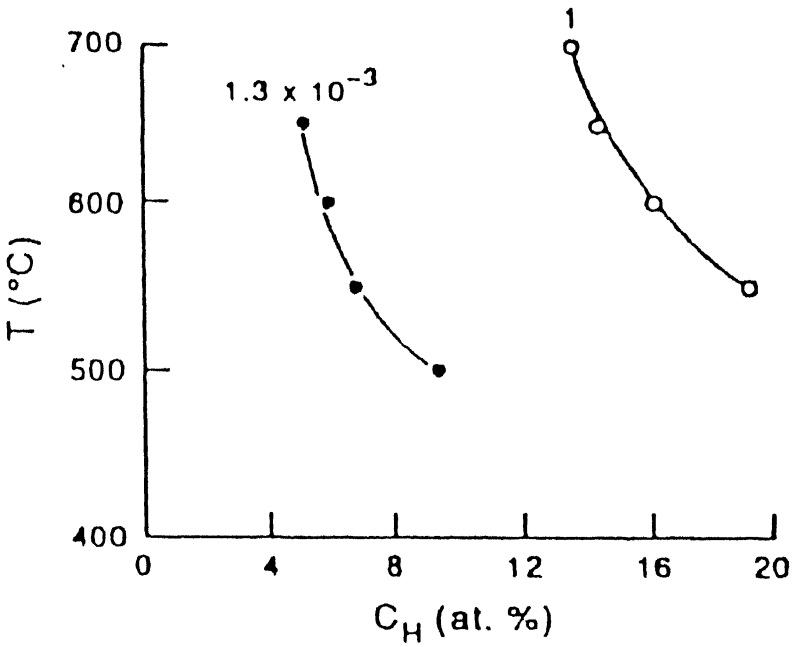

Fig 9 Overall solubility (total uptake) of hydrogen in the α_2 phase vs 1/T for two pressures shown on the curves in units of atm (or 130 Pa and 0.1 MPa) [21].

of hydrogen decreases with increasing temperature. Such a result was also independently confirmed for Ti-24Al-11Nb by Shih et al [37].

There have been no general published reports on the solubility of hydrogen in the β phase of titanium aluminides. The high temperature solubility of several titanium aluminides is shown in Figure 10 [27]. The material for which the chemical activity is lowest will have the highest solubility for hydrogen. β titanium alloys have a lower activity than CP-Ti and hence a higher hydrogen solubility. In contrast, the solubility of hydrogen in the equiatomic γ TiAl is very low, due to the high activity of hydrogen in it. Therefore, the solubility of hydrogen in the β phase should be relatively higher than for the α_2 phase.

The solubility of hydrogen at ambient and high temperatures should be relatively high in the β phase (50 at % H in β-Ti at 700^{o}C [27]) compared to the α_2 phase. At higher temperatures, the solubility of hydrogen is significant in both the α_2 and β phases [21,23,37,38], although the general trend is that solubility decreases with increasing temperature [21,37] due to the negative heat of mixing similar to that observed in the α_2-Ti system. The solubility of hydrogen in the O phase has not been reported, although it is reasonable to assume that it should be similar to that observed for the α_2 phase as the physical metallurgy of the α_2 and O phase are closely related.

2.3.2. HYDRIDE PRECIPITATION

Due to the low solubility for hydrogen in the α_2/O phase, hydrides are expected to precipitate from the α_2 or the O phase. The precipitation of hydrides from the α_2 phase has been extensively documented, whereas the precipitation from the O phase has not been studied in detail as yet. It is reasonable to assume that the precipitation of hydride from the O phase would closely resemble that from the α_2 phase as their physical metallurgy are similar [12].

As regards precipitation of hydrides from the α_2 (O) phase, the important point that needs to be emphasized is that the

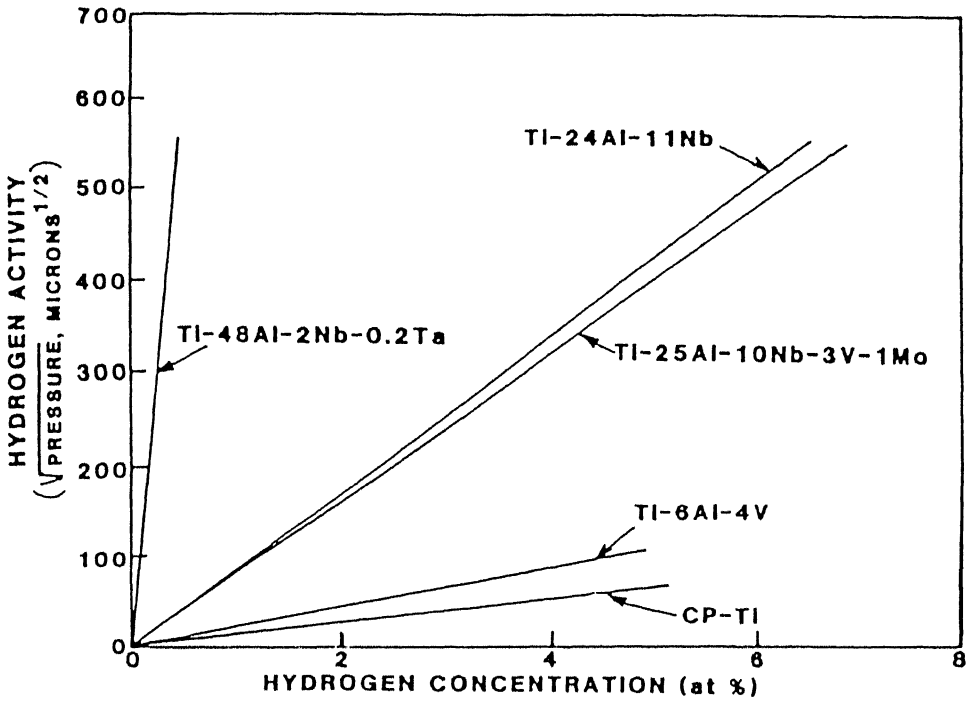

Fig 10 Hydrogen activity for selected titanium alloys at 800^{o}C [27].

hydride(s) that precipitates on ambient temperature cathodic hydrogen charging is not the same as that which precipitates on high temperature gaseous hydrogen charging. These two aspects would be separately discussed below. It should be mentioned at this juncture that the kinetics of hydrogen absorption in stoichiometric titanium aluminide Ti_3Al (α_2 phase) is rapid even at low temperatures of between 0 and 200°C [22]. The initial absorption is rapid (when the H/M reaches 0.6) followed by a sluggish phase (when the H/M reaches about 1.5). In the case of the Ti-24Al-11Nb (heat treated to obtain α_2 completely), hydrogen diffusion is fast, the system becomes saturated with hydrogen and the terminal solid solubility of hydrogen is attained fairly rapidly [21]. After this hydride precipitation takes place. After a certain period of time, there is hardly any effect of hydrogen on this system. The hydrogen absorbing capacity is more temperature dependant than the time dependant [21].

2.3.2.1 AMBIENT TEMPERATURE HYDROGENATION

Rudman et at [22] have found that since the diffusion of substitutional metal atoms is relatively low at room temperatures, the hydrides that form in Ti_3Al at room temperature are necessarily ternary hydrides. They identified two ternary hydrides of composition $Ti_3AlH_{0.35}$ and $Ti_3AlH_{1.6}$ in Ti_3Al. The hydrogen pressure absorption isotherms for Ti_3AlH_x determined at low temperatures is provided in Figure 11a and the estimated equilibrium (metastable) pressure isotherms for the same in Figure 11b. It is to be noted that the hydride β labeled in Figure 11b corresponds to $Ti_3AlH_{0.35}$ and that labeled γ to $Ti_3AlH_{1.6}$. Therefore, at room temperature, the hydride that should exist in the α_2 phase of titanium aluminide and this is of ternary type. It has been shown that when the ternary hydrides were heated above 200°C, the XRD pattern of the hydride TiH_2 emerged indicating that the ternary hydrides formed at room temperature are apparently metastable and they convert to the stable hydride TiH_2 at temperatures higher than 200°C.

There is another interesting observation made by

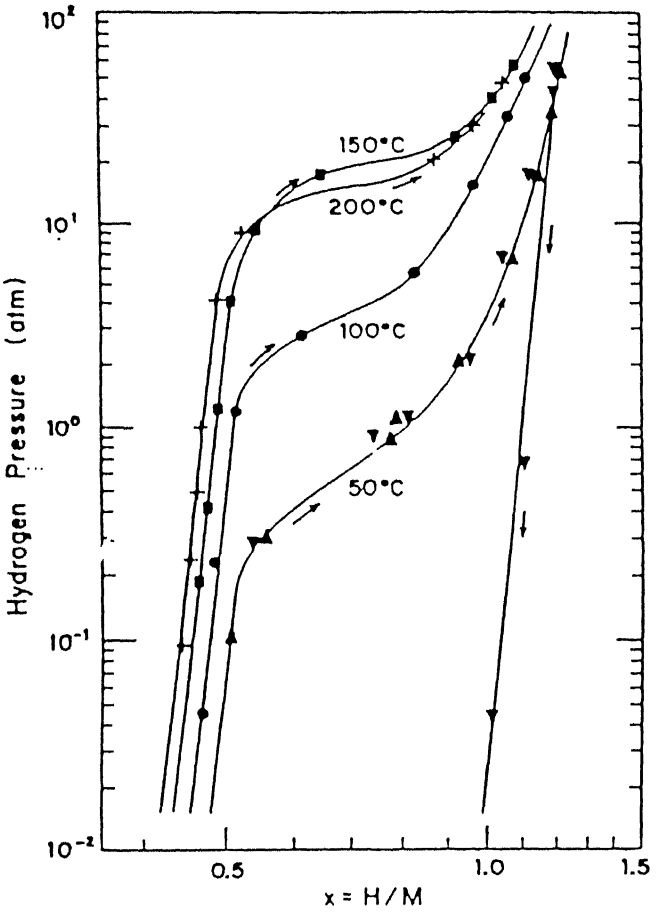

Fig 11(a) Hydrogen pressure absorption isotherms for $Ti_{0.75}Al_{0.25}H_x$.

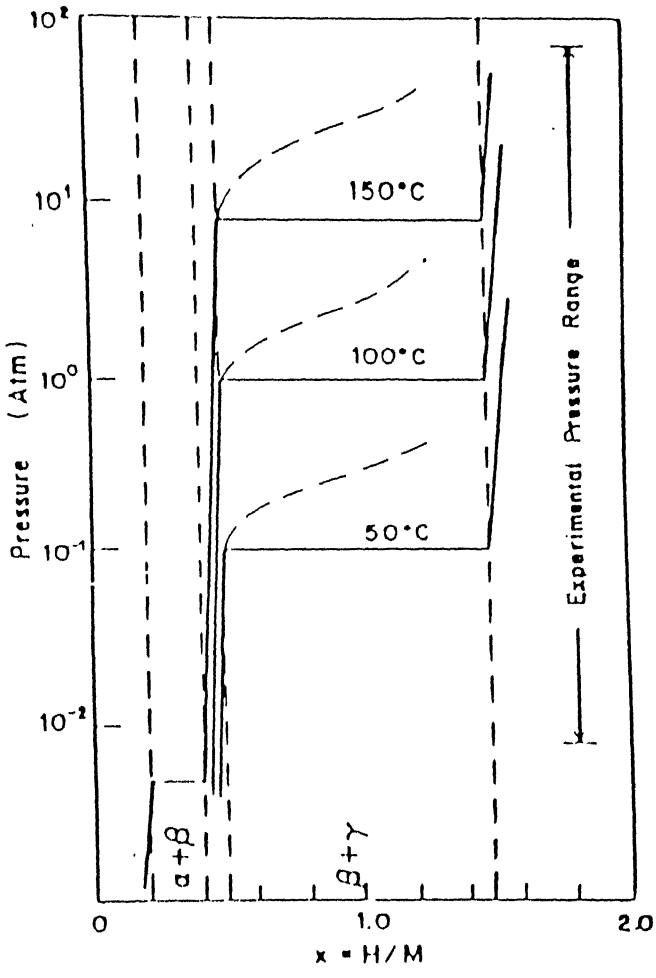

Fig 11(b). Estimated equilibrium (metastable) pressure isothe for $Ti_{0.75}Al_{0.25}H_x$ [22]. For the β hydride x=0.35 for the γ hydride, x=1.6.

Muraleedharan et al [10] when hydrogen is present in titanium aluminides. They noted that when hydrogen was absorbed into the Ti-24Al-15Nb intermetallic during etching (hydrogen content below 20 ppm) after polishing, they observed orthorhombic distortions of the α_2 phase, which they noted to be similar to the hydrogenated phase reported by Shih et al [37]. This phase precipitated as distinct plates at the α_2/β interfaces which were twin related variants of the orthorhombic structure. They noted that this orthorhombic was different from the O phase obtained by heat treatment in that Nb atoms do not occupy specific sub lattice in this case. Moreover, the lattice parameters of the interface orthorhombic phase and the O phase appear to be similar (a = 0.596 nm, b = 0.986 nm and c = 0.467 nm). Whether this phase was a hydride phase or related to the O phase was not resolved by them. They noted that if the latter was the case, it would imply that hydrogen segregates to the α_2/β interface and alters the stability of the α_2 phase such that martensitic transformation to the O structure can occur during etching. Therefore, when hydrogen is introduced into titanium aluminides at room temperature by cathodic processes, the formation of ternary hydrides in the α_2/O phase and the stabilization of the α_2 phase to the orthorhombic structures could be expected.

Manor and Eliezer [39] have stated that a hydride of type (TiNb)H forms in Ti-24Al-11Nb after room temperature cathodic hydrogen charging (1N H_2SO_4 at 5 kA/m^2 for 5 to 20 mins) although they did not provide proof (i.e. TEM pictures, electron and X-ray diffraction patterns) for this identification. They noted that on hydrogenation, cracks formed at the interface between the α_2/β phases and no hydrides could be identified in the crack tip. It is likely that the introduction of hydrogen would have resulted in the stabilization of the orthorhombic distorted phase of the α_2 [10] which could lead to the the cracking noticed. It has been shown by TEM that this the O phase that precipitates from α_2 by the addition of hydrogen at the α_2/β interfaces [10], lending further support to the explanation for the cracking process on hydrogenation. A similar cracking process on room temperature hydrogenation of TEM foils was also reported by Eliezer et al

[40].

2.3.2.2 HIGH TEMPERATURE HYDROGENATION

The hydrides that form on thermally charging hydrogen at high temperatures are different from that which are obtained on room temperature cathodic charging hydrogenation. The difference arises essentially due to the ease of diffusion of Ti (Al and Nb) atoms which results in the stable hydrides being formed. As regards the thermodynamic stability of the hydrides, the titanium hydrides (of varying H/M ratios) are much more stable at any temperature compared to the niobium hydrides (of varying H/M ratios) [28]. For example, the enthalpy and entropy of formation at 298 K are -27300 cal/mol and -25 cal/mol/K for $TiH_{1.6}$, whereas they are -6700 cal/mol and -8 cal/mol/K for $NbH_{0.67}$ [28]. Therefore, the hydrides that are thermodynamically expected to form in the Ti-Nb-Al system are those of Ti. In fact, in a study of hydrogen absorption characteristics of Ti-Nb system by Upadhyaya and McQuillan [41], it was found that in titanium rich alloys, the structure of the hydrided alloy is FCC in all the alloys containing up to 67 at% Nb. The hydrogen absorption remained the same (H/M close to 2) up to this range. In Ti-11 at % Nb alloy, the lattice parameter of the hydrided FCC phase was determined to be 0.443 nm. At higher Nb levels (67-74% Nb), a BCC hydride also coexists with the FCC hydride and beyond 74% Nb, the BCC hydride becomes stable.

Shih et al [37] thermally charged Ti-24Al-11Nb between 500-1050^{o}C and found that small hydride platelets (40-100 nm in size) in the α_2 phase. These hydrides were stable on heating up to 500^{o}C but dissociated at 700^{o}C restoring the original microstructure on out gassing. Based on their TEM work, they indicated that the hydride did not correspond to any of the known variation of titanium hydrides and that it could be of the type Ti_3AlH_x. However, they noted that this hydride phase was a orthorhombic distortion from the α_2 phase and that its habit plane was the basal plane in Ti_3Al and the prism plane in Ti-24Al-11Nb. The change of the hydride habit plane from the basal plane in Ti-25Al to the prism planes in Ti-24Al-11Nb has ben proved to be caused by two mechanism: by increased non basal slip tendency with

Nb addition and by modification in elastic anisotropy because of the Nb addition.

In order to understand the hydride formation in titanium aluminides in greater detail, Guo et al [42] thermally charged hydrogen at 500°C for 6 h in Ti-24Al-11Nb that had been solutionized at 1150°C for 1 h in vacuum and then aged at 760°C for 1 h in vacuum. They estimated the hydrogen content to be about 2500 wppm after the charging treatment. They observed dense oriented hydrides to form in the α_2 matrix and they identified the hydride to be a bct hydride (a= 0.306 nm and c = 0.405 nm) similar to the TiH_2 (a = 0.312 nm and c = 0.418 nm) reported by Jaffe [43]. The hydride was oriented with respect to the α_2 matrix with the (0001) of α_2 parallel to (110) of the hydride and the $[11\bar{2}0]$ of α_2 parallel to [001] of the hydride [42]. Guo et al, in a subsequent paper [44], have provided the mechanism of formation of the hydride phase as a displacement and dilation from the Ti_3Al phase.

Yang et al [26] have also observed dense hydrides of the type observed by Guo et al [42] after high temperature hydrogen charging of several Ti alloys. Under the optical microscopy, the hydrides appeared accicular in Ti-1100 (α phase alloy) while it appeared feather-like in the case of Ti-6Al-4V ($\alpha+\beta$ alloy). However, they could not resolve the hydride under optical microscope in the case of super-α_2 ($\alpha_2+\beta$ alloy). They could resolve the hydride in the TEM and reported that it was similar to that reported by Guo et al [42].

Hydrides in hydrogen thermally charged Ti-24Al-11Nb have also been reported to be plate-like by Chu et al [21]. However, they mention that the hydride phase that forms at high temperatures is the fluorite γ TiH phase based on XRD study of the hydrided specimens. However, there are several complications in understanding the XRD of hydrided samples of titanium aluminides: the peaks of the hydride superimpose on that matrix peaks and the diffraction intensities from the hydride phase are very low [26,38]. Therefore, the identification of the TiH phase could be debated in view of unavailability of concrete proof provided by Chu et al [21].

2.3.2.3 CHARACTERIZATION OF HYDRIDES

Hydride formation in Ti_3Al+Nb alloy can be characterized by several techniques like optical microscopy (OM), scanning electron microscopy (SEM), transmission electron microscopy (TEM) and X-ray diffraction (XRD) techniques. In case of observation by SEM and OM, The hydrides appeared as fine markings or lines on the polished sample without etching after cathodic charging in H_2SO_4 (0.05 mol/lit) with 100 ppm $NaAsO_4$ [21]. The observation was carried out on a scanning electron microscope. Hydrides precipitate as platelets after high temperature hydrogenation. It is interesting to note that the distribution of hydrides was uniform throughout the surface of the sample but locally the hydride platelets were arranged along certain preferential directions [21].

The hydrides can be seen under optical microscopy for some Ti alloys like Ti-1100 (α alloy) and Ti-6Al-4V ($\alpha+\beta$ alloy) after high temperature hydrogenation [26]. However, it was not possible to resolve the hydrides in the more complex titanium aluminides like super-α_2 by optical microscopy. In these two phase (i.e. $\alpha_2/O+\beta$) aluminides, the hydrides appear on a much finer scale and the TEM is required for their characterization. The hydrides that form in titanium aluminides have already been discussed earlier and the detailed information about the same was obtained by TEM.

XRD technique is cannot be effectively used to study hydride formation in titanium aluminides. It must be noted that there are two problems in identifying the presence of titanium hydrides in titanium aluminides by the XRD technique. First, it is possible that due to their small size, the hydride precipitates do not exhibit sufficient long range atomic structure required for detection by XRD. Secondly, the major diffraction peaks due to the reported Ti hydrides [28,43] are almost isomorphous with the α_2 peaks and differentiation becomes a difficulty. For example, the JCPDS XRD files for TiH, TiH_2 and Ti_3Al are compared in Table 3 from which it can be seen that the major peaks of the TiH_2 superimpose on the α (or α_2/O) peaks. Moreover, in the case of the extra spots due to the hydride is observed in the TEM in

Table 3

X-ray diffraction data for TiH, TiH_2 and Ti_3Al obtained from JCPDS files

	Ti_3Al			TiH_2			TiH		
2θ	d_{hkl}	hkl	I/I_o	d_{hkl}	hkl	I/I_o	d_{hkl}	hkl	$I\backslash I_o$
35.9	2.50	220	50	2.50	101	50	2.50	111	50
38.8	2.32	002	70	----	---	---	---	---	---
41.0	2.20	201	100	2.20	110	100	2.20	200	100
53.9	1.70	202	60	----	---	---	---	---	---
59.6	---	---	---	1.55	200	30	---	---	---
61.3	1.51	521	20	----	---	---	---	---	---
64.5	1.44	220	50	----	---	---	---	---	---
70.8	---	---	---	1.33	211	35	1.33	311	35
71.7	1.32	203	60	----	---	---	---	---	---

the case of Ti_3Al is about only 2 degrees apart from the matrix spot [26,37,42]. However, this can be effectively utilized to view the hydride and understand orientation relationships and therefore the TEM technique is best suited to study hydride formation, unlike the XRD technique. Therefore, the above two factors hinder the unambiguous identification of the presence of hydrides in hydrogen charged titanium aluminides by the XRD technique.

In optical microscopy, hair line cracks are seen on the polished, unetched surface due to the presence of hydride in the surface of Ti-24Al-11Nb [21,23]. Moreover, high temperature hydrogenation in a lot of instances leads to fracture and fragmentation of the titanium aluminides [5,6]. Enhanced cracking at the α_2/β interfaces due to room temperature hydrogenation was also observed by Eliezer and co-workers [39,40] by the TEM.

2.3.3 EFFECT OF HYDROGEN ON THE MICROSTRUCTURE

As a way of introduction, it was seen in an earlier study by Chan [6] that the microstructure of titanium aluminide (Ti-24Al-11Nb) produced by different heat treatments affected hydrogen damage tolerance. It was found that the fine basketweave microstructure of α_2 and β is the best hydrogen tolerant microstructure. This was when hydrogen was later added to the system and its properties evaluated. There is another aspect to microstructure when hydrogen is present during the heat treatment and this is dealt with in this section.

Hydrogen is a strong β stabilizing element which can be seen from the Ti-H phase diagram (Figure 5). It can be introduced in Ti alloys in large quantities and can be extracted out by vacuum annealing. The use of hydrogen as a temporary alloying addition in titanium alloys leads to improved workability [27]. The use of hydrogen for this purpose is termed as thermochemical processing (TCP) and it has been shown that this results also in enhancement in mechanical properties due to its beneficial effects in controlling the microstructures [24]. It has also been reported in recent years that the microstructures and corresponding properties of conventional Ti aluminides have been improved by the process of hydrogenation followed by dehydrogenation [27,45,46]. Chu and

Thompson [45,46] showed that the microstructure of Ti-24Al-11Nb was refined by the addition of hydrogen as a temporarily β-stabilizer which resulted in an improvement in the mechanical properties, strength and ductility of alloy. For the 1147°C β solution treating followed by air cooling, hydrogen as a temporary β stabilizer decreased the size of the α_2 phase and increased greatly the retained or transformed β content leading to improvement in strength, ductility, fracture strength and fracture toughness. Slow cooling, on the other hand, did not decrease the size of the α_2 colonies and therefore the mechanical properties were not greatly enhanced. In the $\alpha_2+\beta$ phase field, hydrogen as a temporary β stabilizer changed the size of the transformed α_2 phase and the retained β content, rather than the size and morphology of the primary α_2 phase and some increases were observed in various properties [46]. Therefore thermochemical (hydrogen) processing technique [27] may be a prospective way to improve the ductility of Ti_3Al-based intermetallics by refining and/or changing the microstructure to increase the capability of alloy for deformation. However, further investigations have not been carried out on the effect of different conditions, for example the hydrogenation condition and the subsequent heat treatment on the microstructure of Ti_3Al-based intermetallics so as to optimize this processing technique and effectively improve the alloy properties, as has been well documented for Ti alloys [27].

It has been reported that when the intermetallic designated as super α_2 (Ti-25Al-10Nb-3V-1Mo) is solution treated at 1100°C and then aged at two different temperatures 900 and 950°C, then a large amount of fine accicular α_2 precipitates in the β matrix [25]. Less of the coarse primary α_2 is evident in the hydrogenated specimens but much more primary α_2 is distributed in the unhydrogenated specimens [25]. The higher the aging temperature, the coarser is the α_2 in all specimens especially in the unhydrogenated ones. For the unhydrogenated specimens, it has been reported that the microstructure for the specimen with lowest hydrogen content, contains coarser α_2 phase in the matrix, and that with the highest hydrogen content a greater amount of

retained β matrix with larger accicular α_2 precipitates. The microstructure for the specimen with a medium level of hydrogen content shows a finer and more homogeneous distribution of α_2 phase in the β matrix, which again indicates the importance of extent of hydrogenation to the microstructural variation. The hardness for the hydrogenated specimen under such aging treatments still give higher values than those for the unhydrogenated ones, due to variation of microstructure [25]. Therefore, the presence of hydrogen can influence the microstructure either in continuous cooling or aging of the intermetallics. Hydrogenation of super α_2 followed by a suitable heat treatment will produce a microstructure with a fine α_2 formation and more retained β, and also fine hydrides in the α_2 phase [26]. During dehydrogenation, finer α_2 precipitation will occur in the β phase being dehydrogenated and this finer structure should improve the ductility and strength of the alloy. All these microstructural features reflect the role of hydrogen as a β-stabilizing element during both solution treatment and aging and the possible use of this fact in improving the properties of titanium aluminides.

The microstructural variation of the super α_2 specimens with different hydrogen contents after a solution treatment followed by aging at 800 and 900°C in vacuum (i.e. aging during dehydrogenation) has also been examined [25]. Unlike the above treatment, the precipitation of α_2 in the hydrogenated specimens should be directly influenced by the continuous dehydrogenation. It can be imagined that as the dehydrogenation process goes on, α_2 precipitation should occur continuously within the dehydrogenated β phase. Thus a microstructure with much finer α_2 can be obtained if the heat treatment process is well controlled. It has been seen that the finer accicular α_2 phase has been formed in the hydrogenated specimens, with the existence of coarsened primary α_2 phase, and that the lower the aging temperature, the greater the refinement [25].

It has also been established that the presence of hydrogen effectively lowers the α (or α_2)/β transus temperatures for three different titanium alloy foils (Ti-1100, Ti-6Al-4V and super-α_2) [26], thereby indicating that a better microstructure for hot

deformation can be obtained at a relatively lower temperature for the hydrogen charged titanium alloy foils. The more the hydrogen content, the greater the lowering of the transus temperature [above ref] and therefore the role of hydrogen as a β stabilizer is well established in titanium aluminides.

2.3.4 EFFECT OF HYDROGEN ON THE HARDNESS BEHAVIOR

The microstructures and corresponding phase relationships in Ti_3Al+Nb alloys have been well investigated in recent years. The microstructures in this alloy system may contain the disordered BCC (β), ordered BCC (B2), ordered HCP (α_2), HCP (ω) and an orthorhombic (O) phase [11,47]. However, despite the complexity of phase distribution in these alloys, their microstructures can easily be identified as a mixture of dominant phase of either α_2 or α_2+O and the retained β (or B2) under the optical microscope [12,13]. In the higher Nb containing alloys, the dominant phases are O and β [12].

For the specimen (super α_2) heat treated at 1100°C and then cooled in a furnace, the micro-structure shows a reliable homogeneous distribution of α_2 with retained β phase for the unhydrogenated specimens but inhomogeneous for the hydrogenated ones [25]. Since hydrogen in the specimen is a strong β stabliser, the transformation of β to α_2 during continuous cooling should be strongly affected. For instance, the β phase may be partly or wholly stabliser in a certain temperature range so that the transformation to α_2 occurs at relatively lower temperature. Thus a finer α_2 phase formation with more retained β in micro-structure should be produced in a hydrogenated specimen in continuous cooling. The microstructure for the hydrogenated specimen posses large amount of finer α_2 phase surrounded by the coarsened primary α_2 (undissolved α_2) compared with that for the unhydrogenated specimen [25,26].

It was concluded that when the hydrogenated specimens were slowly cooled from the high temperature, the α_2 phase could not be easily formed in the hydrogen-stabilizer β phase above a certain temperature and coarsening of primary α_2 only occurred when the temperature was low enough [25]. The microstructural difference

among the hydrogenated specimens should be caused by the different extent of β stabilization due to different hydrogen contents in the specimen which implies that an optimized hydrogenation process should be adopted for such treatment; otherwise inhomogeneity may be increased by excessive additions of hydrogen to the alloy [27].

The corresponding hardness of the specimens hydrogenated at any given hydrogen pressure are evidently higher than that of the unhydrogenated ones, whether it has been dehydrogenated or not. This reflects the effect of hydrogen on the microstructure in the super α_2 alloy [25]. The fact that the hardness after dehydrogenation is higher can be attributed to the α_2 phase formed from hydrogen stabilized retained β during the dehydrogenation. The reason why the highest hydrogen content does not corresponds to highest hardness can be explained by the more inhomogeneous microstructure caused by excessive hydrogen in the specimens [25].

It has been found that at higher hydrogen contents, a lower amount of α_2 remain undissolved in the β matrix for the specimen solution treated at 1100°C followed by fast cooling. This demonstrates explicitly the fact that hydrogen lowers the α_2/β transus temperature of titanium aluminide due to its β stabilizing effect, which has been reported elsewhere for the Ti_3Al-Nb system [26]. Microhardness measured for this treatment condition produced the result that the higher the hydrogen content in the specimen, the higher the hardness, which corresponds to the microstructure with less undissolved α_2 in the retained β matrix. This is consistent with previous work showing that the lesser the volume fraction of primary α_2, the higher the strength of Ti-24Al-11Nb intermetallics in the $\alpha_2+\beta$ solution treated condition [48].

2.3.5 EFFECT OF TEMPERATURE ON HYDROGEN EVOLUTION

The dissociation pressure of Ti-H is related to the temperature by the formula [28]

$$\log P = -6671/T + 9.35$$

where P is the pressure in mm Hg and T is the temperature in K. By assuming pressure is equal to 1 atm (760 mm of Hg), the dissociation temperature of Ti-H is equal to 758°C. Below this

temperature there is no decomposition of TiH_2 and so properties do not changes vary much [29]. The TiH_2 decomposes after heating above 760°C and so a large change in properties (strength and ductility) takes place.

In the case of titanium aluminides, as ternary hydrides are supposed to form, the above equation has to be modified. The above equation would be more appropriate than considering the decomposition temperature of the hydride TiH_2 as the hydride that form on room temperature hydrogenation is not this hydride. At atmospheric pressures, the TiH_2 hydride decomposes at 760°C which is obtained from the relation of the decomposition pressure as a function of temperature given as [28]

$$\log p_{H_2}(Ti) = -6679/T + 9.35$$

The dissociation pressure is higher in the titanium aluminide due to blocking of sites due to the presence of Al [23]. The relation between the dissociation pressure in Ti_3Al and in α-Ti is provided by Rudman et al [23] as follows:

$$p_{H_2}(Ti_3Al) \; / \; p_{H_2}(\alpha\text{-}Ti) = [\; (2-x)/(0.25-x) \;]^2$$

where x is the interstitial site per metal atom (=0.25 for Ti_3Al). In the limit of $x \rightarrow 0$, this ratio is 64/1. Therefore,

$$\log \; [\; p_{H_2}(Ti_3Al) \; / \; 64 \;] = -6679/T + 9.35$$

Using the above relation, the decomposition temperature of the ternary hydrides in α_2 (and approximately in also O) can be estimated to be 597°C. It is interesting at this juncture to note that the hydrides that were created by Shih et al [37] after gaseous hydrogen charging of Ti-24Al-11Nb were stable upon heating at 500°C and dissociated only at 700°C. Thereby indicating that the ternary hydrides in the titanium aluminide system are stable to a lower temperatures than TiH_2.

The effect of temperature on hydrogen diffusivity in α-Ti and rutile (TiO_2) is shown in Figure 12 [49]. The data in this figure can be utilized to evaluate the time for diffusing hydrogen out of a specimen of known dimension. It has also been previously established that the titanium oxide layer formed on the α_2 phase is not permeable for hydrogen at 500°C so that hydride evolution

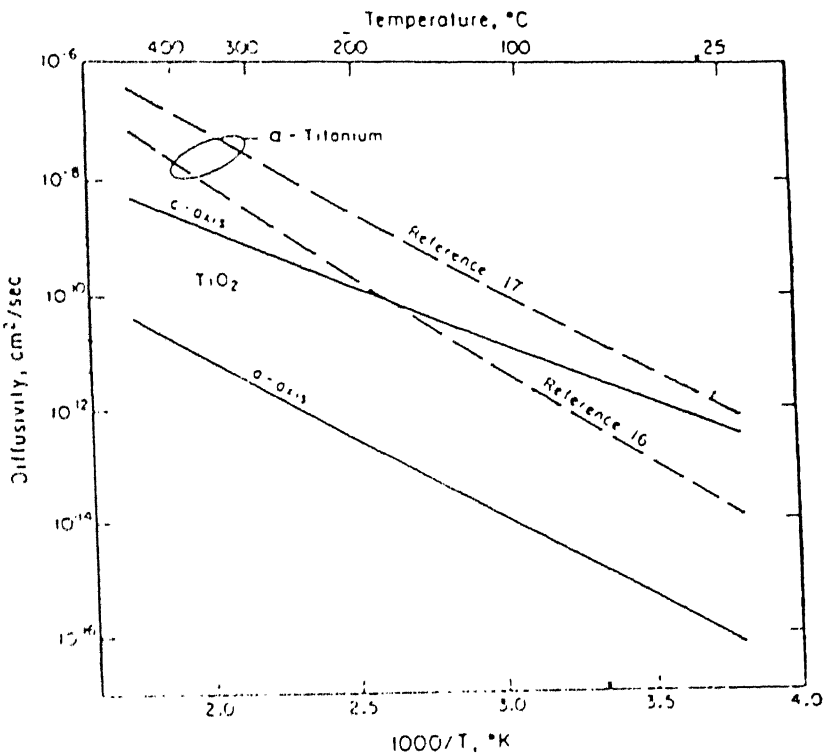

Fig 12 Hydrogen diffusivity in α-Ti and rutile (TiO_2) as a function of temperature [28].

can not occur below this temperature. However, hydrogen can permeate through the oxide layer after 700°C and therefore hydride dissociation and hydrogen evolution can occur above this temperature [19,28]. Figure 12 shows the hydrogen diffusivity in α Ti and rutile (TiO_2) as a function of temperature [49] from where it is seen that hydrogen diffuses at a lower rate in the oxide compared to the base matrix. It should be emphasized that the diffusivity reported is for hydrogen in α-Ti and not in titanium aluminides. It can be expected that the diffusivity would be lower in titanium aluminides as hydrogen diffuses at a lower rate in ordered structures [40]. Therefore, the data in the figure should be used only as a guide and not treated as sacrosanct.

2.4 OXIDATION IN Ti_3Al+Nb INTERMETALLICS

As mentioned in the plan of study, the hydrogen charged intermetallics would be baked at higher temperatures to dissociate the hydride that forms. Therefore, it also becomes important to address the type of oxides that form in the present intermetallics and the following sections are devoted to this aspect.

Irrespective of whether α_2 (i.e. Ti_3Al) based or γ (i.e. TiAl) based alloys are used in monolithic form or as composites, the issue of their oxidation is still of concern. The addition of Nb to binary TiAl improves the low temperature ductility. In general, it has been found to enhance oxidation resistance as well. Metallic material can be protected against high temperature oxidation only by formation of a protective oxide film such as Al_2O_3, Cr_2O_3, and SiO_2. These oxides have sufficiently slow growth rate due to low defect concentration. Out of these oxides Al_2O_3 is favored as a protective oxide. One of the prerequisites for protectiveness of Al_2O_3 scale is that it should be most stable of all possible oxides, so that it does not get reduced by the base metal or the other constituents of the alloy [2].

After annealing the system at high temperatures in air, the weight gain behavior can be analyzed. The oxidation resistance in air is much better than oxygen, resulting in a higher activation energy for oxidation [38]. The examination of oxidation products in super α_2 (Ti-14Al-20Nb-3V-2Mo, wt%) at 700°C showed that the

first step was the formation of a thin rutile layer, independent of atmosphere. In the second stage, there was a build up of a layer consisting of rutile alumina (in oxygen atmosphere) and of rutile, alumina and a trace of TiN (in air). The thin outer layer consists only of rutile of nearly same thickness and relatively poor adherence to the intermediate layer [2]. Only the thickness of second layer seemed to be influenced by the annealing atmosphere, exhibiting a layer formed in oxygen atmosphere which was nearly twice as thick as the one built in air. This indicates that air promoted the formation of a layer which seemed to be more adherent. However, an alternative explanation might involve the lower activity of oxygen (the rate limiting species) in air as compared to pure oxygen [38].

2.4.1 PHASE RELATIONS IN THE Ti-Al-Nb-O SYSTEMS

The oxidation behavior of metals and alloys is related to nature of the scales or product formed. During the parabolic oxidation period of titanium, Kofstad et al. [50] noticed a very thin and extremely adherent grey scale. The oxide color changed to white and yellow during the linear period with poor adherence to the metal. The oxide formed in all the cases was found to be TiO_2. In fact the morphologies and chemical composition of scales are influenced by some factors such as alloying elements, gas composition etc. The binary Ti-Al and ternary Ti-Al-Nb phase diagrams have already been presented earlier. From the Ti-O phase diagram [51], the major stable oxides in Ti-O system are TiO, Ti_2O_3, Ti_3O_4, and TiO_2. Thermodynamically, different oxides of Ti are expected to form as a sequence of layers. However, out of several forms, the rutile structure of TiO_2 has been commonly found below 1273 K in oxygen at near atmospheric pressure [51]. This may be due to kinetic reasons which cause faster oxygen dissolution and consequent rutile formation, as compared to rates of formation of lower oxides. Pure Al forms Al_2O_3, which is closely stoichiometric due to large band gap (about 9.9ev) and a high lattice energy [40]. However, it has several polymorphic forms. The binary Nb-O has a stable monoxide (NbO), and a dioxide (NbO_2). In addition to these, Nb_2O_5 exists in polymorphic forms.

Therefore, there are several oxides that can form in the Ti-Al-Nb system and the type of oxides that form would be discussed in the following section.

2.4.2 EFFECT OF NIOBIUM

The oxidation of alloys and intermetallics in the binary Ti-Al system has been subject of several earlier studies. The scale formed upon oxidation in such cases was mostly multilayered [2]. Ti_3Al as well as TiAl have poor oxidation resistance as compared to $TiAl_3$ [52], because at low Al content, the external scale of the former was not protective Al_2O_3 film but rather TiO_2 or a mixture of TiO_2 and Al_2O_3. Best oxidation resistance is obtained by Al_2O_3 scale formation. The temperature should be high enough to promote Al_2O_3 formation and the Al content must be sufficiently high to develop and maintain an Al_2O_3 layer. The main weakness of Al_2O_3 scale is the susceptibility to cracking and spalling which is caused due to stresses. Addition of a third element may improve the adherence and reduce the growth rate [53].

In general, the addition of Nb to Ti-Al alloys was observed to be beneficial for oxidation resistance by several investigators. The positive role of Nb has been interpreted in many ways. According to some authors [54,55], the addition of Nb reduced the point defect concentration of titania scale which decreases the diffusion rate through titania. while some investigators [56,57] proposed that Nb promotes the formation of protective Al_2O_3. Hoch [58] determined the activity ratios of Al and Ti in Nb containing Ti-36Al (wt %) alloys and observed higher value of the ratios as compared to those in alloys without Nb. Hauffe also reported that the addition of Nb improves the oxidation resistance. The modification of defect structure of TiO_2 caused by Nb ions has also been reported for Ti-25Al-15Nb [59]. However, the mechanism is not properly understood.

On the contrary Subrahmanyam [60] reported detrimental effect of Nb on the oxidation resistance of Ti aluminides . According to the investigator, the presence of Nb_2O_5 in scale was found to be one of the factors leading to spallation. The concentration of Nb also influenced the oxidation behavior. Addition of 5 wt % of Nb

to TiAl caused Al_2O_3 formation at the metal/scale interface even at 1173-1223K. Becker et al [61] held gradual enrichment of Nb in the alloys during the transient oxidation to be responsible for this. According to Singheiser et al. [62] the oxidation rate was parabolic and rate constant values decreases with increasing Nb content and became independent for Nb addition greater than 10 atom %. In another study, Chen et al [63] reported that the oxidation resistance of Ti-Al-Nb system was reduced dramatically when the ratio of Ti to Nb was either too high or too low. The occurrence of Nb_2O_5 for high Nb alloys always leads to decrease in the oxidation resistance. Oxidation at 1173K showed predominantly TiO_2 at Al content lower than 45 atom % and/or Ti/Nb ratio greater than 5 to 6.

It must be noted from the above literature review that there has been no study conducted on the oxidation behavior of high Nb content titanium aluminides. It can be expected that when the Nb content is very high, it can result in the formation of niobium oxides and therefore lower the oxidation resistance as the presence of niobium oxides leads to scale spallation.

2.4.3 OXYGEN DIFFUSIVITY IN TITANIUM ALUMINIDES

Ti_3Al-based alloys are being considered for application in monolithic and composite form in aircraft engines due to their improved high temperature properties over conventional titanium alloys. The inherently poor room temperature ductility of these alloys has been overcome to a great extent by alloying with Nb, Ta, Mo, etc However, their poor oxidation resistance [2] and environmental embrittlement [64,65] at elevated temperatures are still of concern. Embrittlement at higher temperatures is a consequence of hardening caused by dissolution of interstitials such as oxygen and nitrogen in metal lattice [66]. In this regard, values of diffusivity for oxygen and nitrogen in Ti_3Al based alloys would be useful for interpretation of oxidation as well as embrittlement of these alloys. However, only a limited amount of data is available in literature [67-69]. It is therefore important to evaluate the diffusion coefficients of oxygen and nitrogen in Ti-24Al-20Nb and Ti-24Al-27Al (atom%) alloys at 1000°C. and

obtained by profiling microhardness in the matrix after oxidation experiments. Determination of diffusivities by this technique is simple [70], but nevertheless useful as there are many difficulties in the precise measurements of diffusivities.

CHAPTER 3

EXPERIMENTAL PROCEDURE

3.1 MATERIALS

The materials used in the current study are Ti_3Al based intermetallic with high Nb contents. They were obtained in the form of extruded rods 18 mm thick from the Defense Metallurgical Research Laboratory, Hyderabad. There were two compositions that were supplied for the purpose of the study. They had the nominal compositions of Ti-24Al-20Nb and Ti-24Al-27Nb. The first composition is designated as A and the second composition as B throughout the rest of the thesis.

The chemical compositions of these intermetallics were analyzed by a JEOL Electroprobe microanalyzer (JXA-8600 MX). Compositions were obtained from spot analysis. By choosing several different spots, their average compositions were obtained and these are presented in Table 4 in the next chapter. The intermetallic compositions were according to the specifications of the supplier.

3.2 HEAT TREATMENT

A large number of samples of thickness 1 mm were sectioned from the as received rods (in round form). These samples were sealed in a quartz tube under vacuum. For the purpose of heat treatments, a vertical muffle furnace was used. When the desired temperature was attained in the furnace, the sealed quartz tubes were inserted from the top of the cylindrical-type furnace. The heating and soaking was done for the desired time at desired temperature and then cooled according to schedule. Three types of cooling were employed initially to understand the effect of heat treatment on the structure: water quenching, fan cooling and air cooling.

The vacuum sealing of sample containing quartz tube was employed for obtaining the equiaxed and widmanstatten microstructures but for obtaining the fine basketweave and coarse

basketweave microstructures, the heat treatment was performed in argon atmosphere. The lower part of the furnace was closed.The argon gas entered through the plastic tube to the glass pipe which was kept in the furnace and the sample was kept in that glass tube. The exit gas was connected through a bubbler. In this way, the heat treatments in the Ar atmosphere was performed. The heat treatment schedules that were employed in the current study are listed in Table 5.

3.3 SAMPLE PREPARATION

The as received material was in the form of rods of diameter 18 mm. The rod could not be used directly for experiment, so it was cut into pieces. Since Ti_3Al-based intermetallics were very hard and brittle, they could not be cut by a simple cutting machine such as hacksaw. A low speed Isomet saw was used for cutting purposes using a diamond blade. There was an arrangement for adjusting the speed in this machine and oil was used for cooling purposes.

For hydrogen charging experiments, samples of size 10 mm x 1 mm x 4 mm were cut from the as-received rods. A large number of specimens were prepared for hydrogen charging experiments. These specimens were cut by the low speed saw and then polished on a belt grinder, emery paper (1/0 through 4/0) and then on cloth polishing wheel up to 0.3 μm finish using alumina powder. The accurate size of the sample was measured by slide calipers.

The sample for oxidation had a size of 10 mm x 1 mm x 5 mm. A large number of oxidation samples were cut from the as-received rods and polished as described above before the start of the experiments.

3.4 HYDROGEN CHARGING PROCEDURE

Hydrogen charging was performed electrochemically using a potentiostat. The solution used for charging was a 0.05 mol/ liter H_2SO_4 and it contained 100 ppm of hydrogen recombination "poison" $NaHAsO_4$. One liter of this solution was filled in the electrochemical cell and the potentiostat was used to control the charging current such that a current density of 10 mA/cm^2 was

obtained. There were two electrodes in the polarization cell. The counter electrode was a platinum electrode and the specimen was the working electrode . The temperature was maintained constant at 20^{o}C. A cryostat was used for maintaining the temperature. Charging of hydrogen was performed for 24 h, 12 h and 6 h for both the A and B intermetallics. In the initial round of experiments, the potential of the charging electrode was monitored versus saturated calomel electrode (SCE) during the course of charging. The potentiostat was connected with a computer and variation of specimen potential with time was obtained. After charging, the specimen was taken out and washed in water and kept in fridge.The variation of electrode potential as a function of charging time for specimen B is shown in Figure 13. This curve shows that the potential was stabilized fairly quickly.

3.5 BAKING

After hydrogen charging, some samples were also baked in a furnace to understand the stability of hydrides that formed. These samples were introduced in a furnace maintained at the desired temperature and the baking was performed in laboratory air. Two temperatures (400^{o}C and 800^{o}C) were used for baking the hydrogen-charged samples. A freshly hydrogen charged specimen was used for each baking experiment. The baking time at 400^{o}C was 1.5 hrs and at 800^{o}C was 10 minutes. The temperature 800^{o}C was chosen for baking because the decomposition temperature of titanium hydride is 760^{o}C and the temperature 400^{o}C was chosen for the sake of verification whether the hydrides would decompose or not. The time for the baking at both the temperatures were calculated by using formula $x = \sqrt{Dt}$. The D values corresponding to both temperatures were obtained from Figure12. It is 6.9 x 10^{-5} cm^2/s at 400^{o}C and 6.1 x 10^{-7} cm^2/s at 800^{o}C.

It was also likely that the actual diffusivity of hydrogen in the intermetallics could be lower than in α Ti as hydrogen diffusion in ordered structures is slower than in disordered structures. Therefore, the specimens that were baked were further baked at the temperature such that the total baking time was 24 h (i.e. an additional 23h50m for baking at 800^{o}C and 22.5h for

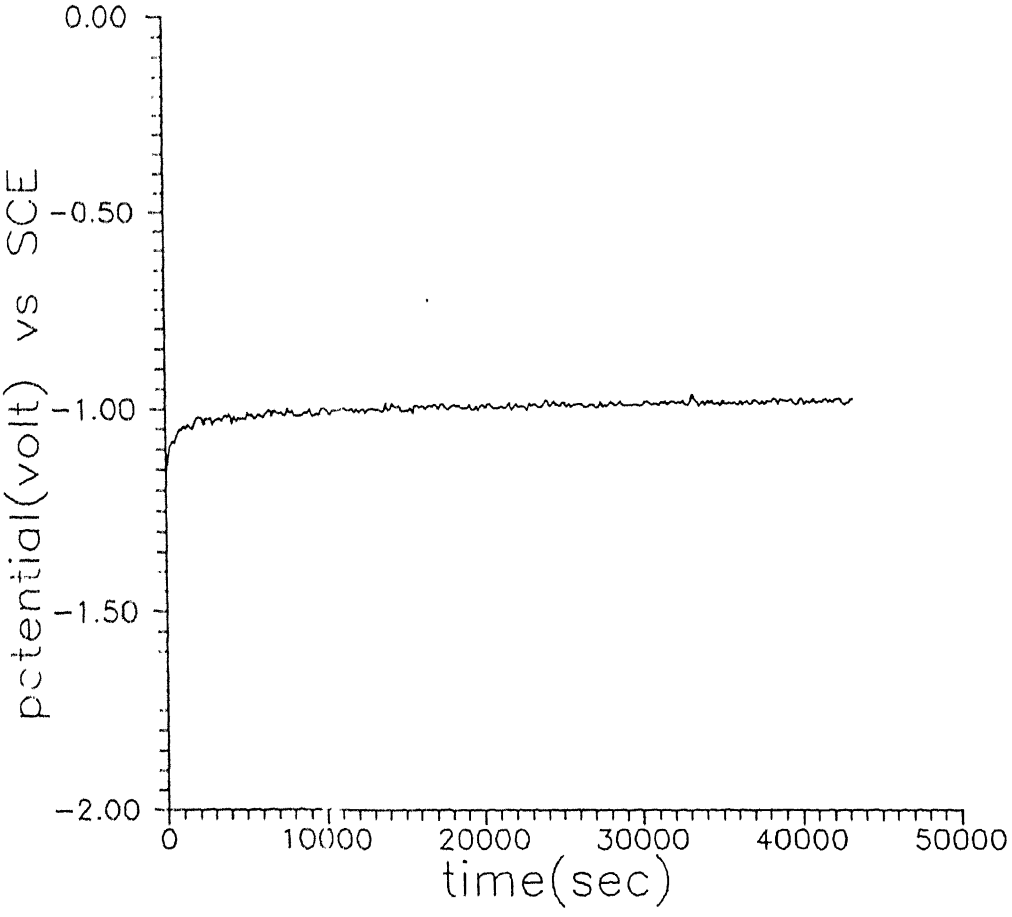

Fig 13 Potential vs. time curve during hydrogen charging in 0.05 mol/lit H_2SO_4 at room temperature for intermetallic A.

baking at 400°C).

For reference purposes, samples of both the intermetallics that were not charged with hydrogen were also provided the above heat treatments at 400°C and 800°C.

In order to understand the long term stability of the hydrides that formed in the samples, some of the samples that were hydrogen charged and baked were allowed to age at room temperature for a fairly long time (1 year) and microhardness obtained.

3.6 OXIDATION

Specimens of size 10mm x 5 mm x 1 mm were prepared for understanding scaling characteristics during exposure of the intermetallics to high temperature. The specimens were polished on 1/0 through 4/0 emery paper and then on cloth polishing wheel to 0.3 μm finish. After polishing, the samples were washed and rinsed with acetone. The temperature of the furnace was maintained at 1000°C. One sample (at each time) was suspended by a Pt wire in the furnace and oxidized for 10 h and 46 h for both the specimens A and B. After the specified time the specimens were taken out, cooled in air, carefully placed in tissue paper and kept in a desiccator.

3.7 CHARACTERIZATION

The following methods were used for characterizing the materials before and after the hydrogen charging, baking, heat treatment and oxidation experiments.

3.7.1 MICROSCOPY (Optical and SEM)

The specimens after various treatments such as hydrogen charging, baking, oxidation and straight heat treatments, were mounted using a cold setting resin and cold setting powder. The specimens were ground on belt grinder, polished with SiC emery papers up to 4/0 and were finally cloth polished using up to 0.3 μm Al_2O_3 powders. The polished specimens were etched with a Kroll's solution (4% HNO_3 and 2% HF in water) to reveal the microstructure. The polished and etched specimens were studied under an optical microscope (Leitz Laborloux) to observe the

microstructure and distribution of phases.

The specimens used for scanning electron microscopy were observed in a JEOL JSM 840 A scanning electron microscope. They were also prepared as described above. However, sometimes they were also coated with a thin silver layer on the surface (after the etching treatment) prior to observation. The microstructures were obtained in both normal and back scattered mode. In the back scattered electron mode, the elements having different atomic number scatter the electrons with different intensities and therefore the contrast between different phases (containing different amounts of the elements) could be obtained. The α_2/O phases in titanium aluminides appear dark whereas the β phase appears as bright in the back scattered electron mode. X-ray elemental mapping of Ti, Al and Nb was also performed for hydrogen charged and oxidized samples using the energy dispersive X-ray analysis (EDX) unit attached to the SEM..

3.7.2 HARDNESS MEASUREMENT

The microhardness was obtained using a microhardness tester attached to a Carl Zeiss Jena Microscope. The measurements were obtained on polished and etched specimens. A 40 gm load was used for the hydrogen charged and baked specimens and a 30 gm load for the oxidized specimen. In the case of heat treated specimens, a 40 gm load were used. Indentations were made from one surface to another along the width at a fixed interval of distance. The load was applied and then after unloading, the size of indentation was measured on a vernier scale. The formula used for Microhardness measurements was

$$MHV = 1854.18\ P\ /\ D^2$$

where P is load in gm and D is the diagonal length of indentation in μm. By using this formula, the value of microhardness (MHV) was calculated.

For the microhardness profiling experiments, three sets of microhardness readings (i.e. three different microhardness profiles) were obtained and the average value at a particular location was computed and these data are presented in the next chapter.

3.7.3 X-RAY DIFFRACTION

After hydrogen charging, baking and oxidation, the samples were fitted in a sample holder of a Rich Seifert 2002D X-ray diffractometer. XRD patterns were obtained for 2θ from 15° to 110° for uncharged, hydrogen charged and baked specimens and from 20° to 70° for oxidized specimens using Cu K_{α} radiation.. With the help of powder diffraction files, these ranges of angle were chosen since all the possible phase provide major reflections from planes in this range of angles. The interplanar spacing (d) values were calculated from the patterns by using Bragg's law and the diffraction lines in the patterns were indexed. In this way, the presence of various phases was studied.

The radiation used was CuK_{α} and the speed of scanning was 1.5 and 3°/min. The chart speed was 15 and 30 mm/min and the counts per minutes was 5K and 10K. These interplanar (d) values were matched with the d value of different phases obtained from powder diffraction files in order to identify the phases present.

CHAPTER 4

RESULTS AND DISCUSSION

The results obtained from the various experiments carried out for the thesis work are discussed in this chapter. The chemical compositions of samples A and B have been checked by EPMA. The effect of several heat treatments on the microstructure has been discussed. The effect of hydrogen charging and subsequent baking treatment on microhardness profiles of the samples have been discussed. The effect of other variables such as charging time, baking temperature and baking time have also been addressed. In the oxidation studies, the spalling behavior of the oxides formed after oxidation has been addressed. Moreover, the diffusivity of oxygen in the intermetallics has been determined by subscale microhardness profiling. All the above effects have been understood by material characterization using optical and scanning electron microscopy and x-ray diffraction analysis.

4.1 COMPOSITION ANALYSIS BY EPMA

The compositions of samples A and B were analyzed using a JEOL electron probe microanalyser. The compositions obtained at five different random points and the average composition of the intermetallics are presented in Table 4. The compositions are as per the specification provided by the supplier (DMRL).

4.2 EFFECT OF HEAT TREATMENT

The heat treatment schedules listed in Table 5 were utilized for intermetallics A and B with the main objective of obtaining different microstructures. The solutionizing temperatures (1050^{o}C for intermetallic A and 750^{o}C for intermetallic B) for the two

Table 4

Compositions of intermetallics analyzed by EPMA

	Point I	Point II	Point III	Point IV	Point V	Avg.
Elements	At%	At%	At%	At%	At%	At%
			Sample A			
Ti	57.0086	56.9554	56.1821	56.1891	55.0019	56.2674
Al	23.7746	24.4966	24.2702	24.2706	25.1103	24.3844
Nb	19.2171	18.5480	19.5476	19.5403	19.8878	19.3481
			Sample B			
Ti	49.2067	49.2269	49.5708	50.1248	49.3086	49.4875
Al	23.8264	23.3858	23.6674	23.7801	24.0146	23.7348
Nb	26.9669	27.3879	26.7618	26.0951	26.6768	26.1777

Table 5

The heat treatment schedules used for developing different microstructures of intermetallics A and B.
(WQ represents water quenched and FC represents fan cooling)

Sample A

	Expected Microstructure	Heat Treatment Schedule
(a)	Equiaxed $\alpha_2+\beta$	1050°C/0.5hr/WQ
(b)	Widmanstatten $\alpha_2+\beta$	1040°C/1hr/WQ 976°C/1hr/WQ 715°C/1hr/WQ
(c)	Coarse Basketweave $\alpha_2+\beta$	1035°C/1hr/FC 976°C/1hr/FC 715°C/1hr/FC
(d)	Fine Basketweave $\alpha_2+\beta$	1035°C/1hr/FC 767°C/8hr/FC

Sample B

	Expected Microstructure	Heat Treatment Schedule
(a)	Equiaxed $\alpha_2+\beta$	680°C/0.5hr/WQ
(b)	Widmanstatten $\alpha_2+\beta$	750°C/1hr/WQ 680°C/1hr/WQ 510°C/1hr/WQ
(c)	Coarse Basketweave $\alpha_2+\beta$	750°C/1hr/FC 680°C/1hr/FC 510°C/1hr/FC
(d)	Fine Basketweave $\alpha_2+\beta$	750°C/1hr/FC 560°C/8hr/FC

intermetallics were chosen on the basis of the β-transus temperatures from the phase diagram of Ti_3Al-Nb presented in Figure 3. It was expected that the intermetallics would be obtained in the β condition after the solutionizing treatment and later the heat treatments would precipitate α_2 and O phase in intermetallic A and the O phase in intermetallic B. However, it was observed that after treating both the specimens according to heat treatment schedules, the microstructures were similar for all the heat treatments for both intermetallics A and B. Therefore the microstructure could not be changed by heat treatment of the as-received intermetallics according to the schedules listed in Table 5. Typical SEM photographs are shown in Figures 14 and 15 for intermetallics A and B, respectively.

In Figure 14, the intermetallic A had been provided heat treatment marked "a" and intermetallic B heat treatment marked "a" in Table 5. In the case of intermetallic A, it was found that the all the heat treatments resulted in microstructures of equiaxed α_2/O phase in a matrix of β. The O phase precipitates in the matrix of β for heat treatments lower than 1253 K (in the Ti-24Al-15Nb intermetallic) whereas for heat treatments above this temperature, an orthorhombic distortion of the hexagaonal phase is observed and not the O phase [10-12]. It must be noted that the dark phase that reveal in the case of titanium aluminides is the α_2 or the O phase (light grey contrast) and the light phase is the Nb-rich β phase. In the case of the Ti-24Al-20Nb (intermetallic A), both the α_2 and the O phase can precipitate in the matrix of β while in the case of the Ti-24Al-27Nb (intermetallic B), the O phase precipitates in the matrix of β [71]. The α_2 phase can also precipitate in the interphase regions of the higher Nb alloy [71]. The grey phase is α_2 and O and white phase is β in Figure 14. Therefore, from Figure 14, it can be concluded that all the heat treatments resulted in α_2/O phase precipitation in the β matrix in intermetallic A. The issue of differentiating between the α_2 and the O phase can be resolved only by transmission electron microscopy, which was unfortunately not attempted in this thesis work. The as-received microstructure of the intermetallic A is presented in Figure 16a and this shows fine precipitation of α_2/O

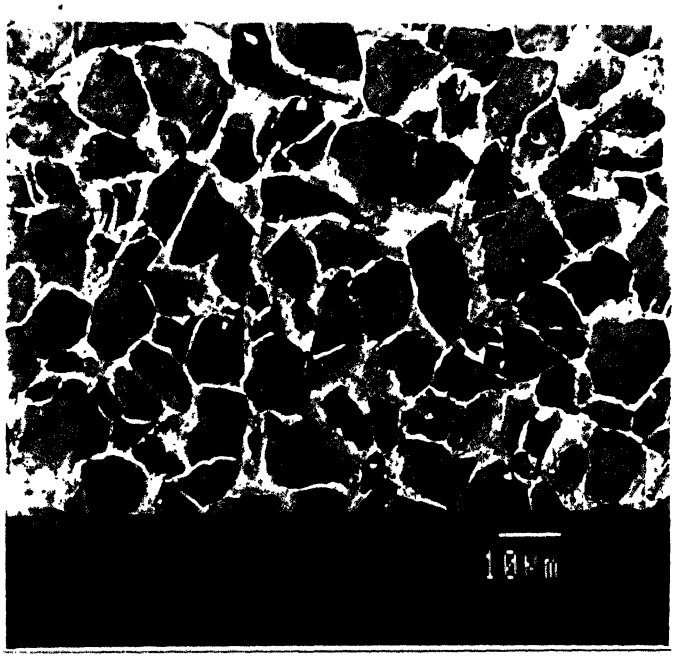

Fig 14 SEM photograph of sample A obtained after heat treatment marked "a" in Table 5.

in the β matrix. Upon further heat treatment according to schedules listed in Table 5, the precipitated phases α_2 and the O phase grow in the matrix of β, which results in the microstructure of Figure 14.

In the case of the Ti-24Al-27Nb (B) intermetallic, the heat treatments resulted in fine precipitation of O in a matrix of β (Figure 15). The as-received microstructure of the intermetallic B is presented in Figure 16b, which reveals a fine distribution of the O phase in the β matrix. The solutionizing temperature used for intermetallic B was not sufficient to solutionize the intermetallic (in order to form the complete β phase) and upon further heat treatments provided according to the schedules listed in Table 5, the precipitated O phase only exhibited growth and coarsening as can be seen in Figure 15. As noted earlier, in the high-Nb titanium aluminides, the O phase precipitates for heat treatments below 1253 K. The Nb level in this phase is intermediate between that in the α_2 and β phases, as is seen from the contrast obtained [12]. The Nb atoms in the O phase occupy a sublattice distinct from that of the Ti and Al atoms, and this structure is derived by a small distortion of the "a" and "c" axes of the close packed hexagonal α_2 structure. In the α_2 structure, the Nb atoms show no distinct sublattice occupancy [12].

The microstructures of both the intermetallics could not, therefore, be altered by the heat treatments listed in Table 5. It can be reasonably concluded that this was due to the relatively low solutionizing temperatures provided in the heat treatments. It was later communicated by the supplier [71] that the β transus of these alloys are 1130^{o}C and 1110^{o}C for alloys A and B, respectively. Moreover, the effect of prior thermomechanical treatment on the subsequent heat treatments could also have affected the microstructure. In view of these results, the as received condition was used for all further studies for both the intermetallics. The microstructures of the as-received intermetallics are shown in Figure 16. The microstructure of Ti-24Al-20Nb consists of fine distribution of α_2 and O in β, while that of Ti-24Al-27Nb shows a fine distribution of O in β. The XRD patterns from the as-received intermetallics (Figures 17 and 18)

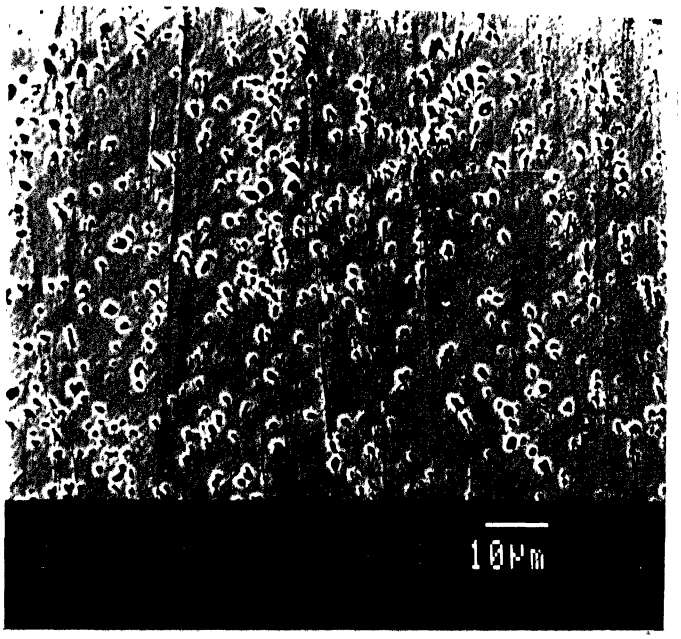

Fig 15 SEM photograph of sample B obtained after heat treatm
marked "a" in Table 5.

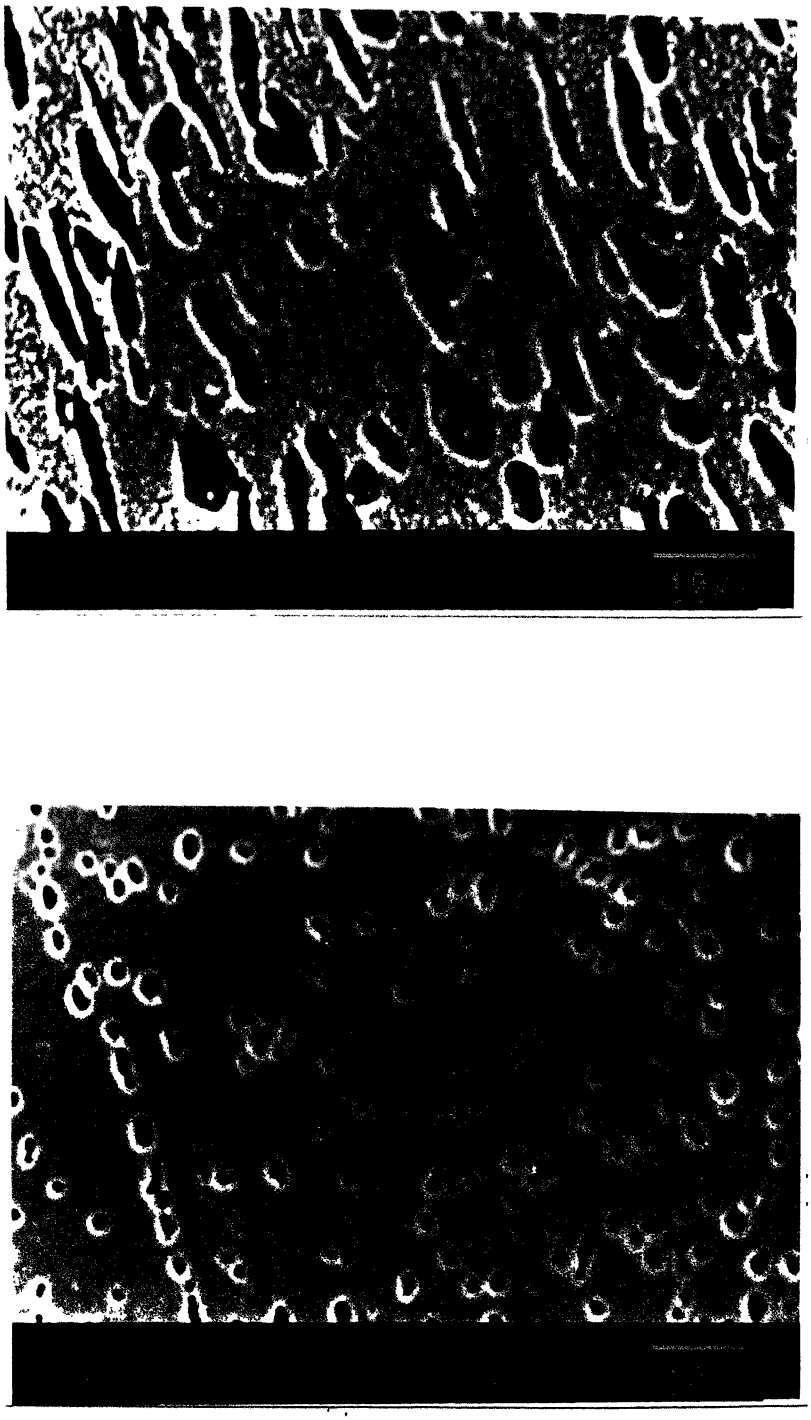

Fig 16 As-received microstructures of intermetallics (a) A and (b) B.

showed that the Ti-24Al-20Nb contained both the α_2 and O phases while the Ti-24Al-27Nb contained the O phase, as no significant peak from the α_2 phase could be identified. The area fraction of the dark phase (either α_2 or O) and the light phase (β) was obtained by quantitative microscopic calculations. The area fraction of the dark phase (α_2/O) is 21% and 7% in intermetallics A and B, respectively, while that of the β phase is 79% and 93% in intermetallics A and B, respectively.

4.3 HARDNESS VARIATION OF UNCHARGED SPECIMENS

In the case of the specimens that were not charged with hydrogen, the hardness profiles across the cross-section remain constant along the width. This is the case for both the intermetallics as shown in Figures 19 and 20. It is to be noted that the hardness of intermetallic B is higher than that of A in the as-received condition. The possible reasons for this could be the following. The percentage of niobium is higher in intermetallic B (27% Nb) as compared to A (20% Nb). The orthorhombic O phase is the major precipitating phases in this alloy (refer to Figure 3) and as the hardness of the O phase is greater than that of the α_2 and β phase [11], the intermetallic B exhibits a higher hardness than that of intermetallic A. The orthorhombic phase is the phase which appears as dark in optical and SEM photographs (see, for example, Figure 16b). It can be unambiguously identified by transmission electron microscopy [10-12]. Therefore, one reason for the higher hardness of intermetallic B could be the presence of the harder O phase. In the case of the intermetallic A, the microstructure (Figure 16a) shows a distribution of a dark phase in the β matrix. It is reasonable to assume that this dark phase is predominantly α_2 (with minor amount of O) since the composition contains a lower amount of Nb. This has also been borne out by XRD studies (Figure 17). Therefore, it appears that the hardness of the intermetallic is higher for a lower volume fraction of the O phase in a matrix of β (i.e. intermetallic B) than for a higher volume fraction of the α_2 phase in a matrix of β (i.e. intermetallic A). Secondly, the size of the precipitates in intermetallic B is finer than that

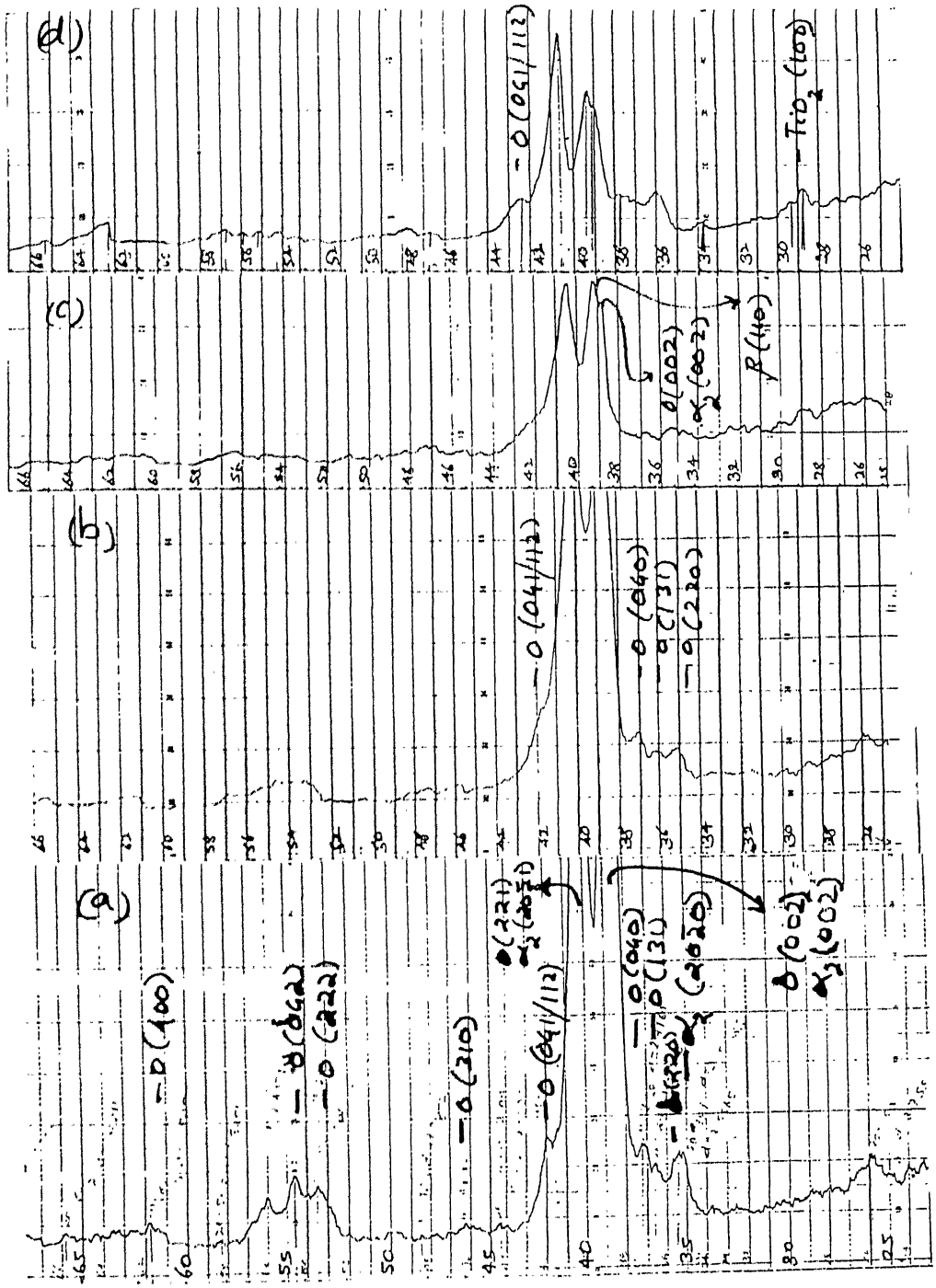

Fig 17 XRD patterns taken at a scan rate of 3^{o}/minute of intermetallic A : (a) uncharged (b) hydrogen charged for 24 hours (c) baked at $400^{o}C$ for 1.5 hours (d) baked at $800^{o}C$ for 10 minutes.

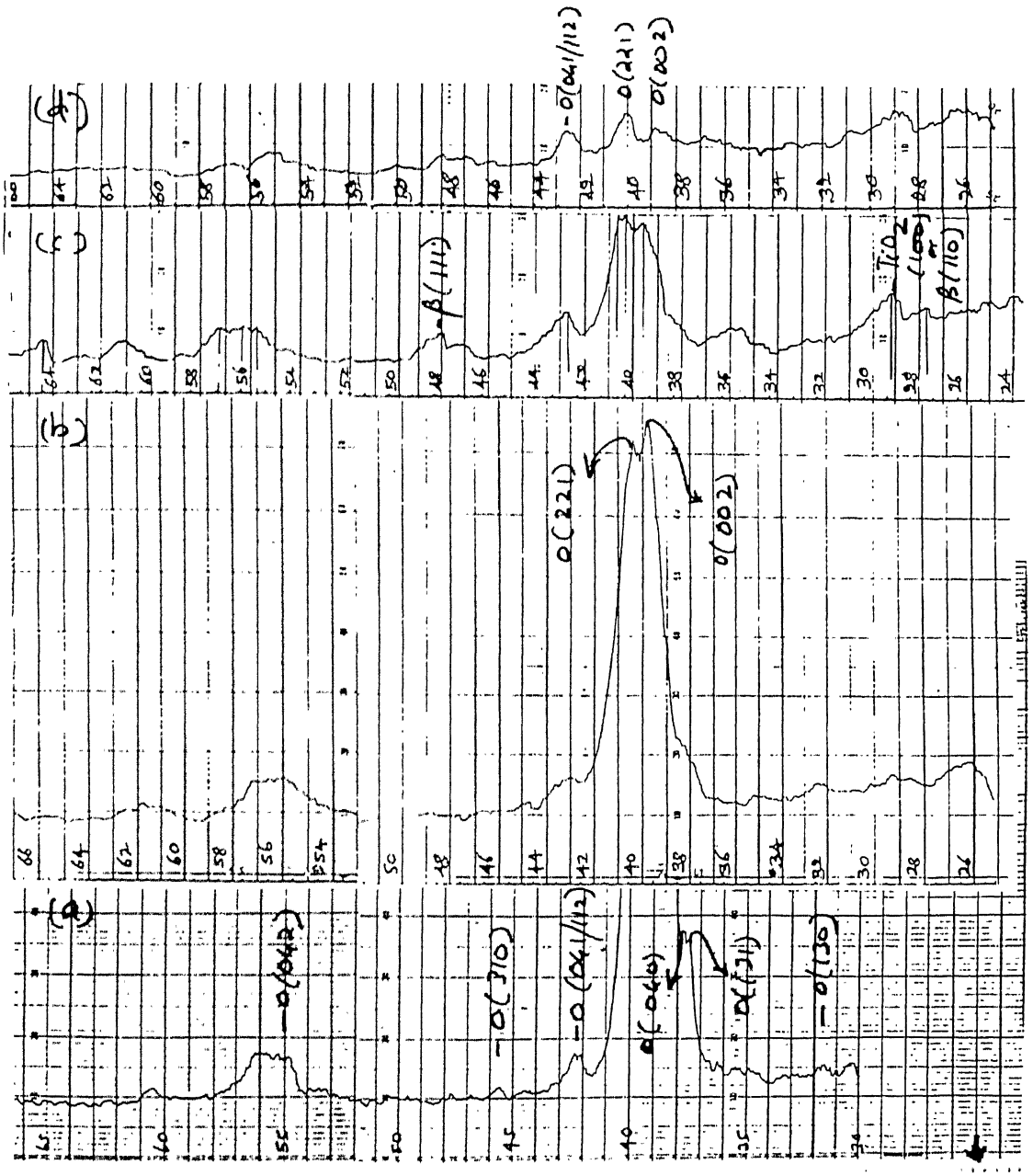

Fig 18 XRD patterns taken at a scan rate of 3°/minute of intermetallic B : (a) uncharged (b) hydrogen charged for 24 hours (c) baked at 400°C for 1.5 hours (d) baked at 800°C for 10 minutes

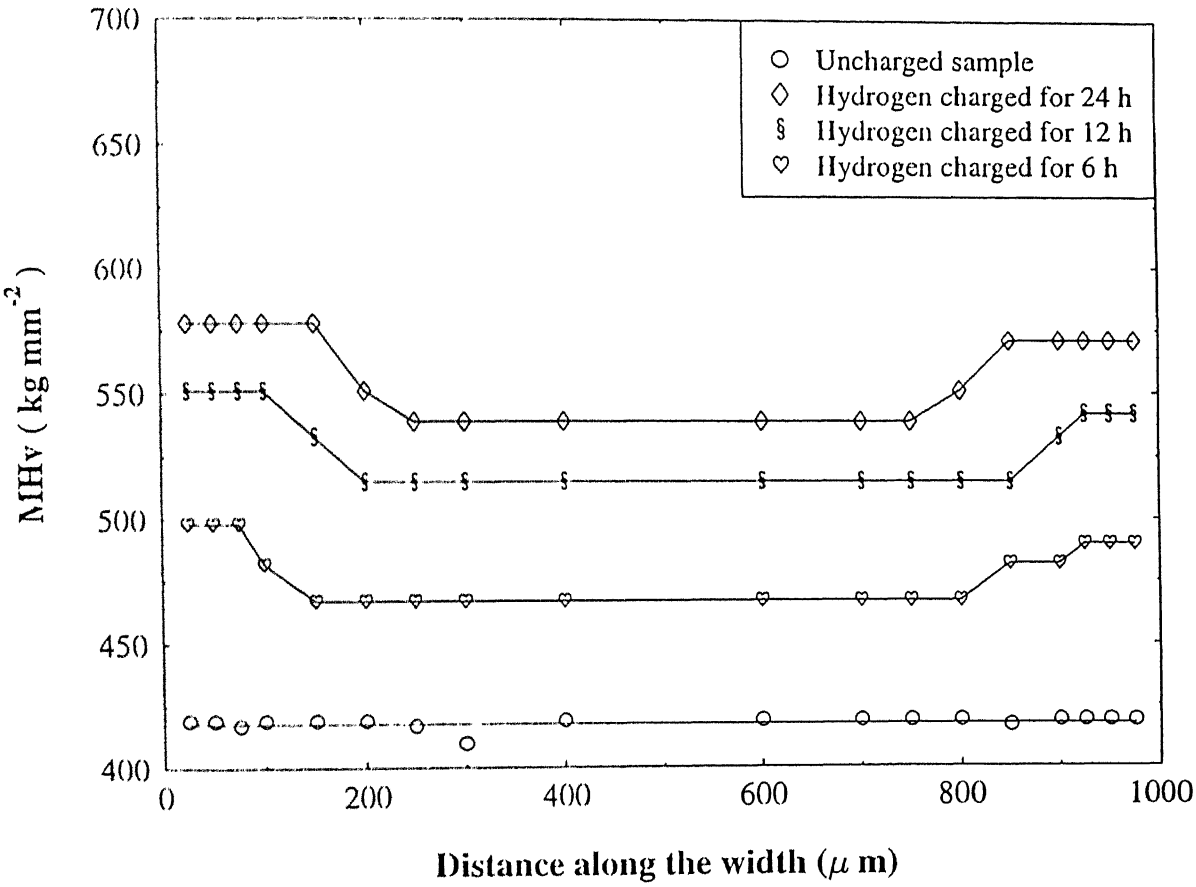

Fig 19 Microhardness profiles for intermetallic A for the following conditions: uncharged; hydrogen charged for 6, 12 and 24 hours.

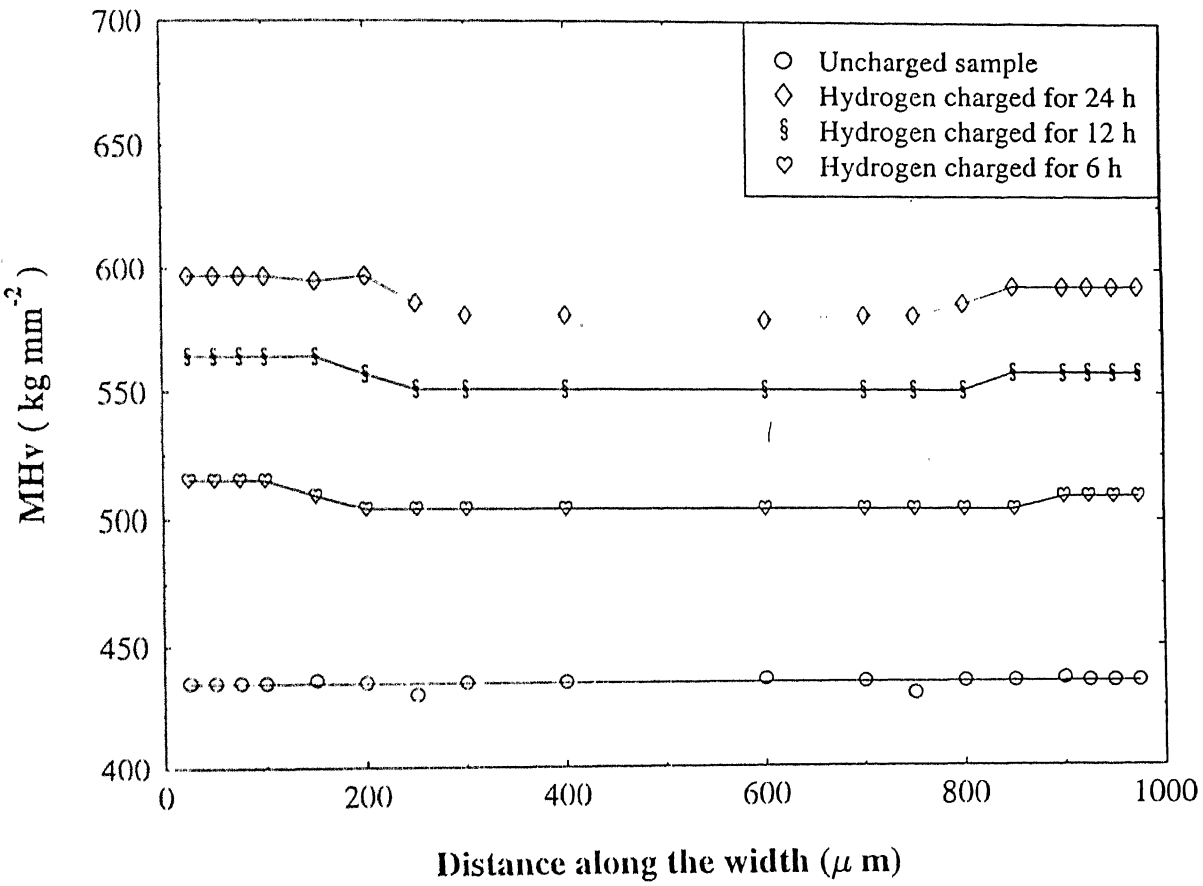

Fig 20 Microhardness profiles for intermetallic B for the following conditions: uncharged; hydrogen charged for 6 12 and 24 hours.

in intermetallic A and this could have also contributed to the higher hardness observed for intermetallic B. It is also to be noted that the microstructure did not vary as a function of the cross section of the specimens for both the intermetallics.

As noted earlier, the microstructures of both the intermetallics is a matrix of β in which precipitation has taken place. Although the exact thermomechanical treatment provided to the samples were not indicated by the supplier, it appears that the samples had been solutionized to the β phase and then extruded into rod shapes at a fairly high temperature. The standard practice at DMRL (from where the extruded rods were obtained) consists of mill annealing the cast intermetallics (i.e. 1373K, 4 hours, furnace cool) which results in grains of α_2/O with β at the triple points [11]). The β phase does not show superlattice spots at positions expected for the ordered B2 structure. These starting structure have been used for solution treatment in the α_2/O + β phase region. This consisted of 1140°C/1h/2.5°C per sec + 750°C/24h/AC for Ti-24Al-20Nb and 1120°C/1h/0.1°C per sec + 750°C/24h/AC [71]. The same temperature must have been used for heat treating both the intermetallics as the presence of a larger volume fraction of α_2/O precipitates in β matrix in the case of sample A is indicative of a higher α_2(O)/β transus for this alloy compared to alloy B (Figure 3). Incidentally, the as-received microstructure of the intermetallics A and B resemble that of Ti-24Al-11Nb after the α_2+β anneal at 1373K provided in Figure 4a of Reference 11. The precipitation of the α_2 and O phases would have occurred in intermetallic A and of the O phase in intermetallic B could have occurred during the heat treatment. This would result in a fine distribution of the precipitating phases in the β matrix as observed for the as-received condition (Figure 16). Moreover, that this is likely if borne out by further heat treatments (as per schedules listed in Table 5) of the intermetallics which lead to the coarsening of the precipitated phases in the matrix of β, since the solutionizing temperatures employed in the present study were not sufficient (high enough) to dissolve the precipitated phases.

4.4 HARDNESS VARIATION AFTER HYDROGEN CHARGING

The hardness profiles for intermetallics A and B after hydrogen charging for 24 h are also presented in Figures 19 and 20 for intermetallics A and B, respectively.

The hardness remains constant up to a distance of about 150 μm for intermetallic A and about 200 μm for intermetallic B from the surface and then it decreases to a lower value after which it again remains constant across the central region of the cross section. It will be seen later that this behavior is characteristic of the hydrogen-charged titanium aluminides used in this study. The constant values of hardness obtained in the surface and central regions of the specimen have been listed in Table 6. It should be also be noted that the increase in hardness is realized across the cross section of the specimens and this indicates that hydrogen has diffused through the thickness of the specimen for the duration of the experiment. Diffusion of hydrogen is expected to be high. Although the diffusivity is lower in ordered structures when compared to disordered structures [40].

The microhardness variation of the hydrogen charged specimens indicates two distinct features: a region near the surface that exhibits a higher hardness than the interior with the interior region itself exhibiting higher hardness compared to the reference uncharged specimen. As the hardness increase is noticed only after charging with hydrogen, it is reasonable to propose that this is due to the presence of hydrogen. Hydrogen can be present either as a solid solution or could lead to the precipitation of hydrides in the microstructure. The solubility of hydrogen at ambient and high temperatures should be relatively high in the β phase (50 at % H in β-Ti at 700°C [37]) compared to the α_2 phase [22,23]. At ambient temperatures, the solubility of hydrogen is low in the α_2 phase such that ternary hydrides precipitate [23]. At higher temperatures, the solubility of hydrogen is significant in both the α_2 and β phases [21,23,37,38], although the general trend is that solubility decreases with increasing temperature [21,37] due to the negative heat of mixing similar to that observed in the α_2-Ti system. The solubility of hydrogen in the O phase has not been reported, although it is reasonable to assume that it should

Table 6a

Hardness data from the surface and bulk region of the reference hydrogen charged and baked specimen. The depth of the surface hardened zone is also provided.

Intermetallic A

Conditions	Bulk MHv (kg/mm^2)		Surface MHv (Kg/mm^2)		d (μm)
	Value	% change	Value	% change	
U	419	---	419	---	--
24 h C	539	28.7	578	37.9	150
12 h C	515	22.9	551	31.5	100
6 h C	467	11.5	498	18.8	75
H. T. at 800°C/10 min	434	---	434	---	--
24 h C+B 800°C/10 min	475	9.4	498	14.7	150
12 h C+B 800°C/10 min	462	6.5	488	12.4	100
6 h C+B 800°C/10 min	439	1.1	453	4.4	75
H. T. at 400°C/1.5 h	448	---	448	---	--
24 h C+B 400°C/1.5 h	509	13.6	527	17.6	150
12 h C+B 400°C/1.5 h	498	11.2	515	14.9	100
6 h C+B 400°C/1.5 h	453	1.1	467	4.2	75
H. T. at 800°C/24 h	426	---	426	---	--
24 h C+B 800°C/24 h	430	0.9	434	1.9	75
12 h C+B 800°C/24 h	426	0.0	430	0.9	50
6 h C+B 800°C/24 h	426	0.0	426	0.0	0
H. T. at 400°C/24 h	438	---	438	---	--
24 h C+B 400°C/24 h	453	3.4	458	4.6	75
12 h C+B 400°C/24 h	448	2.3	453	3.4	50
6 h C+B 400°C/24 h	444	1.4	448	2.3	25

Where U = Uncharged, C = Charged, B = Baked , H.T. = Heat treated and d = Surface hardened zone depth (μm)

Table 6b

Hardness data from the surface and bulk region of the reference hydrogen charged and baked specimen. The depth of the surface hardened zone is also provided.

Intermetallic B

Conditions	Bulk MHv (kg/mm^2)		Surface MHv (Kg/mm^2)		d (μm)
	Value	% change	Value	% change	
U	435	---	435	---	--
24 h C	581	33.6	597	37.2	200
12 h C	551	26.8	564	29.6	150
6 h C	504	15.9	515	18.4	100
H. T. at $800^{O}C$/10 min	453	---	453	---	--
24 h C+B $800^{O}C$/10 min	498	9.9	515	13.7	200
12 h C+B $800^{O}C$/10 min	488	7.7	509	12.3	150
6 h C+B $800^{O}C$/10 min	457	0.9	467	3.0	100
H. T. at $400^{O}C$/1.5 h	477	---	477	---	--
24 h C+B $400^{O}C$/1.5 h	539	13.0	558	17.0	200
12 h C+B $400^{O}C$/1.5 h	527	10.5	539	13.0	150
6 h C+B $400^{O}C$/1.5 h	483	1.2	498	4.4	100
H. T. at $800^{O}C$/24 h	444	---	444	---	--
24 h C+B $800^{O}C$/24 h	448	0.9	453	2.0	100
12 h C+B $800^{O}C$/24 h	444	0.0	448	0.9	75
6 h C+B $800^{O}C$/24 h	444	---	444	---	--
H. T. at $400^{O}C$/24 h	462	---	462	---	--
24 h C+B $400^{O}C$/24 h	487	5.4	493	5.5	100
12 h C+B $400^{O}C$/24 h	477	3.2	483	4.5	75
6 h C+B $400^{O}C$/24 h	472	2.2	477	3.2	50

Where U = Uncharged, C = Charged, B = Baked, H.T. = Heat treated and d = Surface hardened zone thickness.

be similar to that observed for the α_2 phase as the physical metallurgy of the α_2 and O phase are closely related. Therefore, it is very likely that both the intermetallics A and B dissolve a large amount of hydrogen liberated by cathodic charging and this could be one of the reasons leading to the increase in hardness after hydrogen charging. Hydrogen would exist in solid solution essentially in the β phase as the terminal solid solubility of hydrogen in the α_2/O phase is small [21]. This is indirectly indicated in the higher hardness increase obtained for intermetallic B which contains a larger volume fraction of the β phase compared to intermetallic A (Figure 16).

The second plausible reason for the increase in the hardness would be precipitation of hydrides in the alloys. Hydrides are expected to precipitate from the α_2 or the O phase. The precipitation of hydrides from the α_2 phase has been extensively documented [26,37,42,44], whereas the precipitation from the O phase has not been studied in detail as yet. It is reasonable to assume that the precipitation of hydride from the O phase would closely resemble that from the α_2 phase as their physical metallurgy are similar [11,12]. This is also reasonable as the nature of hardness variation for intermetallic B after hydrogen charging is similar to that for intermetallic A. As regards precipitation of hydrides from the α_2 (O) phase, there are several points that need to be emphasized. First, the hydride that precipitates after ambient temperature cathodic hydrogen charging is not the same as that which precipitates after high temperature gaseous hydrogen charging. Rudman et al [22] have found that the hydrides that form in Ti_3Al at room temperature are necessarily ternary hydrides. They attributed this to the relatively low diffusion of substitutional metal atoms at ambient temperatures. They identified two ternary hydrides of composition $Ti_3AlH_{0.35}$ and $Ti_3AlH_{1.6}$ in Ti_3Al. However, they noted that when the ternary hydrides were heated above 200°C, the XRD pattern of the TiH_2 hydride emerged indicating that the ternary hydrides formed at room temperature are apparently metastable. Of course, it must be borne in mind that Rudman et al studied the bulk hydriding of the α_2 Ti_3Al intermetallic and not the precipitation of the ternary

hydrides in the α_2 matrix.

There is another interesting observation made by Muraleedharan et al [10] when hydrogen is present in titanium aluminides. They noted that when hydrogen was absorbed into the Ti-24Al-15Nb intermetallic during etching (hydrogen content below 20 ppm) after polishing, they observed orthorhombic distortions of the α_2 phase, which they noted to be similar to the hydrogenated α_2 phase reported by Shih et al [37]. This orthorhombic phase precipitated as distinct plates at the α_2/β interfaces which were twin related variants of the orthorhombic structure. They noted that the orthorhombic phase obtained on hydrogenation was different from the orthorhombic O phase obtained by heat treatment in that Nb atoms do not occupy specific sublattice in the former. Moreover, the lattice parameters of the interface orthorhombic phase and the O phase appear to be similar (a = 0.596 nm, b = 0.986 nm and c = 0.467 nm). Whether this phase was a hydride phase or related to the O phase was not resolved by them. They noted that if the latter was the case, it would imply that hydrogen segregates to the α_2/β interface and alters the stability of the α_2 phase such that martensitic transformation to the O structure can occur during etching. Therefore, when hydrogen is introduced into titanium aluminides at room temperature by cathodic processes, the formation of ternary hydrides in the α_2/O phase and the stabilization of the α_2 phase to the orthorhombic structures could be expected.

Manor and Eliezer [39] have stated that a hydride of type (TiNb)H forms in Ti-24Al-11Nb after room temperature cathodic hydrogen charging (1N H_2SO_4 at 5 kA/m^2 for 5 to 20 mins) although they did not provide proof (i.e. TEM pictures, electron and X-ray diffraction patterns) for this identification. Manor and Eliezer [39] and Eliezer et al [40] noted that on hydrogenation, cracks formed at the interface between the α_2/β phases and no hydrides could be identified in the crack tip. It is likely that the introduction of hydrogen would have resulted in the stabilization of the orthorhombic distorted phase of the α_2 [10] which could lead to the the cracking noticed. It has been shown by TEM [10] that the orthorhombic phase that precipitates from α_2 on addition

of hydrogen at the α_2/β interfaces [10], lending further support to the explanation for the cracking process on hydrogenation.

The hydrides that form on thermally charging hydrogen at high temperatures are different from that which are obtained on room temperature hydrogenation by cathodic charging. Shih et al [37] thermally charged Ti-24Al-11Nb between 500-1050^{o}C and found that small hydride platelets (40-100 nm in size) precipitated in the α_2 phase. These hydrides were stable on heating up to 500^{o}C but dissociated at 700^{o}C restoring the original microstructure on out gassing. Based on their TEM work, they indicated that the hydride did not correspond to any of the known stated titanium hydrides and that it could be of the type Ti_3AlH_x. However, they noted that this hydride phase was a orthorhombic distortion from the α_2 phase and that its habit plane was the basal plane in Ti_3Al and the prism plane in Ti-24Al-11Nb. In order to understand the hydride formation reported by Shih and co-workers, Guo et al [42] thermally charged hydrogen at 500^{o}C for 6 h in Ti-24Al-11Nb that had been solutionized at 1150^{o}C for 1 h in vacuum and then aged at 760^{o}C for 1 h in vacuum. They estimated the hydrogen content to be about 2500 wppm after the charging treatment. They observed dense oriented hydrides to form in the α_2 matrix and they identified the hydride to be a bct hydride (a= 0.306 nm and c = 0.405 nm) similar to the TiH_2 (a = 0.312 nm and c = 0.418 nm) reported by Jaffe [43]. The hydride was oriented with respect to the α_2 matrix with the (0001) of α_2 parallel to (110) of the hydride and the [11$\bar{2}$0] of α_2 parallel to [001] of the hydride [42]. Guo et al, in a subsequent paper [44], have provided the mechanism for formation of the hydride phase as a displacement and dilation from the Ti_3Al phase. Yang et al [26] have also observed dense hydrides of the type observed by Guo et al [42] after high temperature hydrogen charging of several Ti alloys. Under the optical microscopy, the hydrides appeared acicular in Ti-1100 (α phase alloy) while it appeared feather-like in the case of Ti-6Al-4V ($\alpha+\beta$ alloy). However, they could not resolve the hydride under optical microscope in the case of super-α_2 ($\alpha_2+\beta$ alloy). They could resolve the hydride in the TEM and reported that it was similar to that reported by Guo et al [42]. Hydrides in hydrogen thermally

charged single α_2 phase Ti-24Al-11Nb have also been reported to be plate-like by Chu et al [21]. However, they mention that the hydride phase that forms at high temperatures is the florite γ TiH phase based on XRD study of the hydrided specimens. However, there are several complications in understanding the XRD of hydrided samples of titanium aluminides: the peaks of the hydride superimpose on that matrix peaks and the diffraction intensities from the hydride phase are very low [26, 38]. Moreover, the presence of hydrogen leads to stabilization of additional phases (orthorhombic phase at ambient temperatures [10] and the β phase at high temperatures [26]) and therefore the identification of the TiH phase could be debated. Moreover, the TiH peaks appear very near to the TiH_2 peaks [20].

The increased hardness at the near-surface regions could also result from additional factors like stabilization of additional phases in the presence of hydrogen. It has been reported that the presence of even a small amount of hydrogen (200 ppm) leads to the transformation of of α_2 to an orthorhombic phase, very similar to the O phase [10]. It is still to be resolved whether the orthorhombic artifact is a hydride or related in some manner to the Nb rich O phase [10]. It has been proposed that hydrogen segregation to the α_2/β interface alters the stability of the α_2 phase with respect to the O phase such that a *martensitic* transformation to the O structure occurs [10]. It is interesting to note that Shih et al [37] have also reported the formation of a hydride Ti_3AlH_x in a hydrogenated Ti-24Al-11Nb intermetallic which they indicated was definitely different from any of the three titanium hydride phases previously determined (i.e. fct γ with c/a>1, fcc δ and fct ε with c/a<1). They did not determine the crystal structure of this hydride but they reported it to posses an orthogonal distortion of the hexagonal structure. Based on these two studies, it can be stated that the presence of hydrogen results in the stabilization/formation of additional phases and the propensity for these processes would be greater near the surface regions as the hydrogen concentration is greater and the stresses generated due to the phase transformations can be accommodated easily near the surface regions because of relief of

transformation stresses due to the presence of the free surface. In such a case, the microhardness would be higher at the surface regions than the interior. Such a surface hardened layer in the presence of hydrogen has also been reported in the commercially available super alpha-2 alloy (Ti-14Al-20Nb-3V-2Mo, wt %) by Blank-Bewersdorff and Peters [38]. They also have noted that the hardness of the alloy charged with hydrogen increased from 403 $HV_{0.5}$ to 510 $HV_{0.5}$ after hydrogenation for 1 h at 700°C (corresponding to a concentration of 33.8 at. % hydrogen). They also noted that the mechanism of formation of the hardened layer was unclear and it is quite likely that this could have occurred due to stabilization of the orthorhombic "hydride".

In case it is assumed that the higher hardness obtained in the near-surface regions of the intermetallics after hydrogen charging could be due to hydride formation or stabilization of additional phase in the presence of hydrogen, some additional points can be discussed in this light. The hardness of intermetallic A is similar to that of intermetallic B in the near-surface region after 24 hour hydrogen charging (Figures 19 and 20). The drop in the hardness towards the center is more drastic in the case of the intermetallic A compared to B indicating that the concentration of the phase (α_2), from which the hydride precipitates or the new phase is stabilized in the presence of hydrogen is present in larger concentration in intermetallic A. The α_2 phase is present in larger concentration in the intermetallic with lower Nb (i.e. A). Therefore, as the intermetallic A contains a higher volume fraction of the α_2 phase compared to the intermetallic B, a higher amount of hydride/stabilized O phase can form.

It appears likely that the first process (i.e. dissolution of hydrogen in the β matrix) would be the important factor determining the increase in the hardness at both the surface and the center of the specimens as it is noted that there is a relatively large increase in the hardness of the charged specimen in the intermetallic B which contains a higher amount of the β phase compared to the intermetallic A. As regards the increase in hardness in the surface regions of the specimens, the increase

could be additionally due to precipitation of hydrides or stabilization of orthorhombic phase from the α_2 and O phases.

The microstructures of these hydrogen charged intermetallics are shown Figure 21. It was observed in the SEM that there was no visible change in the microstructure after hydrogen charging. Similar findings have also been reported by Blank-Bewersdorff and Peters [38] who state that the microstructure by optical microscopy showed no significant deviation from the annealed state for a super-alpha2 alloy. A similar result has also been reported by Yang et. al. [26] for the case of titanium aluminide super-α_2 where there was no change in microstructure under low magnification whereas Ti-1100 (α alloy) and Ti-6Al-4V ($\alpha+\beta$ alloy) showed dense, feather-like hydrides even under optical microscopy. It has earlier been reported that the presence of hydrides in titanium aluminides is revealed in scanning electron microscopy by characteristic surface releifs on surfaces of polished (unetched) specimens [21]. However, these surface reliefs were not observed in the present study for both the intermetallics. It is for certain that the terminal solid solubility of hydrogen must have been exceeded due to the long charging time employed and therefore it implies that hydrides would have formed and this must have occurred on a microscopic scale, far too small to be resolved by SEM. All the earlier studies on hydride formation in $\alpha_2+\beta$ titanium aluminides have utilized the TEM for identifying hydride platelets in the α_2 matrix. Therefore, the presence of hydrides can be best studied by transmission electron microscopy as several investigators have shown in earlier studies on hydride formation in titanium aluminides [26,37,42,44]. The hydrides that form in titanium aluminide can be resolved only at much higher magnifications and therefore the TEM is best suited for proving its presence. Unfortunately, the microstructures could not be studied by TEM and therefore no direct conclusions can be drawn regarding hydride formation in these intermetallics although several indirect evidences are available, which would discussed in the section on baking experiments of the charged intermetallics.

In order to determine if hydrides did form in these

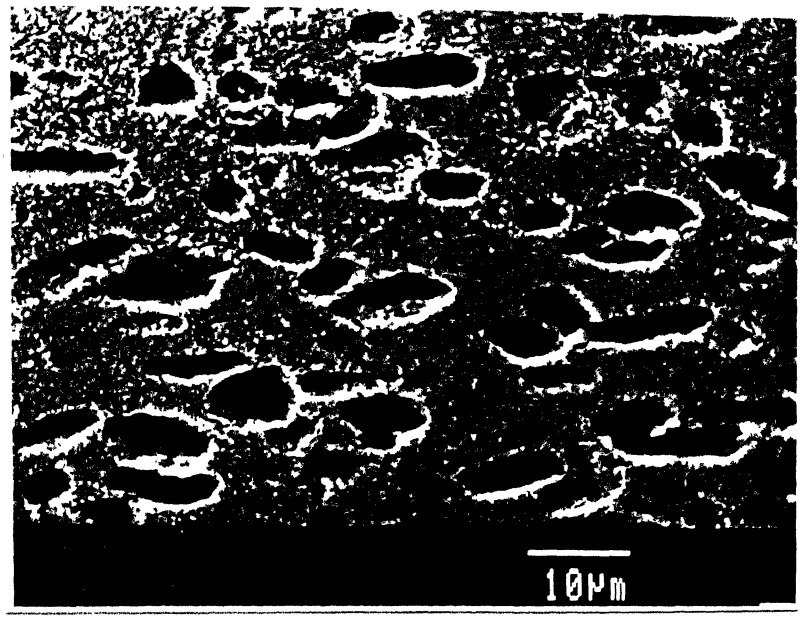

(a)

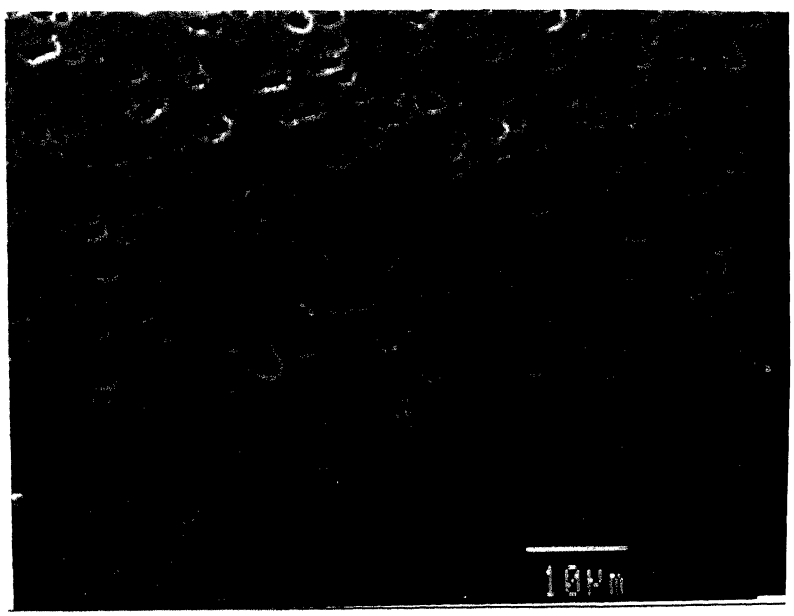

(b)

Fig 21 SEM micrographs of the intermetallics (a) A and (b) B after hydrogen charging for 24 hours.

intermetallics, XRD patterns were obtained from the freshly hydrogen charged (24 h) specimens. It must be noted that there are two problems in identifying the presence of titanium hydrides in titanium aluminindes by the XRD technique. First, it is possible that due to their small size, the hydride precipitates do not exhibit sufficient long range atomic structure required for detection by XRD. Secondly, the major diffraction peaks due to the reported Ti hydrides [28] are almost isomorphous with the α_2 peaks and differentiation becomes a difficulty (Table 3). These extra spots due to the hydride is observed in the TEM to be about only 2 degrees apart from the matrix (α_2) spot [26,37,42,44]. Therefore, the above two factors hinder the unambiguous identification of the presence of hydrides in hydrogen charged titanium aluminides by the XRD technique.

The diffraction patterns for the reference specimens and the 24 hour hydrogen charged specimens are provided in Figures 17 and 18 for intermetallics A and B, respectively. The uncharged intermetallic A exhibits diffraction peaks corresponding to both the α_2 and O phases whereas most of the peaks in the uncharged intermetallic B corresponded to that of the O phase with some minor peaks corresponding to the α_2 phase. It is to be noted that distinct additional peaks do not arise after hydrogen charging which might indicate that hydrides of Ti (and also Nb) did not form in these intermetallics. However, this cannot be concluded unambiguously because the significant peaks of titanium hydride TiH_2 (in case this is the hydride that forms in the system, which is very unlikely) and the Ti_3Al phases nearly coincide with each other (Table 3). The peaks of TiH_2 and TiH overlap on major peaks of α_2/O phase(Table 3) and therefore the presence of these phases cannot be conclusively proved just by XRD studies. Moreover, as noted earlier, the hydride would most likely be of a ternary hydride present in the α_2/O phase [22]. The diffraction peaks from this hydride is also expected to be very weak as it is likely to be present in small amounts and also its peaks would overlap on the peaks of the α_2/O phase. The XRD patterns that are presented in Figures 17 and 18 were taken at a scan rate of 3 degree per minute. Therefore, several scans were performed through the angles

where the significant peaks of TiH and TiH_2 were expected (34 to 38, 58 to 62 and 70 to 73 degrees) with the scanning speed reduced to 0.6 degree per minute for obtaining more counts in these regions. The first observation that was noted is that diffraction peaks corresponding to the TiH_2/TiH phase does not appear and therefore this proves that the hydrides that form in these intermetallics on room temperature hydrogen charging must be of the ternary type, as has been observed in titanium aluminides charged with hydrogen at room temperature [22,37]. Secondly, it is observed that the peaks showed a broadening thereby indicating the expansion of the lattices due to the presence of hydrogen. The intensity of the α_2 peak in the intermetallic A showed a decrease on hydrogenation thereby indicating the possible conversion of a part of the α_2 phase to the O phase in presence of hydrogen [10]. In the case of intermetallic B, there was broadening of the peaks and a simultaneous decrease in the intensity of the peaks on hydrogenation, indicating the dilation caused by the presence of hydrogen. Additional peaks corresponding to the hydride TiH_2/TiH were missing also in intermetallic B. However, as the hardness of the intermetallic B is also higher in the near surface region compared to the interior, this could imply the formation of ternary hydrides from the O phase upon room temperature hydrogenation, similar to hydride formation from the α_2 phase.

It was earlier seen that the hardness remains constant up to a certain distance from the front and back faces of the intermetallics. The near-surface hardness of the back face side is lower than that of front face side (Figures 19 and 20). This behavior is due to the varying amount of hydrogen liberated on the front face and back face side during the cathodic polarization. The solution resistance would be higher near the back side of the specimen and this would result in a lower hydrogen overpotential on this surface. Therefore, the concentration of surface hydrogen on the front face side (i.e. facing the counter electrode) is higher than that on back face side and this results in the observed behavior.

The plot of the depth as a function of charging time is presented in Figure 22 which shows that the parabolic growth law is obeyed for the growth of the surface hardened layer for both the intermetallics A and B. From the slopes of the curves in Figure 22, the value of k_p for intermetallics A and B are 2.5×10^{-9} and 4.8×10^{-9} cm^2/sec, respectively. The obedience to parabolic growth kinetics indicates that the surface hardened layer progresses into the material in a parabolic fashion which is indicative of diffusion-controlled growth. The similarity between the growth of this layer can be compared with that of the internally oxidized zone in internal oxidation where a similar behavior is generally observed [72]. This indicates that the surface hardened layer is composed of ternary hydrides in addition to hydrogen in solid solution. It is likely that at the progress of this front is dependent on the amount of hydrogen that reaches the zone front. Diffusivity of hydrogen in titanium aluminides have not been measured as yet. However, the parabolic rate constant for the layer growth must be proportional to the permeability of hydrogen (i.e. diffusivity) and inversely proportional to the concentration of the hydriding phase, similar to that in the case of internal oxidation where the parabolic rate constant for the growth of the internal oxidation zone is proportional to the permeability of oxygen and inversely proportional to the concentration of the oxidizing element that results in internal oxidation [72]. Therefore, the k_p can be expressed as

$$k_p = \frac{A\, N_H D_H}{N_X}$$

where A is the proportional constant, $N_H D_H$ is the permeability of hydrogen and N_X the concentration of the hydriding species. If it is assumed that the α_2/O phase that hydrides in A and the O phase in B, then theoretical ratio of $(k_p)_A/(k_p)_B$ should be equal to $(N_X)_B/(N_X)_A = 0.33$ since $(N_X)_A$ is 0.21 and $(N_X)_B$ is 0.07 (i.e. the volume fraction of the hydriding phase in the microstructure). The estimated ratio of $(k_p)_A/(k_p)_B$ is 0.53, thereby indicating that

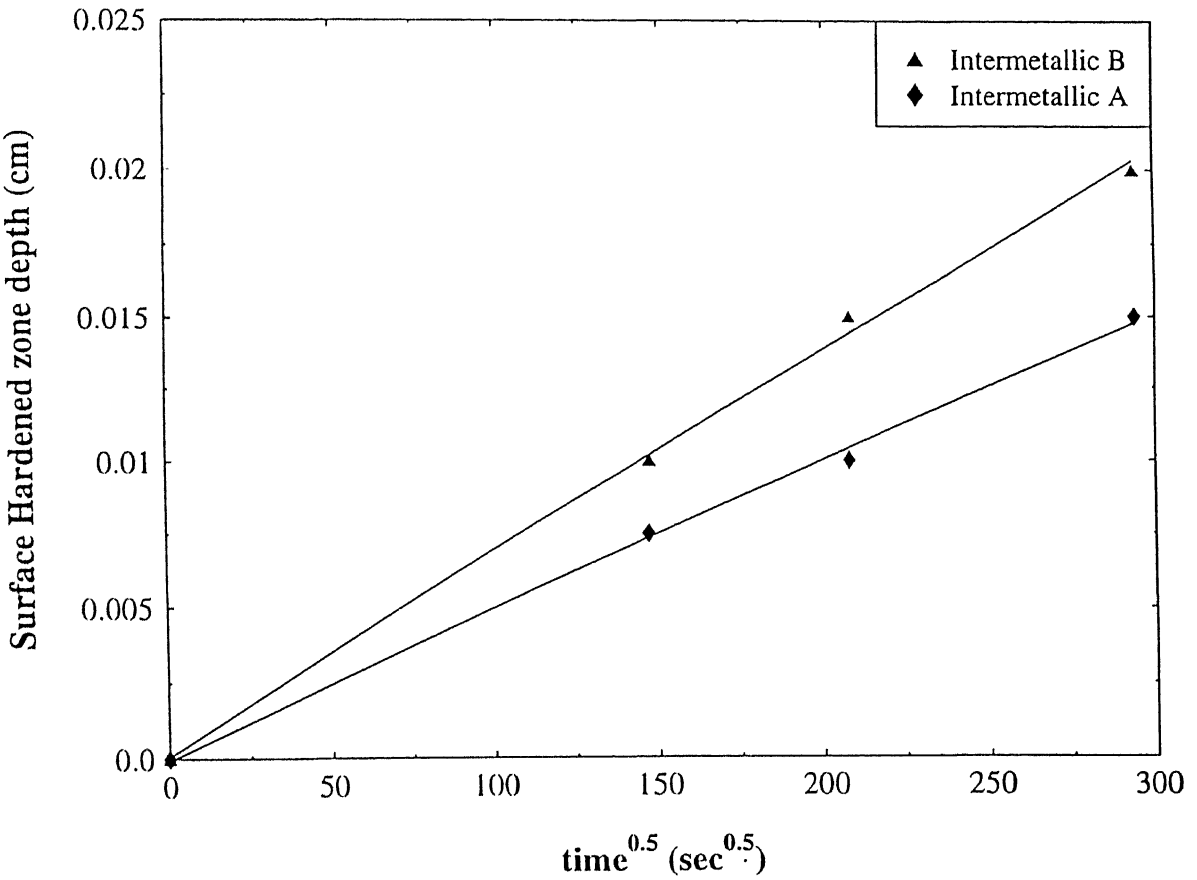

Fig 22 Variation of the surface hardened layer in intermetallics A and B as a function of hydrogen charging time showing parabolic growth nature.

the surface hardened layer corresponds to the internally hydrided region.

Therefore, based on the k_p for growth of the surface hardened layer, it can be reasonably concluded that the growth of the surface hardened layer in intermetallic A is lower than that in intermetallic B, assuming similar hydrogen permeabilities in both the intermetallics. The reasons for this could be the higher volume fraction of the α_2/O phase in sample A which act as blocking sites for permeability of hydrogen. Moreover, the lower k_p also indicates that the concentration of the hydriding phase (α_2/O) in sample A is higher than in sample B, as is known from the analysis of the microstructures (Figure 16). However, a major difference between internal oxidation should be noted in that unlike the oxygen concentration which is zero at the zone front, the concentration of hydrogen at the hydriding zone front is not zero but is finite. This is reflected by the fact that the hardness of the central portion also increases with increasing charging time. The hardness increase in the central zone could be both due to hydrogen in solid solution or precipitation of ternary hydride of lower hydrogen content (as Rudman et al [22] have observed) with the hydrogen reaching the central regions by short circuit paths (i.e the defects in the β phase or the $\alpha_2(O)/\beta$ interfaces).

Moreover, it is seen that the hardness in the central regions increases with increasing charging time indicating that this results due to enhanced presence of hydrogen in the intermetallics. Hydrogen can exist in the central portion either in solid solution or in the form of hydrides. However, it must be pointed out that the concentration of hydrogen in the central portions could be higher due to short diffusion path, for example through the defects in the β phase or through the interfaces between the β and α_2/O phases. In order to ascertain the presence of hydrides in the central region, baking experiments were conducted on the hydrogen charged specimens and this is discussed

below.

4.6 EFFECT OF BAKING

It was seen in the earlier section that the presence of hydrogen in the intermetallics leads to an increase in the hardness in both the near-surface and central regions of the intermetallics. The possible reasons for the increase in hardness in the presence of hydrogen was attributed to three causes: (i) dissolution of hydrogen (which should be primarily in the β matrix as it has a higher solubility for hydrogen than the α_2/O matrices), (ii) hydride formation from the α_2/O phases present in the microstructures, and (iii) stabilization of the orthorhombic phase in the presence of hydrogen from the α_2 phase (in intermetallic A). All these above processes would result in increase in the hardness over the base uncharged intermetallics. In order to understand the effect of hydrogen in causing these changes, it was decided to conduct baking experiments at different temperatures for varying amounts of time on the hydrogen charged and the reference as-received intermetallics. The baking experiments were also performed on the as-received intermetallics in order to understand the effect of exposure of these intermetallics at the baking temperatures on the microstructure (and hence the hardness) so that the effect of the microstructural changes can be excluded while analyzing the effects of hydrogen. The baking temperatures were chosen based on the published decomposition temperature of the ternary titanium aluminide Ti_3AlH_x (x=0.35 and 1.6) by Rudman et al [23]. This would be more appropriate than considering the decomposition temperature of the hydride TiH_2 as the hydride that form on room temperature hydrogenation is not this hydride. At atmospheric pressures, the TiH_2 hydride decomposes at around 760^{o}C [28] which is obtained from the relation of the decomposition pressure as a function of temperature given as [28]

$$\log p_{H_2}(Ti) = -6679/T + 9.35$$

The dissociation pressure is higher in the titanium aluminide due to blocking of sites due to the presence of Al [23]. The relation

between the dissociation pressure in Ti_3Al and in α-Ti is provided by Rudman et al [23] as follows:

$$p_{H_2}(Ti_3Al) \; / \; p_{H_2}(\alpha\text{-}Ti) = [\; (2-x)/(0.25-x) \;]^2$$

where x is the interstitial site per metal atom (=0.25 for Ti_3Al). In the limit of $x \rightarrow 0$, this ratio is 64/1. Therefore,

$$\log \; [\; p_{H_2}(Ti_3Al) \; / \; 64 \;] = \; -6679/T + 9.35$$

Using the above relation, the decomposition temperature at 1 atm pressure of the ternary hydrides in α_2 (and approximately in also O) can be estimated to be 597°C. It is interesting at this juncture to note that the hydrides that were created by Shih et al after gaseous hydrogen charging of Ti-24Al-11Nb were stable upon heating at 500°C and dissociated only at 700°C [37], thereby indicating that the ternary hydrides in the titanium aluminide system are stable only to a lower temperatures compared to TiH_2.

Therefore, if baking is performed at a temperature above the hydride decomposition temperature, it should result in the decomposition of the hydride which would indirectly be indicated as a decrease in the hardness after the baking experiment. On the other hand, if the baking is performed at a temperature lower than this temperature, the hydrides should not decompose and hardness would remain the same in case hydride formation is the reason for the increase in hardness in the first place. In case the hardness decreases after the lower temperature baking treatment, it would imply that the hydrogen that is held in the intermetallics in solid solution is released indicating that hydrogen is present in the materials in solid solution. However, the situation is not as simple as outlined above due to the following two reasons: (i) hydrogen is a β stabilizer and its presence, say from the decomposition of the hydride phase, would lead to stabilization of the β phase and (ii) the growth of the precipitated α_2 and O phases would occur at higher temperatures. Moreover, it is also not known if the reversion of the stabilized O phase to the α_2 structure does or does not occur in the absence of hydrogen. In case the absence of hydrogen results in the reversion of the O phase to the α_2 phase, then it can also be anticipated that

lowering of the hardness should occur at both the lower and higher temperatures. However, in spite of these complications, the baking experiments are useful experiments to elucidate the role of hydrogen in causing the microhardness changes.

Two baking temperatures were chosen for the baking experiments : 400^{o}C (below the decomposition temperature) and 800^{o}C (above the decomposition temperature). The time of baking at these temperatures were determined using the published diffusivity of values of hydrogen in α-Ti [28]. The time that it would take to diffuse out of from the center of the specimen of thickness 1 mm was calculated from the diffusivity equation. It was estimated that hydrogen should diffuse out of the intermetallics in 10 minutes at 800^{o}C and in 90 minutes at 400^{o}C. Therefore, the intermetallics that had been initially charged for different times (24 h, 12 h and 6 h) were baked at these temperatures for these times. The environment used for these experiments was laboratory air. It is known that the oxides on these intermetallics do not completely cover the surface even at the higher temperature (800^{o}C) for the time studied [2]. Therefore, there would have been no surface oxide to hinder the release of hydrogen. Moreover, it has been found that the oxide (rutile TiO_2) that form on the surface of α-Ti are permeable for hydrogen at 500^{o}C [28] and the major constituent of the oxides on these titanium aluminides is TiO_2 (to be discussed in later section).

4.6.1. BAKING AT 800^{o}C

The hardness profiles after the 800^{o}C baking treatment for the intermetallics A and B initially charged for 24, 12 and 6 hours are provided in Figures 23 and 24, respectively. The nature of the hardness profiles are similar to that obtained after hydrogen charging. However, there is a relative decrease in the near-surface and central region hardness compared to the hydrogen charged specimens. The hardness data obtained from the surface and central plateau regions of the specimens are tabulated in Table 6. In order to understand the effect of exposure of the intermetallics (not containing hydrogen) at this temperature, the intermetallics were heat treated at 800^{o}C for 10 minutes and the

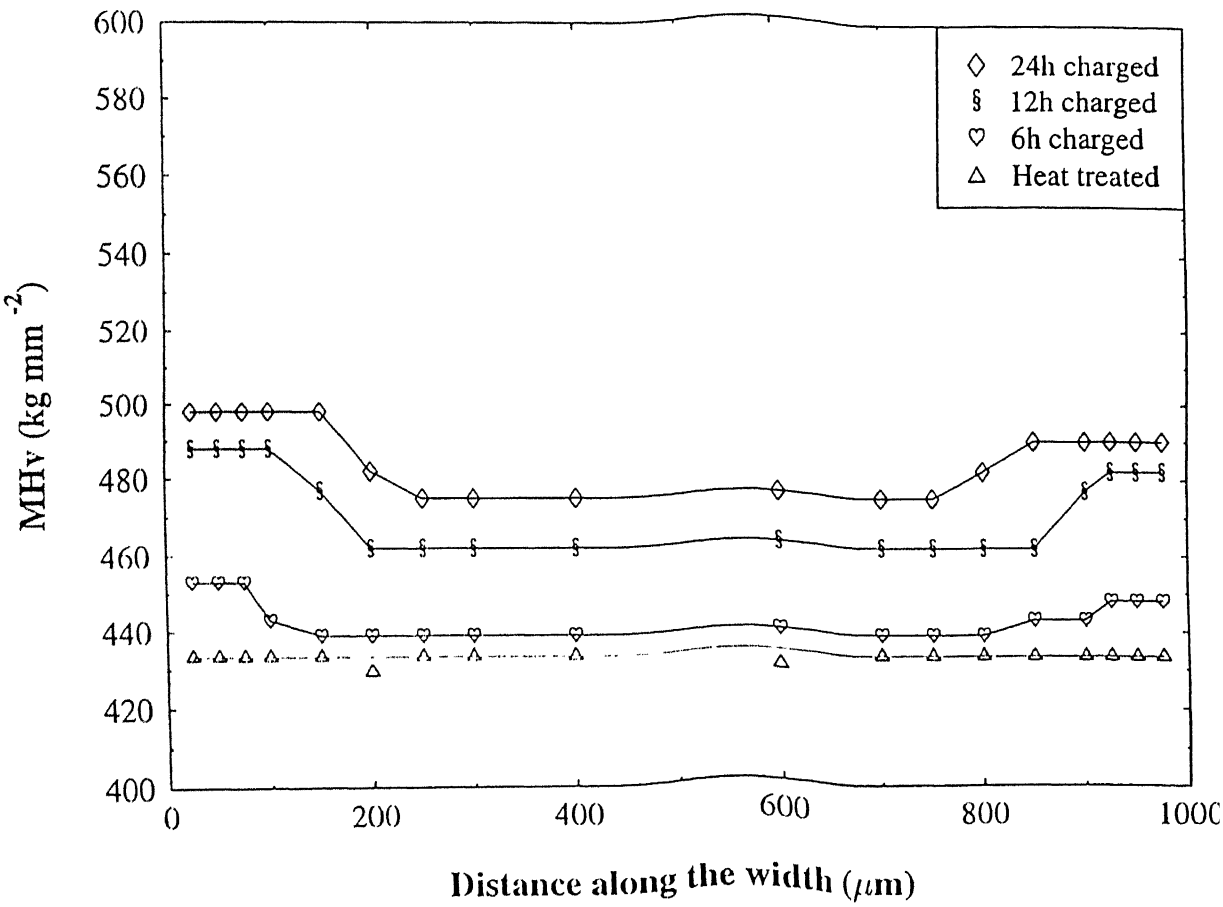

Fig 23 Microhardness profiles for intermetallic A for the following conditions: baked at 800°C for 10 minutes after 24 hour, 12 hour and 6 hour hydrogen charging and heat treatedat 800°C for 10 minutes without prior hydrogen charging.

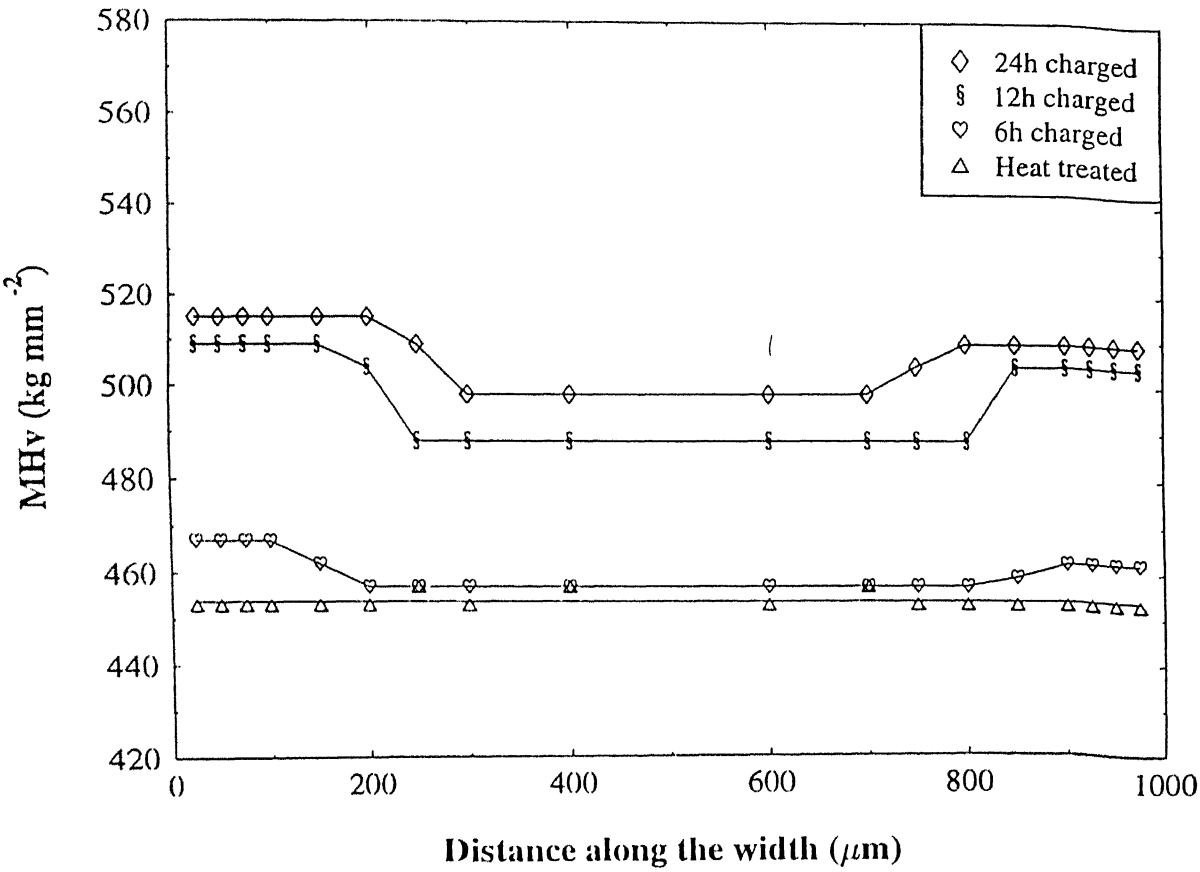

Fig 24 Microhardness profiles for intermetallic B for the following conditions: baked at 800°C for 10 minutes áfter 24 hour, 12 hour and 6 hour hydrogen charging and heat treated at 800°C for 10 minutes without prior hydrogen charging.

microhardness profiles after this treatment are also provided in Figures 23 and 24 for both the intermetallics. There is an increase in the hardness of the as-received intermetallic upon heat treating it at 800°C for 10 minutes. It was revealed by microscopy that coarsening of the precipitates occurred in both the intermetallics and this could possibly explain the increase in hardness of the as-received intermetallics after the high temperature heat treatment. The kinetics of coarsening of the precipitates in titanium aluminides is relatively fast at 800°C [9].

The hardness in the near-surface and central regions decreases for both the intermetallics upon baking at 800°C. This could indicate that hydrogen could either be present in the form of hydrides and/or in solid solution in the intermetallics as the high temperature employed is sufficient for both decomposing the hydride as well as releasing the hydrogen in solid solution. The relative change in the hardness of the central regions indicates that for the 6 h charged specimens, the original hardness is restored indicating that hydrogen is removed whereas the hydrogen is not removed from the surface regions. In the case of the 12 h and 24 h charged specimens, higher hardness are obtained over the reference value in spite of the treatments provided. In order to check if this is due to the short time (10 min) employed for the high temperature heat treatment, the baked specimens were further baked at 800°C for another 23 hours and 50 mins (total 24 hours) and the microhardness profiles again obtained. The reference uncharged specimens were also provided the 24 hour heat treatment. The microhardness profiles obtained for these conditions are provided in Figures 25 and 26, respectively. The surface and central region hardness are tabulated in Table 6, from which it can be noticed that after the 24 hour baking treatment, the relative hardness change is insignificant for the both the surface and central regions indicating that nearly all the hydrogen has been out gassed from these regions in the intermetallics. However, the small relative hardness increase in the surface and bulk regions of the 24 h hydrogen charged specimens of A and B indicates that a small amount of hydrogen still remains in the

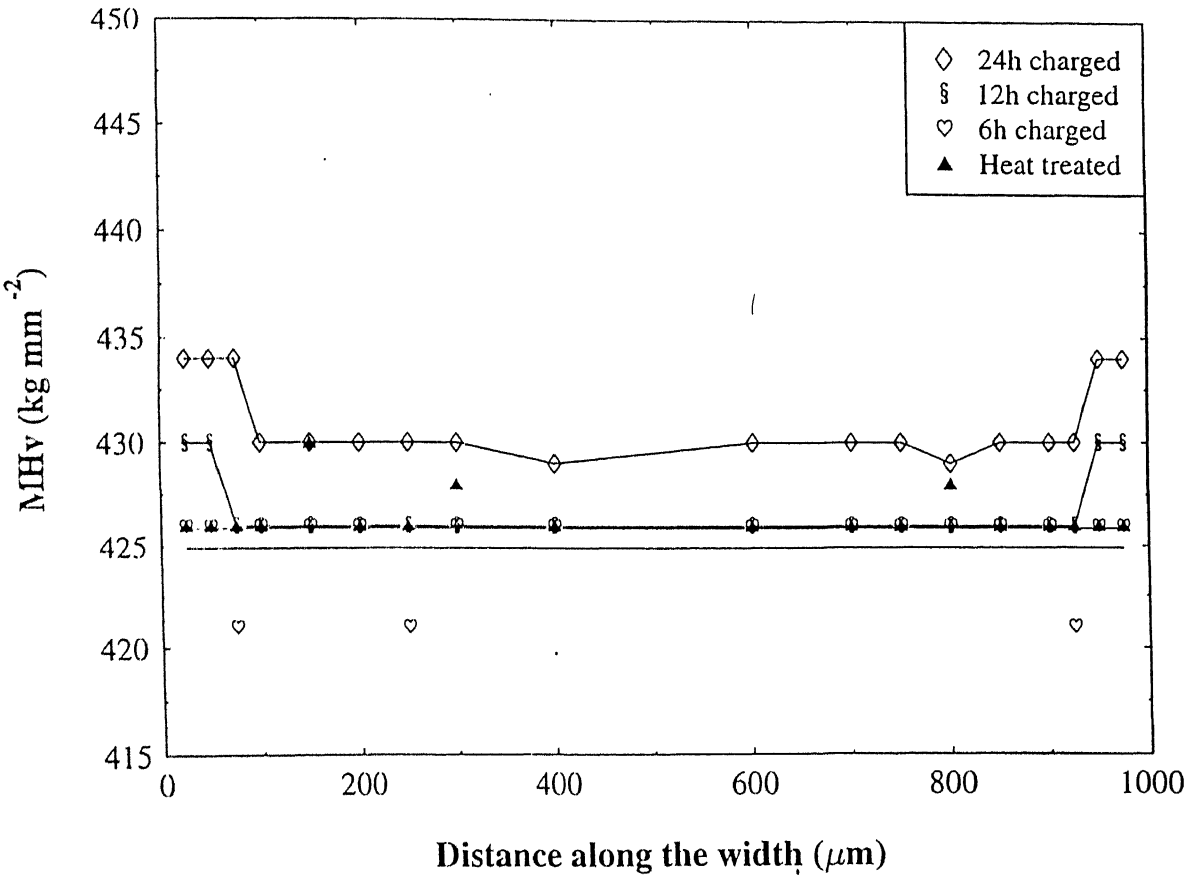

Fig 25 Microhardness profiles for intermetallic A for the following conditions: baked at 800°C for 24 hours after 24 hour, 12 hour and 6 hour hydrogen charging and heat treated at 800°C for 24 hours without prior hydrogen charging.

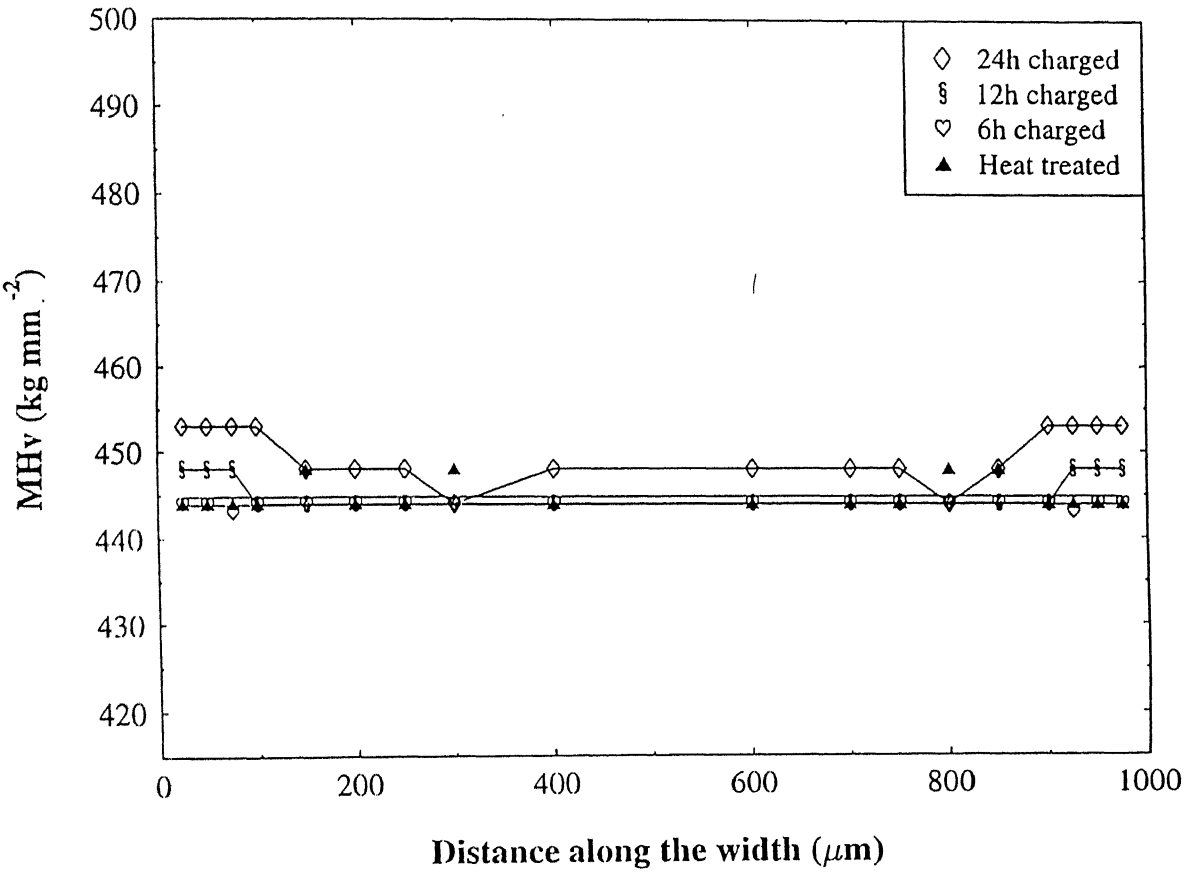

Fig 26 Microhardness profiles for intermetallic B for the following conditions: baked at 800°C for 24 hours after 24 hour, 12 hour and 6 hour hydrogen charging and heat treated at 800°C for 24 hours without prior hydrogen charging.

central and surface regions even after 24 hours of baking at 800°C and this could be the hydrogen in solid solution in the β phase.

The surface hardened layer thickness remains the same after the short time of baking at 800°C (i.e. similar to that observed after the hydrogen charging). This coupled with the fact that the relative hardness change in the central and bulk portions after the short baking time is significant indicates that all the hydrides in these region have not decomposed. The fall in hardness after the 10 min baking treatment could be therefore indicative of out gassing of hydrogen in solution and decomposition of part of the hydride. On increasing the baking time to 24 hours, it is seen that the surface hardened layer is non-existent in the case of the 6 hour hydrogen charged specimen, whereas it has decreased for the 12 h and 24 h charged specimens. The relative change in hardness in the surface region is small for both these cases with the 24 h hydrogen charged specimen showing a slightly higher change. This would imply the presence of hydrogen (either in solid solution or as hydrides) in these samples, with their volume fraction being very small. For the central region, the reference hardness is obtained for the 6 h and 12 h hydrogen charged samples, whereas it is insignificant (1%) for the 24 h charged sample. This would imply that the the hydrides in the central region of the samples have decomposed and the hydrogen in solid solution out gassed after the 24 hour baking treatment.

4.6.2. BAKING AT 400°C

The high temperature baking treatment was performed above the decomposition temperature of the hydride. Therefore, baking experiments were also performed at 400°C, a temperature at which decomposition of the stable TiH_2 (or the ternary hydrides as they anyway transform to the stable TiH_2 hydride above 200°C [22]) is not feasible.

The hardness profiles after the 400°C baking treatment for 90 minutes for the intermetallics A and B initially charged for 24, 12 and 6 hours are provided in Figures 27 and 28, respectively. The nature of the hardness profiles are again similar to that obtained after hydrogen charging (i.e. a surface hardened layer

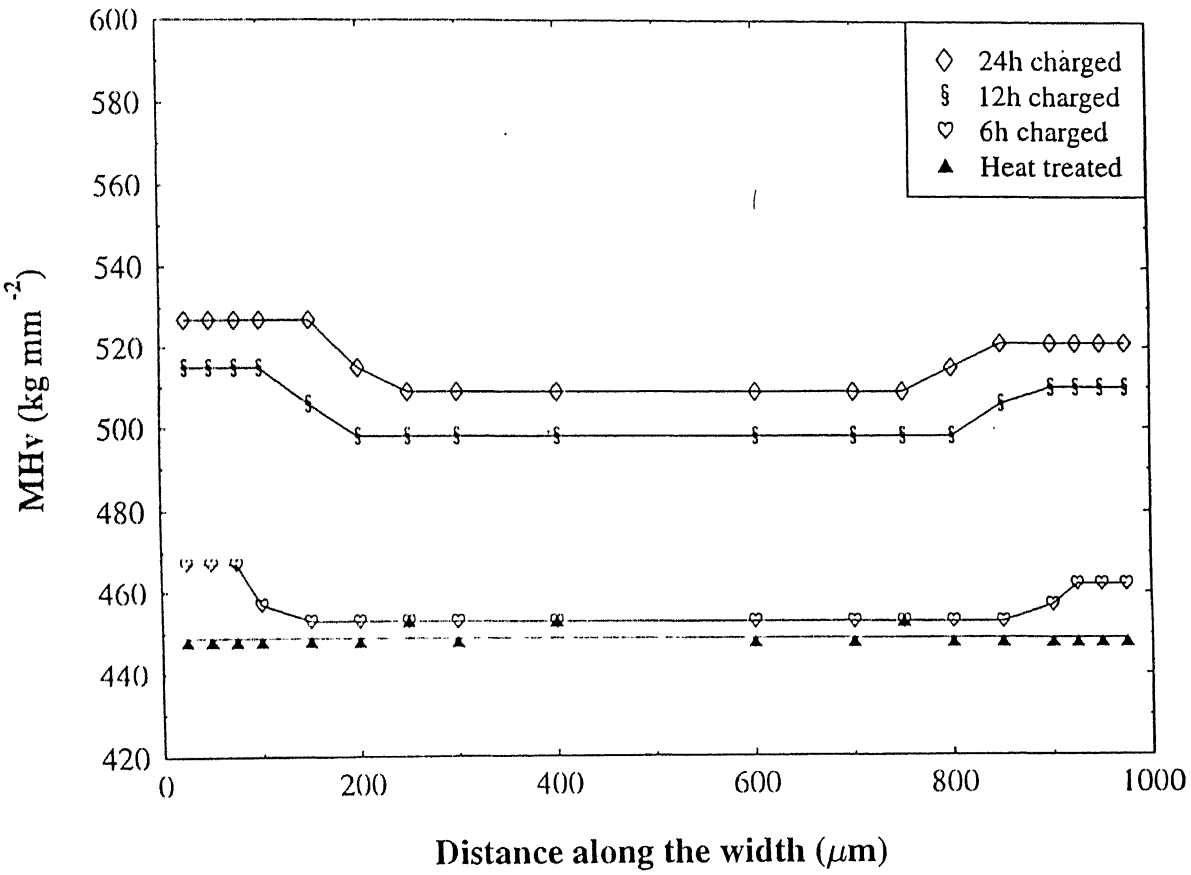

Fig 27 Microhardness profiles for intermetallic A for the following conditions: baked at 400°C for 90 minutes after 24 hour, 12 hour and 6 hour hydrogen charging and heat treated at 400°C for 90 minutes without prior hydrogen charging.

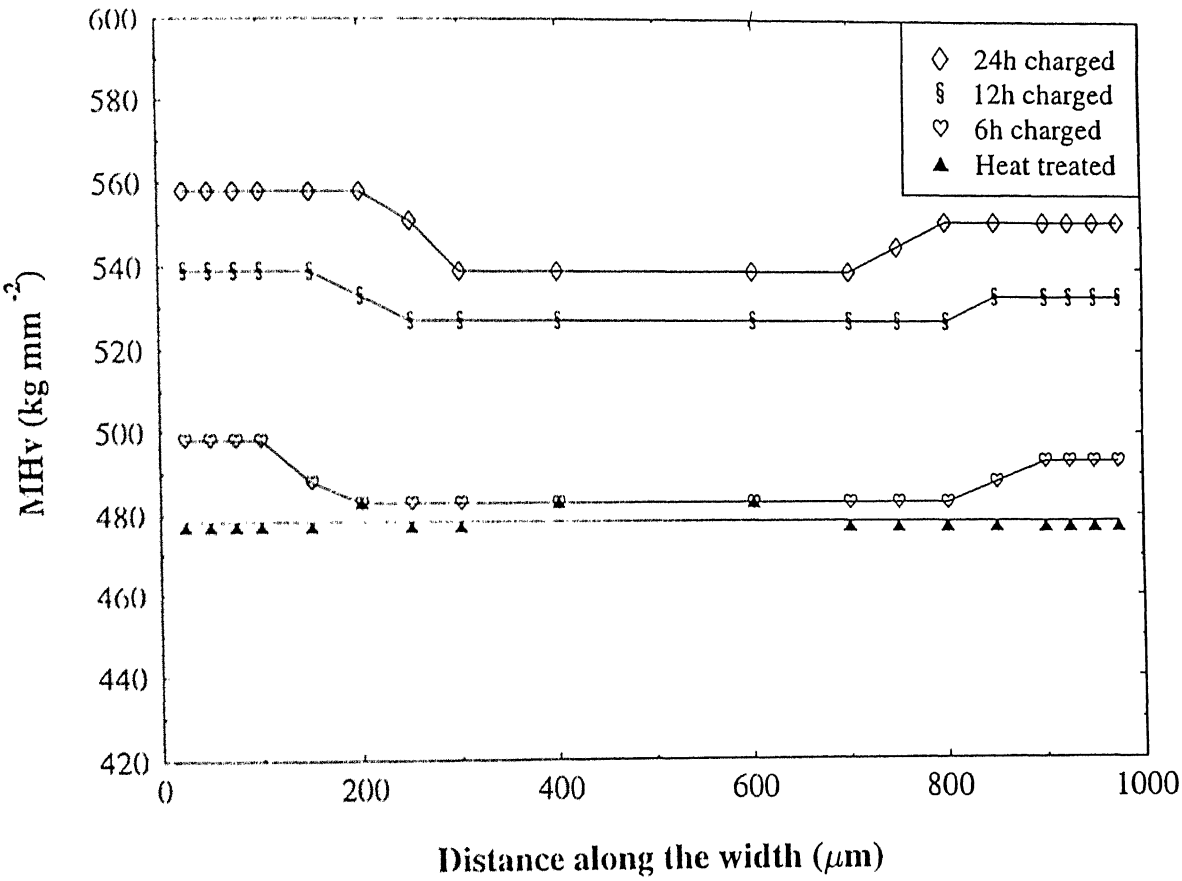

Fig 28 Microhardness profiles for intermetallic B for the following conditions: baked at 400°C for 90 minutes after 24 hour, 12 hour and 6 hour hydrogen charging and heat treated at 400°C for 90 minutes without prior hydrogen charging.

and a central region with a higher hardness than the uncharged condition). There is a relative decrease in the near-surface and central region hardness compared to the hydrogen charged specimens. The hardness data obtained from the surface and central plateau regions of the specimens are tabulated in Table 6. In order to understand the effect of exposure of the intermetallics (not containing hydrogen) at this temperature, the intermetallics were heat treated at 400°C for 90 minutes and the microhardness profiles after this treatment are also provided in Figures 27 and 28 for both the intermetallics. There is an increase in the hardness of the as-received intermetallic upon heat treating it at 400°C for 90 minutes. It was revealed by microscopy that coarsening of the precipitates occurred in both the intermetallics and this could possibly explain the increase in hardness of the as-received intermetallics after the low temperature heat treatment. Possible precipitation of the ω phase cannot also be discounted as it has been reported that the kinetics of precipitation this phase is rapid in super-α_2 alloy in the temperature range of 300 to 500°C, with the maximum rate obtained around 400°C [9]. Transmission electron microscopy should be able to resolve this issue.

The hardness in the near-surface and central regions decreases for both the intermetallics after baking for 90 mins at 400°C. This indicates that a part of hydrogen is held reversibly in solid solution in the surface and central regions of both the intermetallics. It is reasonable to assume that hydrogen is present in solid solution in the β matrix as it has a higher solubility for hydrogen than the other phases (either α_2 or O) [28]. It is also interesting to note that after charging for relatively shorter time (6 h) and then baking the specimen at 400°C, the expected hardness of the intermetallics in the absence of hydrogen is obtained thereby indicating that hydrogen present in solid solution in the central regions of the specimens is responsible for the increase in hardness. However, there is still a noticeable change in hardness at the surface for the 6 h charged specimen, indicating that all the hydrogen has not been out gassed from this region. For the cases of 12 h and 24 h hydrogen charging

experiments, the relative change in hardness is significant (i.e. not zero) indicating that all the hydrogen from the central region have not been removed by the 400°C baking treatment. It is also to be noted that the near-surface hardness after the baking experiment for the hydrogen charged specimens is higher than the expected hardness of the intermetallics in the absence of hydrogen. This observation indicates that in addition to hydrogen being present in solid solution in the near-surface regions, ternary hydrides could be present in the surface regions that have still not decomposed or the titanium hydride resulting from the decomposition of the ternary hydride has not decomposed.

As was seen earlier in the case of baking at 800°C, it was felt that the time provided for the 400°C baking could have been insufficient and therefore, it was decided to bake the specimens for an additional period of 22.5 hours (total 24 hours). The specimens that was charged initially for 24, 12 and 6 hours was baked at 400°C for a total period of 24 hours and the microhardness profiles again obtained. The as-received intermetallics were also provided this heat treatment in order to understand its effect on the microstructure and the hardness. The hardness profiles for these conditions are provided in Figures 29 and 30 for intermetallics A and B, respectively. The results are tabulated in Table 6. For all the charging times (6, 12 and 24 h), both the bulk and surface hardness values of the intermetallics do not revert to the reference values and there is a noticeable relative change in hardness even after the 24 h baking treatment at 400°C. The relative change is apparent for both the bulk and surface regions in both the intermetallics, with the surface region indicating a slightly higher relative change in hardness compared to the inner regions. This indicates that the hydrides that have formed in the material have not decomposed and hence this indirectly proves the existence of hydrides both in the surface and central regions of the hydrogen charged specimens.

Regarding the depth of the surface hardened layer after the 400°C baking, it is seen that this does not show a change for the short 90 min baking time employed and it remains the same as that observed for the hydrogen charged specimens. This behavior is seen

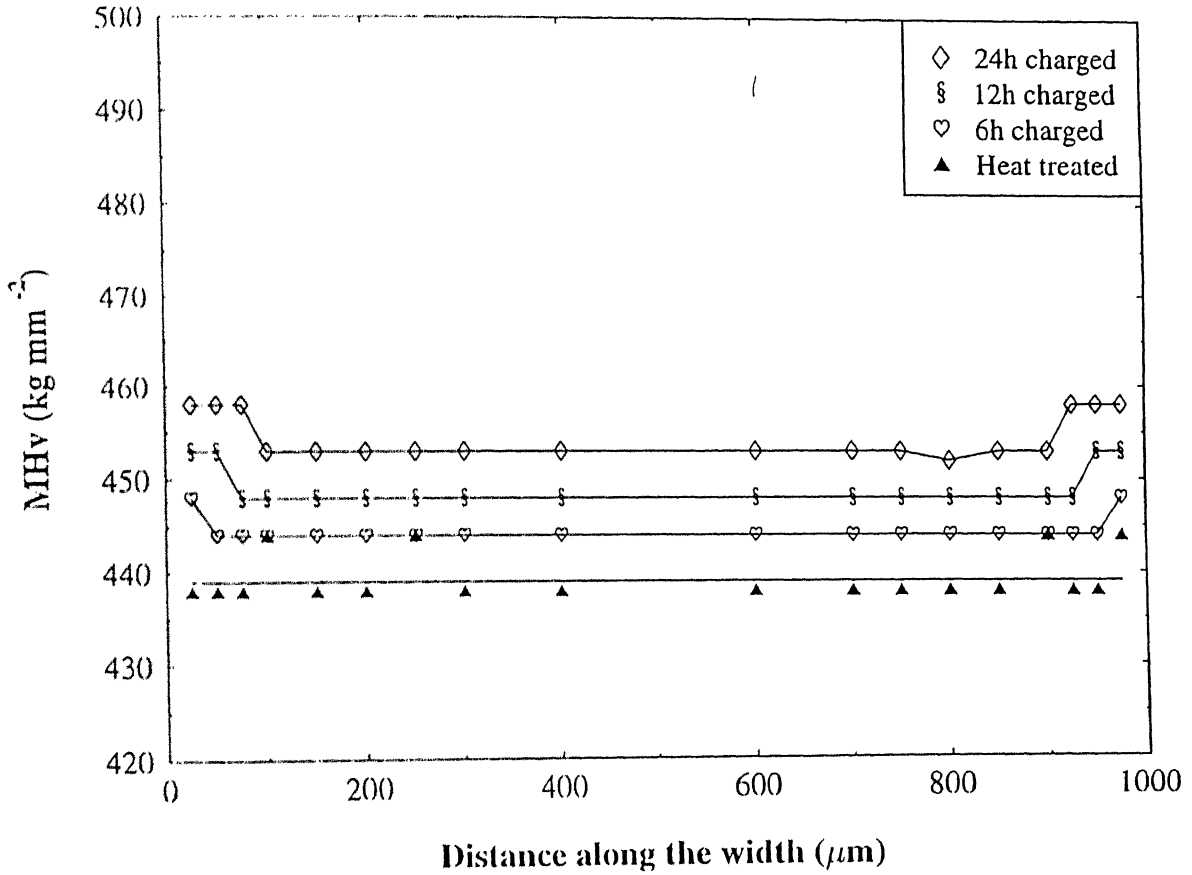

Fig 29 Microhardness profiles for intermetallic A for the following conditions: baked at 400°C for 24 hours after 24 hour, 12 hour and 6 hour hydrogen charging and heat treated at 400°C for 24 hours without prior hydrogen charging.

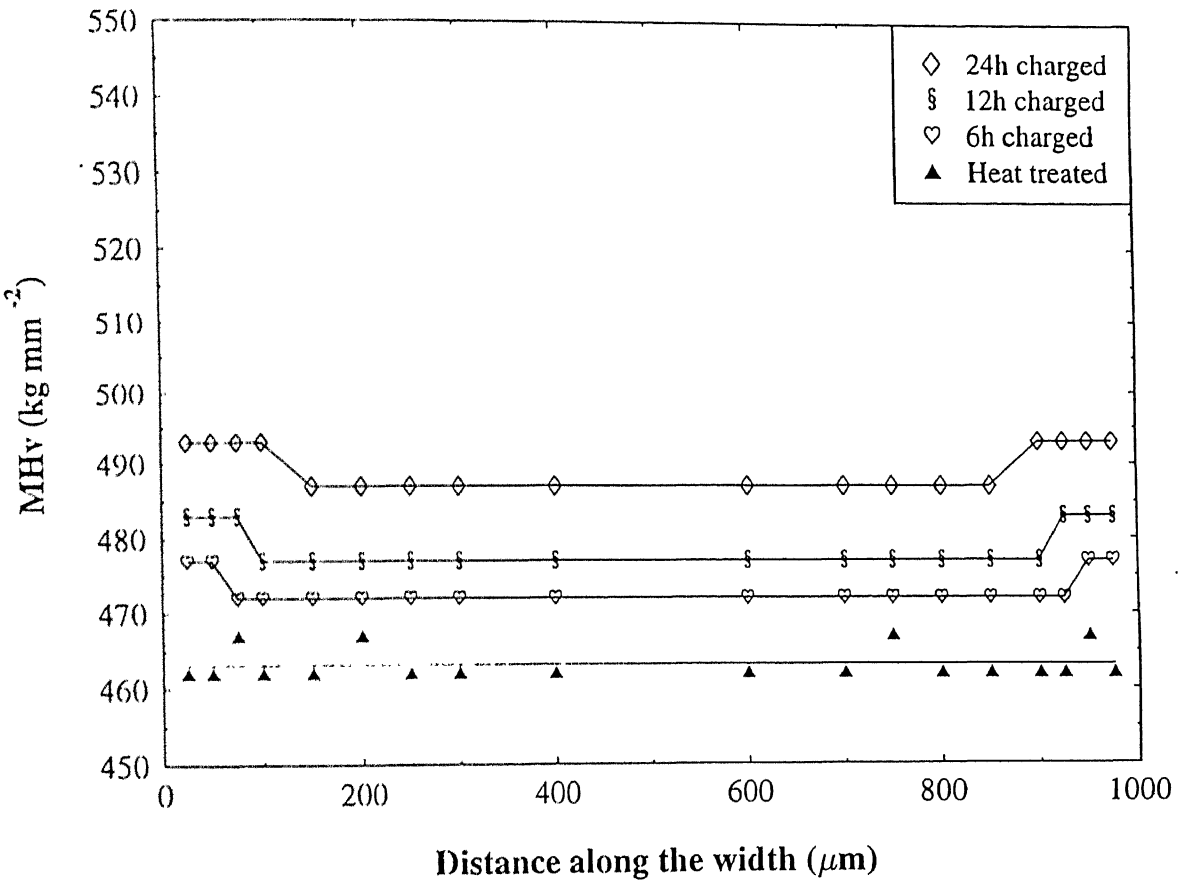

Fig 30 Microhardness profiles for intermetallic B for the following conditions: baked at 400°C for 24 hours after 24 hour, 12 hour and 6 hour hydrogen charging and heat treated at 400°C for 24 hours without prior hydrogen charging.

for both the intermetallics. However, on baking for longer time (24 h), the depth of the zone is clearly reduced to lower values for both the intermetallics. This is indicative of the surface hardened layer being composed of primarily hydrogen in solid solution as there is a decrease in the hardened layer even after baking at 400°C when the hydrides are not expected to decompose.

The XRD patterns taken from the 24 hour hydrogen charged specimen and reference specimen treated at 800°C and 400°C for a total of 24 hours are presented in Figures 31 through 34. It is noted that additional peaks due to the presence of hydrides could not be found in the case of the 400°C baked specimen and the same was also found in the case of the 800°C baked specimens.

For the case of the 800°C baking and heat treatment, the following observations can be made on the XRD patterns. The intermetallic A after baking revealed three prominent peaks of the O phase with the α_2 phase peak that occurred at 36° missing in the baked sample. The intensity of the peaks had also decreased after the baking and heat treatment (Figure 31). The heat treated sample also showed a decrease in the intensity of the peaks. However, additional O phase peaks were observed. Moreover, the α_2 peak occurring around 36° could also be observed. The intermetallic B revealed essentially O phase peaks in the baked and heat treated conditions (Figure 32). Additionally, the O phase peak at 36° had become much more intense while that at 38° showed a decrease in intensity. In the case of the baked sample, some additional peaks that could not be indexed to the O phase were also found. Some of them could be indexed to the β phase. Notice especially the peak that occurs at 40° which clearly shows resolution into two peaks for the baked condition. The smaller of these two peaks corresponds to the β phase. Therefore, it is likely that the presence of hydrogen in solution has stabilized the β phase in the near surface regions such that it is present in larger proportions resulting in the XRD peaks.

For the case of the 400°C baked specimens, the following observations could be made. In the intermetallic A, the peaks were generally less intense than in the uncharged condition (Figure 33), with the heat treatment condition resulting in a greater

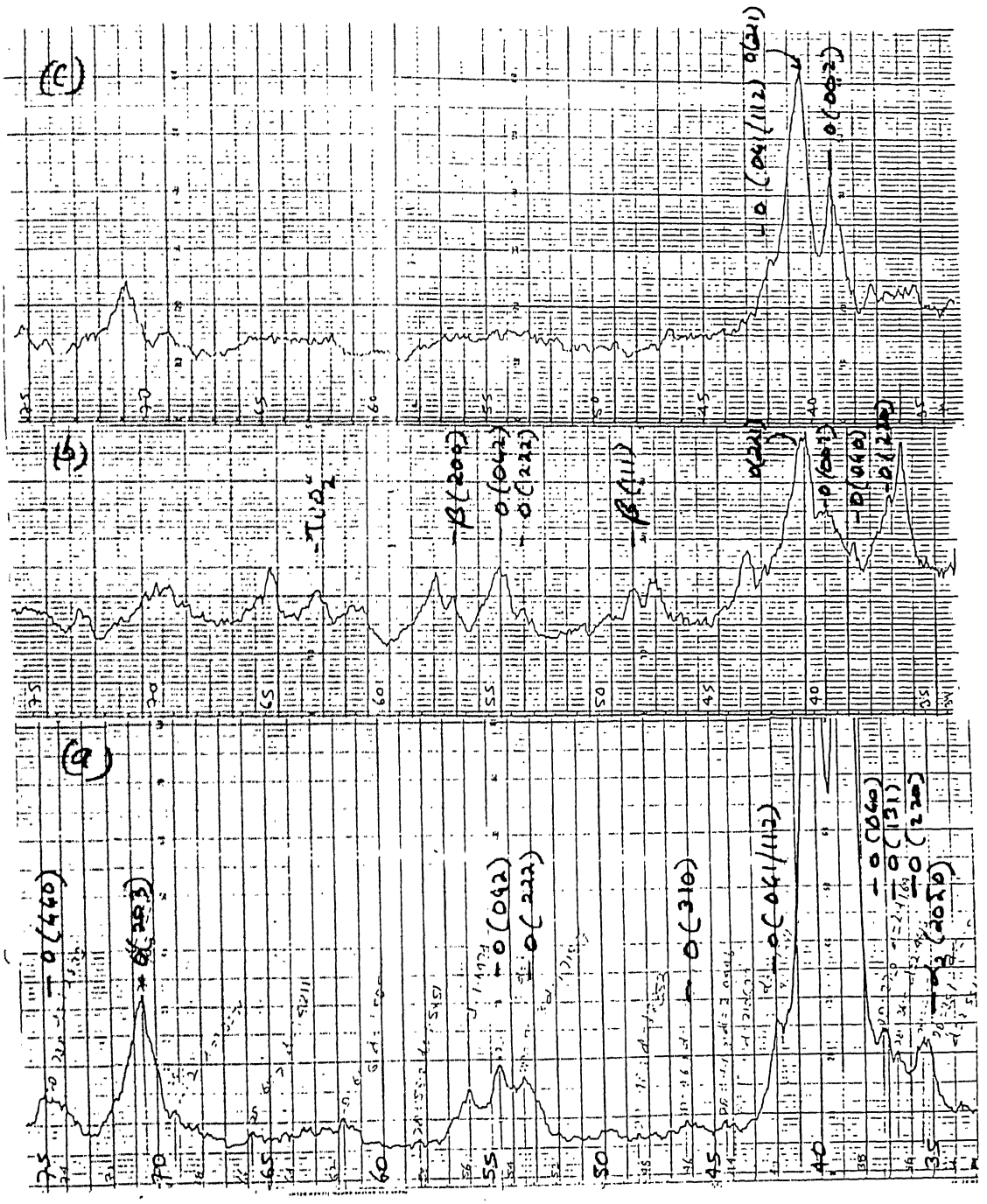

Fig 31 XRD patterns taken at a scan rate of 3^{o}/minute of intermetallic A :(a) uncharged (b) 24 hour hydrogen charged sample baked at 800^{o}C for 24 hours (c) heat treated at 800^{o}C for 24 hours.

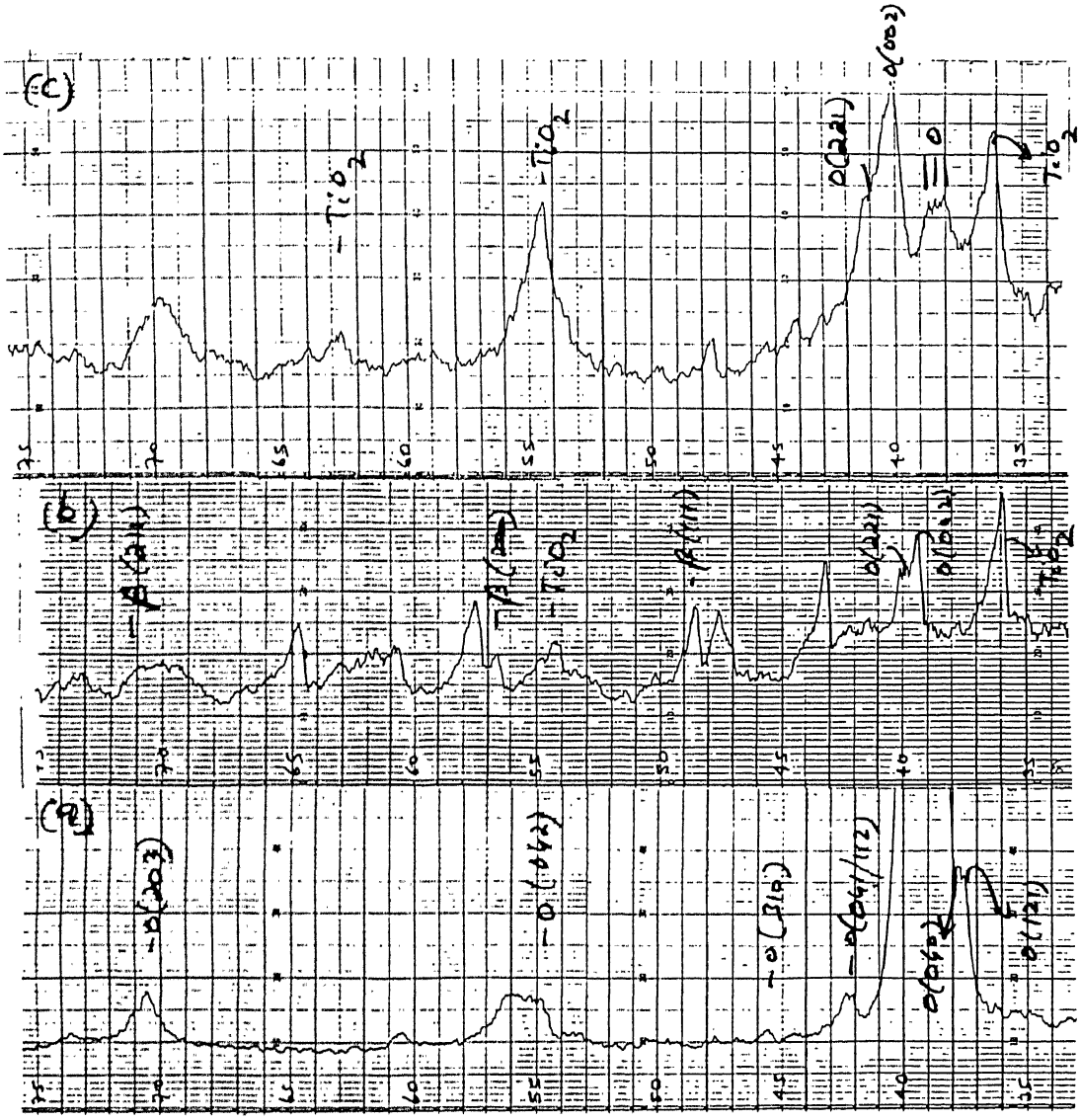

Fig 32 XRD patterns taken at a scan rate of 3^{o}/minute of intermetallic B : (a) uncharged (b) 24 hour hydrogen charged sample baked at 800^{o}C for 24 hours (c) heat treated at 800^{o}C for 24 hours.

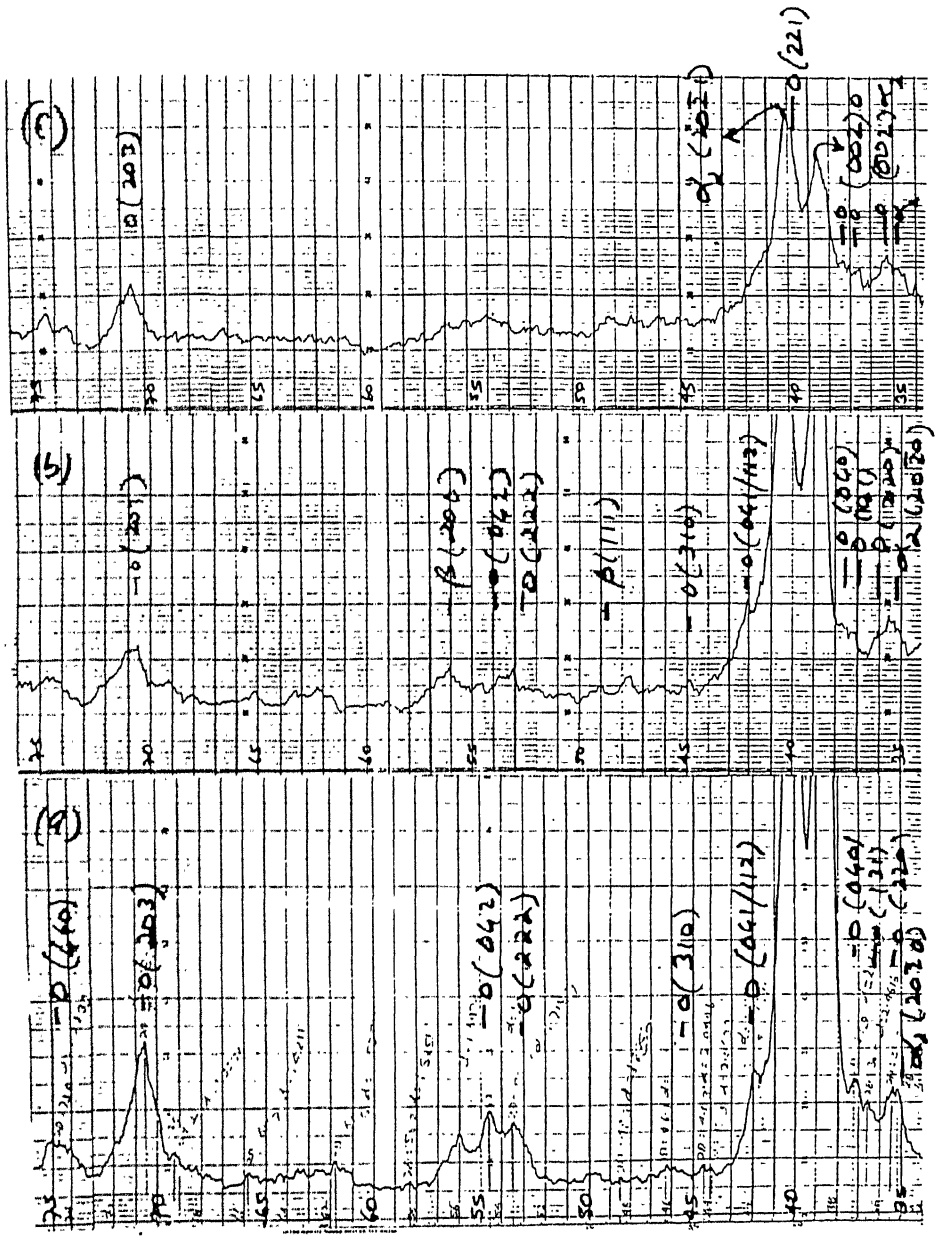

Fig 33 XRD patterns taken at a scan rate of 3^{o}/minute of intermetallic A : (a) uncharged (b) 24 hour hydrogen charged sample baked at 400^{o}C for 24 hours (c) heat treated at 400^{o}C for 24 hours.

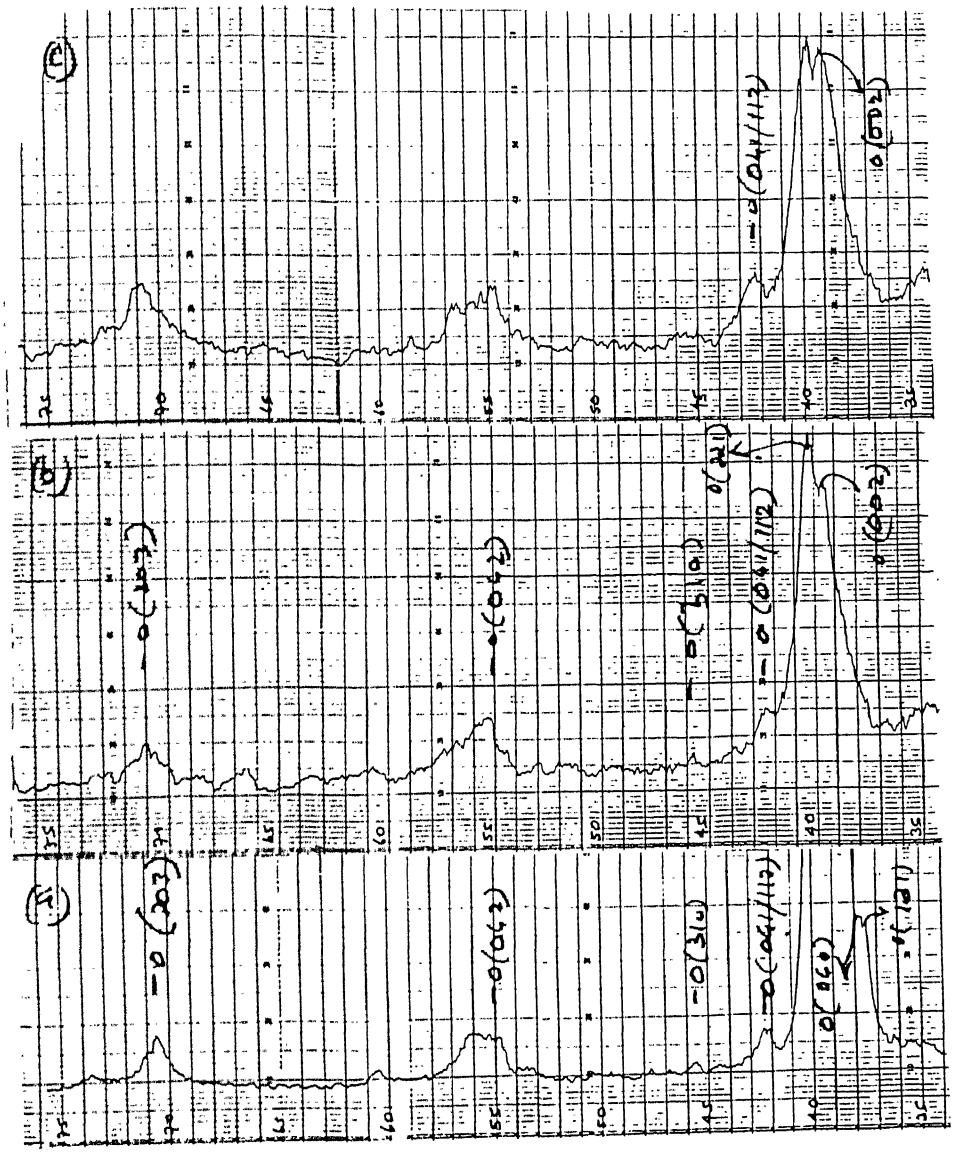

Fig 34 XRD patterns taken at a scan rate of 3^{o}/minute of intermetallic B : (a) uncharged (b) 24 hour hydrogen charged sample baked at 400^{o}C for 24 hours (c) heat treated at 400^{o}C for 24 hours.

decrease in intensity. Additional peaks due to the presence of hydrides (TiH_2) could not be identified. In the intermetallic B, a similar situation obtains (Figure 34).

In order to ascertain whether the hydrogen present in the intermetallics is strongly bound, the samples that were charged with hydrogen for 24 hours and later baked at 400°C and 800°C for 90 and 10 mins, respectively, were baked at room temperature for 1 year and the microhardness profiles again taken. It was observed that there was no change in the microhardness profiles after the fairly long room temperature baking treatment thereby indicating that the hydrogen present in the system is strongly bound. Room temperature baking is not sufficient to bake out the hydrogen.

4.7 SCALING BEHAVIOR DURING ISOTHERMAL OXIDATION

Specimen coupons of both the intermetallics were exposed to 1273 K in laboratory air for different times and the weight gain and surface scale characteristics were noted. The surface scale formed in both the intermetallics were yellow in color on visual observation and in cases where the surface scale had spalled during oxidation or during removal of the specimens from the furnace, the surface appeared grey. In the case of both the intermetallics, the presence of $TiO_2$and Al_2O_3 was clearly indicated. There were additional peaks that did not correspond to either these phases or the matrix peaks and a detailed analysis of the XRD files of the oxides, nitrides and carbides of Ti, Al and Nb was undertaken. XRD peaks of Nb_2O_5 were identified in intermetallics A and B. Some of the peaks from the oxidized sample of A could be identified with the phase $AlNbO_4$. The presence of TiN was indicated in intermetallic A but not in B. The signals from TiN were much more strong after 10 hour oxidation compared to 46 hour oxidation for sample A. This is seen in the XRD patterns of the oxidized intermetallics after 10 hrs and 46 hrs of oxidation at 1273 K presented in Figures 35 and 36 for intermetallics A and B, respectively. In the case of intermetallic A, it is seen that the relatively strong signal from the Nb_2O_5 peak at around 28° becomes weaker after the longer exposure time. However, the TiO_2 peaks are stronger in intensity

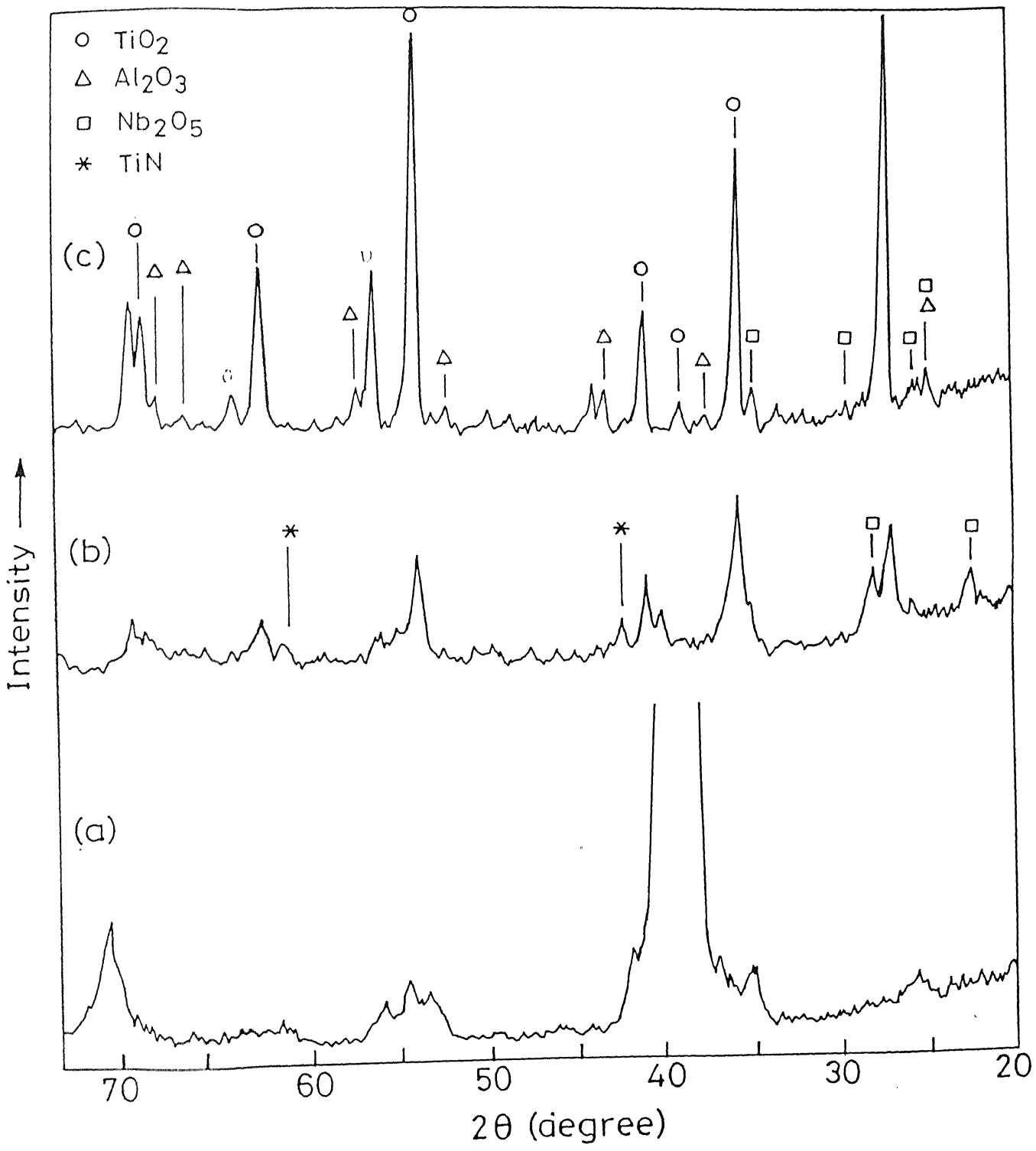

Fig 35 XRD patterns of intermetallic A: (a) reference unoxidiz after oxidation at 1000°C for (b) 10 hours and (c) 46 hours

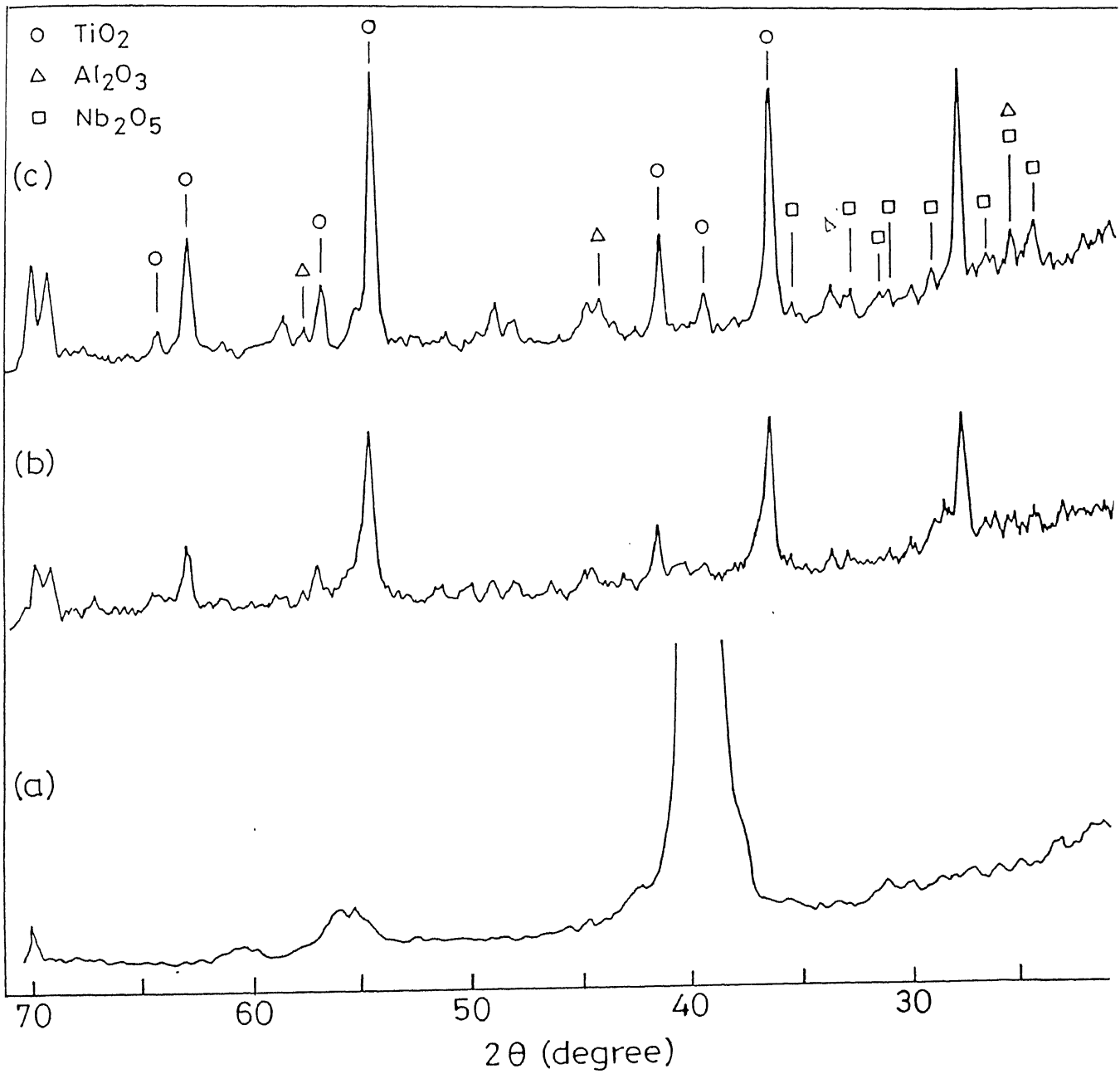

Fig 36 XRD patterns of intermetallic B: (a) reference unoxidize after oxidation at 1000°C for (b) 10 hours and (c) 46 hour

after the longer oxidation. The matrix peaks are relatively of lower intensity indicating that the x-rays have not penetrated all the way through the oxide. In the case of intermetallic B, extra peaks due to Nb_2O_5 could be identified even after longer oxidation time.

The weight gain data after oxidation was analyzed. The rate constant (K_p) was obtained from the relation between weight gain per unit area vs square root of time as given below

$$(\Delta w/A)^2 = K_p\ t$$

The rate constants calculated from the observed weight gains after 10 h and 46 h exposure in air is provided in Table 7. It is seen that K_p decreases with increasing exposure time for both the intermetallics.

The oxidation rate of intermetallic A is compared with that of other titanium aluminides from the literature. The K_p values for oxidation at 1300 K of three titanium aluminides of composition Ti-25Al, Ti-24Al-11Nb and Ti-25Al-15Nb in a 80:20 (volume) nitrogen:oxygen mixture earlier determined by Roy [2,59] are (K_p in $kg^2m^{-4}s^{-1}$) 6.05×10^{-7}, 1.10×10^{-8} and 4.82×10^{-9}, respectively. It therefore appears from the initial study on the oxidation of Ti-24Al-20Nb intermetallic (A) that the oxidation rate in air is further reduced with increasing additions of Nb.

The scale morphology of the 46 hour oxidized intermetallic A and X-ray mapping of the scale area (of Ti, Al and Nb) are shown in Figure 37. The scale appears multi layered with the outer scale showing separation from the inner scale (Figure 37a). Both the scales are essentially TiO_2 containing Al and Nb in solid solution. The concentration of Al in the scales is much lower than that of Nb as can be seen in the X-ray maps of Al and Nb in Figure 37. Moreover, there appears to be a Nb depleted layer next to the scale in the intermetallic due to the diffusion outside of Nb into TiO_2. The doping of Nb in TiO_2 should result in lower oxidation kinetics. The presence of Nb_2O_5 cannot be conclusively stated from the X-ray mapping although it appears that there is a large concentration of Nb in the outermost layer indicating its likely presence in this region. This is further substantiated by the observation that the outer scale has separated from the inner

Table 7

Oxidation data analysis

Intermetallic	A		B	
Oxidation time (t) (sec.)	36000	165600	36000	165600
Area (A) (m^2)	2.62×10^{-4}	2.69×10^{-4}	2.00×10^{-4}	1.89×10^{-4}
Initial weight (w_i) (Kg)	0.364×10^{-3}	0.567×10^{-3}	0.569×10^{-3}	0.405×10^{-3}
Final weight (w_f) (Kg)	0.365×10^{-3}	0.569×10^{-3}	0.571×10^{-3}	0.408×10^{-3}
dw/dA (Kg/m^2)	3.81×10^{-3}	7.43×10^{-3}	10.02×10^{-3}	15.87×10^{-3}
K_p ($Kg^2m^4s^{-1}$)	4.04×10^{-10}	3.33×10^{-10}	2.79×10^{-9}	1.52×10^{-9}
Scale	Less compact , yellow color.	More compact , yellow color.	Less compact , yellowish white colour	Least compact, yellow color

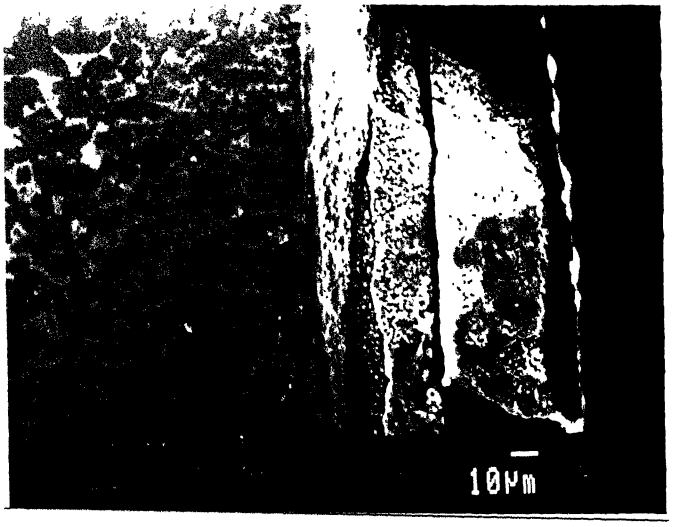

(a)

(b)

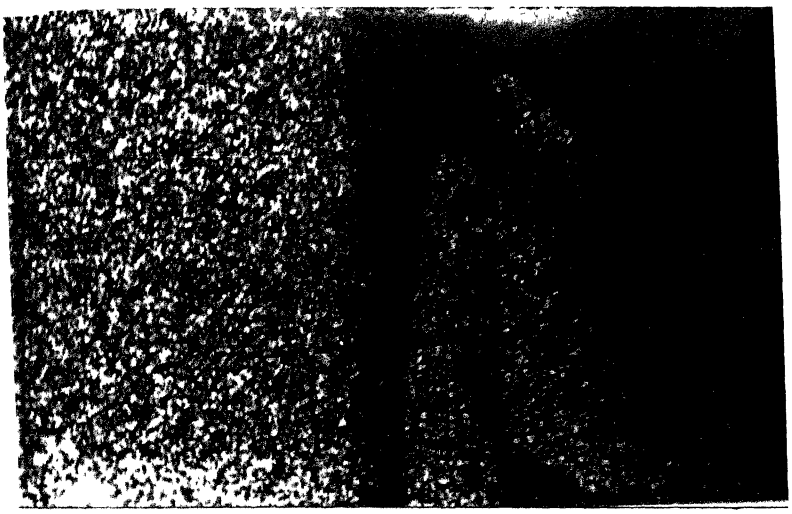

(c)

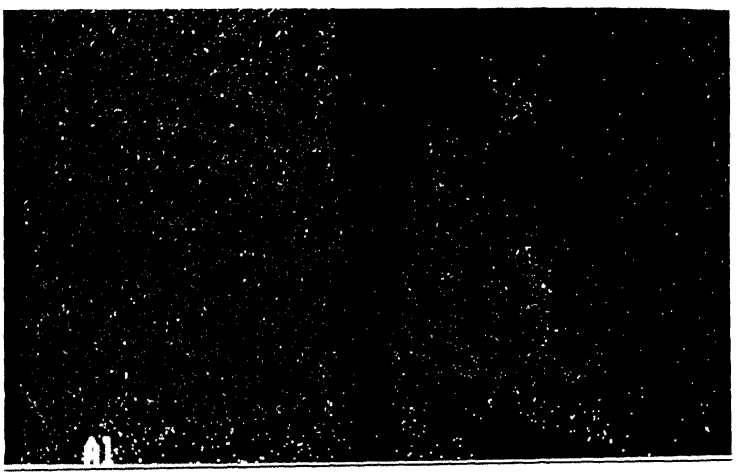

(d)

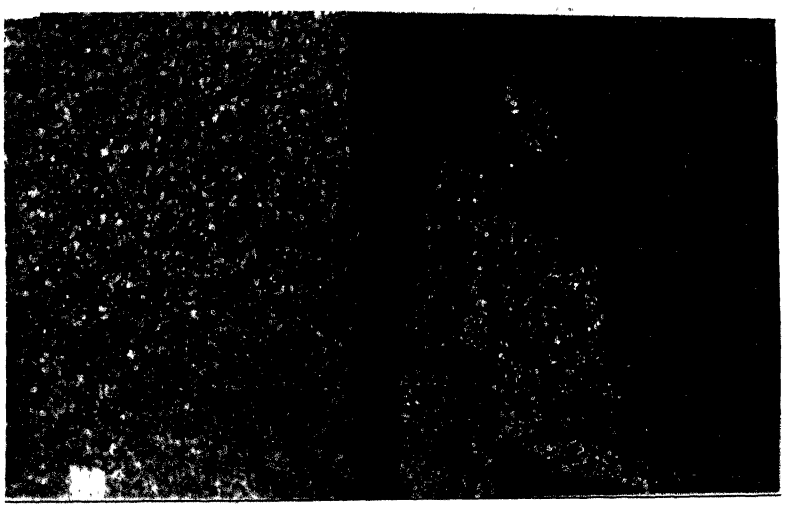

(e)

Fig 37 (a) SEM micrographs of scale morphology (b) subscale back scattered electron image of the intermetallic A after 46 h oxidation at 1000^{o}C; X-ray composition maps of (c) Ti, (d) Al and (e) Nb from the scale area shown in (a).

(a)

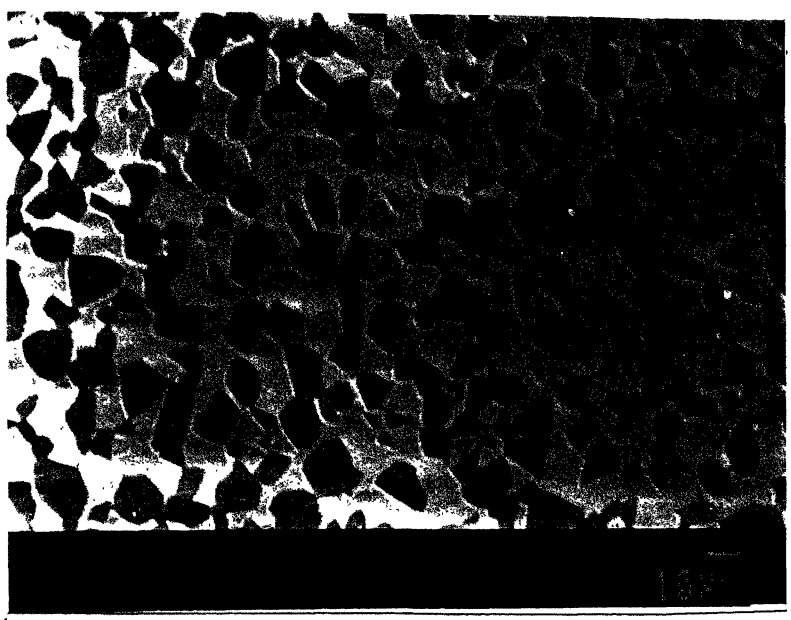

(b)

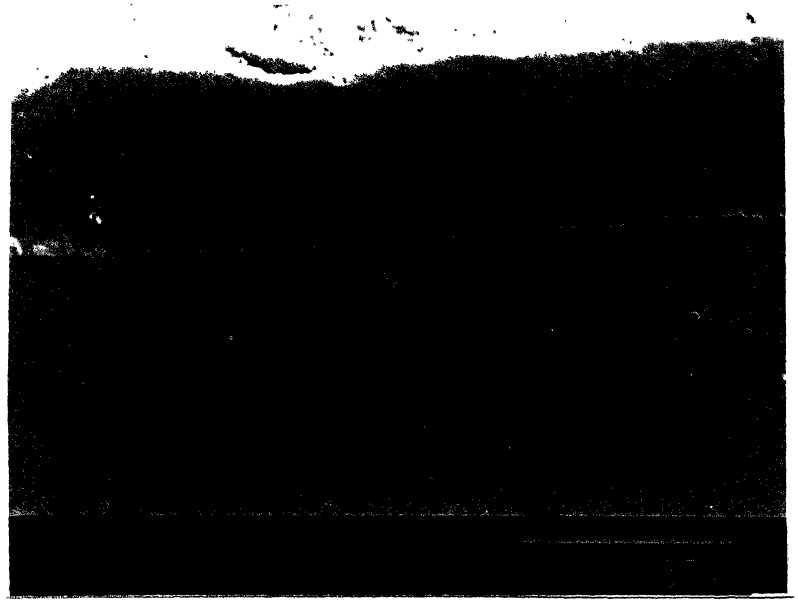

(c)

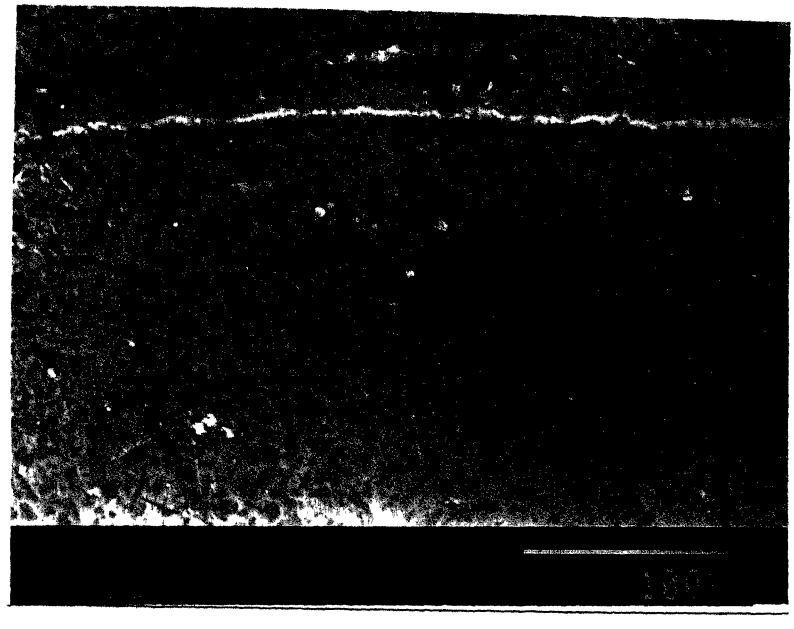

(d)

Fig 38 EPMA micrographs of subscale microstructure of intermetallics (a) A near the surface, (b) A much below the surface, (c) B near the surface and (d) B much below the surface after oxidation at 1000^{o}C for 46 h.

scale indicating the large molar volume increase on Nb_2O_5 oxide formation.

Additionally, the presence of TiN was also indicated by XRD in the oxidized sample A and its presence has been well documented in the case of oxidation of titanium aluminides in air [59]. The presence of TiN is generally beneficial in lowering the oxidation rate [59] and this is the reason why the titanium aluminides , in general, exhibit lower oxidation rates in air when compared to pure oxygen. It has been reported that TiN forms in the interface between the metal substrate and the oxide in Ti-25Al-10Nb-3V-1Mo by Wallace et al [69] oxidized in air over a range of 973 to 1273 K and in Ti-24Al-5Nb oxidized in nitrogen containing environment between 1100 and 1300 K [59]. Two different nitride layers, TiN and Ti_2AlN were identified by Becker et al [61] beneath the Al_2O_3 layer formed on TiAl in air. The innermost layer was TiN and the middle layer was Ti_2AlN with the outermost layer was a single Al_2O_3 layer [61]. Rawe and Rosa [74] also observed a very thin TiN layer in the innermost scale of Ti-4.3Nb (wt pct) alloy exposed to air, which resulted in superior oxidation resistance. The reasons for the improvement in the oxidation resistance in the presence of TiN has been attributed to the barrier qualities of TiN [74], the protective nature of the scale due to the Pilling-Bedworth ratio being 1.1 [59] and to the metallic nature of TiN which would be able to accommodate more stresses before cracking [59]. Thermodynamic analysis of nitride formation [59] indicates that the TiN should form only when the partial pressure of oxygen is much lower compared to that of nitrogen and this is possible if either oxygen diffusion through the scale is orders of magnitude lower compared to that of nitrogen or both oxygen and nitrogen reach the surface at comparable rates but the oxygen gets consumed primarily in dissolution in the alloy or internal oxidation of Al to Al_2O_3. The diffusivity of oxygen is greater than that of nitrogen in α-Ti [73] and therefore once a protective scale forms on the surface, the formation of TiN becomes feasible.

The apparent oxidation rate of the intermetallic B calculated from the weight gain data after isothermal exposure and removal from furnace is relatively lower compared to that of intermetallic

A. The calculated value of K_p in the case of intermetallic B could be in error as there was significant scale spalling during oxidation experiments and also during removal from the furnace and this would result in a lower weight gain being recorded than actually obtained. The continuous weight gain assessment technique should be used to obtain further insights on the oxidation behavior of intermetallic B. The scale morphology could not be studied as the scales were generally not adherent to the substrate in the case of intermetallic B.

The non-adherent nature of the scale formed on intermetallic B during high temperature oxidation could be due to the formation of Nb_2O_5. The presence of this phase was indicated by XRD in the sample B oxidized for 10 and 46 hours, with the XRD signals being much more prominent after the 46 hour oxidation. There is a large molar volume change on the formation of this oxide and this results in spalling of the scale. The spallation of scales on pure Nb has been well documented in the literature [51]. The breakaway oxidation behavior (i.e. linear oxidation rate following parabolic oxidation rate) is observed at lower temperatures in pure Nb and this is essentially due to the formation of Nb_2O_5 [51]. The Nb_2O_5 layer is porous and offers little resistance to oxidation. At higher temperatures (above 650°C), Nb is rapidly oxidized to Nb_2O_5 through the intermediate formation of NbO and NbO_2. The reaction rates become too rapid at high temperatures that it has been stated that accurate studies of the kinetics of Nb oxidation cannot be made, unless the oxygen partial pressure is lowered. Therefore, the poor oxidation resistance of Nb_2O_5 has also been well documented in the literature.

Another reason for the poor oxidation resistance and spallation of the scales on intermetallic B is the absence of TiN. As stated earlier, thermodynamic analysis of nitride formation indicates that much lower oxygen partial pressures (or more precisely low ratio of partial pressure of oxygen to nitrogen) are required in order to form TiN. This can be achieved if oxygen and nitrogen do not arrive at the same rate and if oxygen gets consumed in other processes like dissolution and internal oxidation. The absence of TiN in intermetallic B indicates that

low oxygen partial pressures were not attained in the scale formed on this intermetallic during high temperature oxidation. It is reasonable to therefore conclude that such low oxygen pressures could not be achieved at the metal oxide/substrate interface in intermetallic B due to the non-protective and spalling nature of the scale. This further aggravates the oxidation problem as the formation of TiN is hindered. Therefore, the spallation of the scale on intermetallic B is detrimental to its oxidation resistance due to non-protective scale formation and absence of TiN.

The non-adherent nature of the scale was also indicated by substantial microstructural changes in the near-surface regions of the intermetallic B. The microstructural changes occur primarily due to the presence of oxygen which stabilizes the α_2/O phase [28]. The subscale microstructures of intermetallics A and B after 46 h exposure to the air environment are presented in Figure 38. The presence of oxygen in the substrate has lead to significant microstructural changes in case of B as compared to A. This further indicates that the scale in the case of intermetallic B was non-protective leading to substantial dissolution of oxygen that caused the phase changes. In the case of intermetallic A, the microstructural changes are not as significant as that of B. It is interesting to note that the volume fraction of the dark phase (α_2) is higher at the inner regions than the surface region whereas it is expected that this should have been higher had oxygen stabilized the α_2 phase. This could possibly indicate the outward diffusion of Ti and Al as the scales were primarily TiO_2 and Al_2O_3 which would result in depletion of the α_2 phase amount. In contrast, very drastic microstructural changes can be noticed in the case of intermetallic B. It can also be noticed that there are pores that are present in the regions where the microstructural changes are visible in intermetallic B. High magnification images of the interface between the regions that show and do not exhibit microstructural changes for intermetallic B are presented in Figure 39. It is seen that the white phase (i.e. β) has undergone a transformation in the regions where oxygen is present. At the interface region, it can be further noticed that the pores are formed at the interface between the β

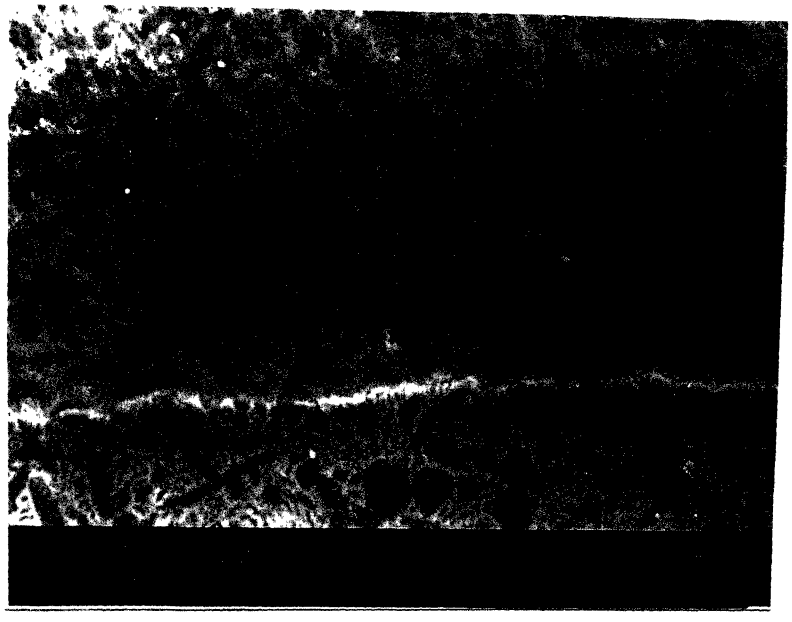

(a)

(b)

Fig 39 EPMA micrographs of the subscale microstructure of intermetallic B taken at the interface between the oxygen affected and unaffected regions at (a) low magnification and (b) high magnification. Intermetallic B had been oxidized at 1000^{o}C for 46 h.

and O phase boundary. The pore formation should be related to the stabilization of the α_2/O phase in the presence of oxygen. These significant changes occur due to the presence of oxygen. Oxygen must be present in larger amount in specimen B compared to A to affect such changes and this is also reflected in subscale microhardness profiles (to be discussed below). Higher oxygen solubilities again indicates the poor adherent nature of the scale formed on intermetallic B. Additionally, it should be realized that oxygen stabilized the O phase in intermetallic B and therefore the mechanism of stabilization of the O phase in the presence of oxygen may be different such that the pore formation may be a result of this stabilization, unlike in the case of stabilization of the α_2 phase in the presence of oxygen.

4.8 SUBSCALE HARDNESS PROFILING OF OXIDIZED INTERMETALLICS

Subscale hardness profiles obtained from the oxidized intermetallics A and B after oxidation at 1273 K for 10 h and 46 h are shown in Figures 40 and 41, respectively. The subscale hardness values are higher for intermetallic B after both 10 h and 46 h when compared to intermetallic A. This further indicates the non-protective nature of the scale formed on the intermetallic B when compared to that on intermetallic A.

The depth of hardened substrate zone varied from 40 to 60 μm in case of sample A and from 60 to 80 μm in case of sample B (Figures 40 and 41) for the oxidized samples. This hardening has earlier been attributed to the diffusion of oxygen/nitrogen into the alloys by neglecting the counter-diffusion of metal [66,70,73,74]. The variation of microhardness (MH) in the subscale is due to the variation of concentrations of diffusing species, viz. oxygen and nitrogen. Assuming $(C-C_b)$ to be proportional to increase of MH over the bulk value [59], viz. $(MH-MH_b)$,

$$\frac{C - C_b}{C_s - C_b} = \frac{MHv - MHv_b}{MHv_s - MHv_b} \qquad (1)$$

where

C_s = surface concentration of diffusing species

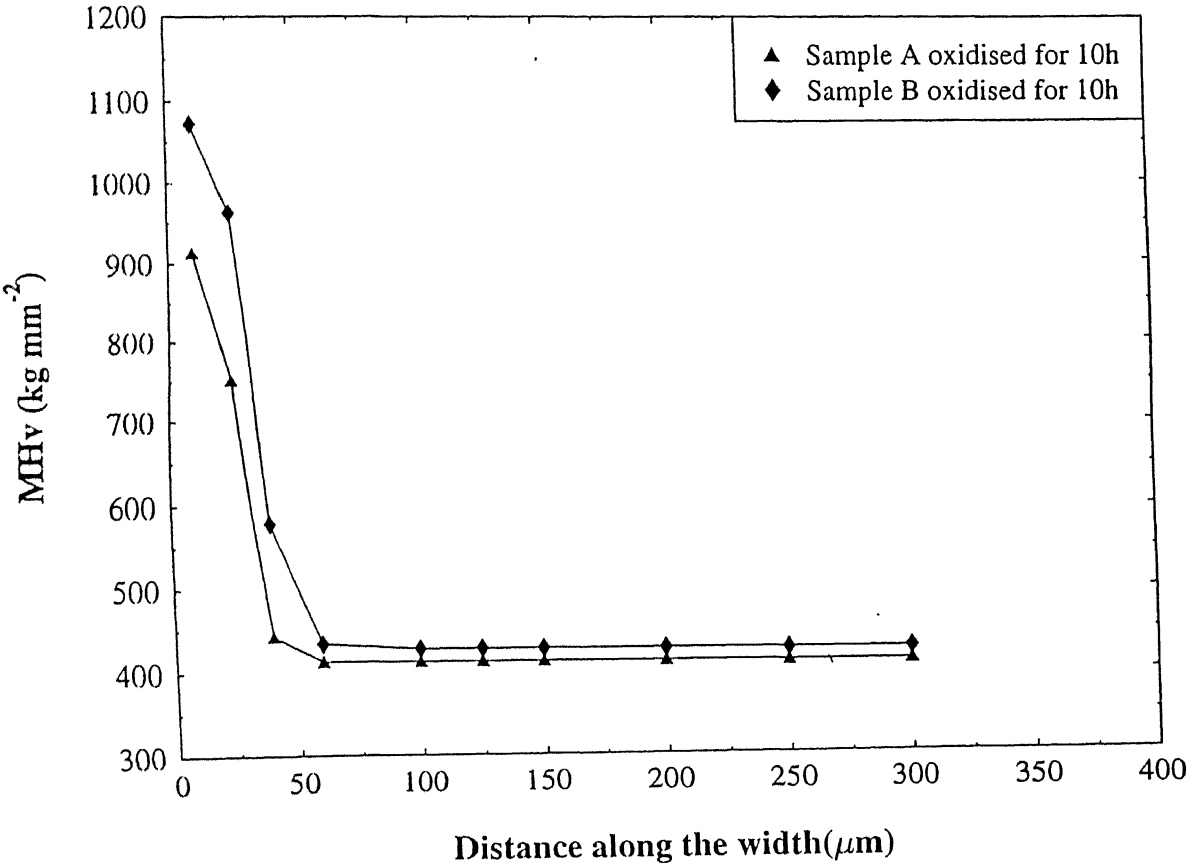

Fig 40 Subscale microhardness profiles taken from the intermetallics A and B after oxidation at 1000^{o}C for 10 h.

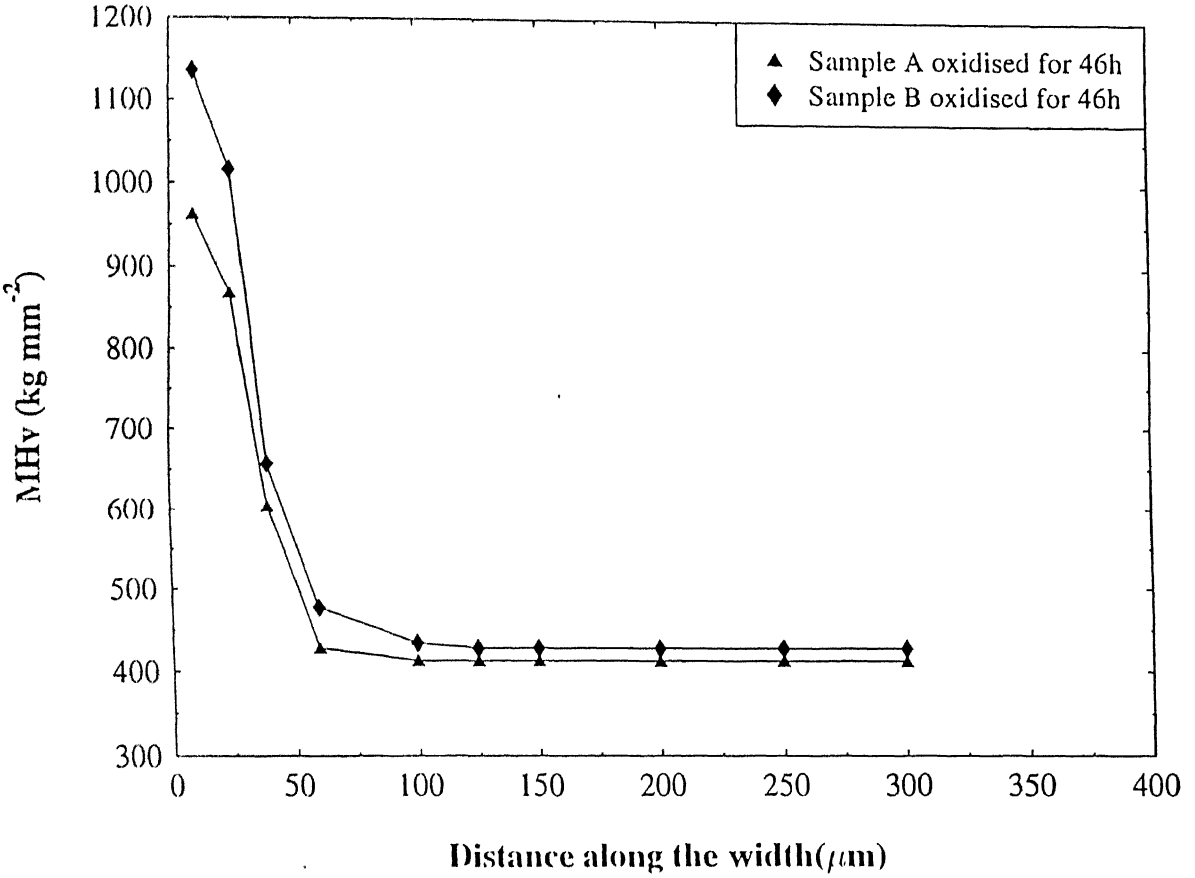

Fig 41 Subscale microhardness profiles taken from the intermetallics A and B after oxidation at 1000°C for 46 h.

C_b = bulk concentration of diffusing species

C = concentration of diffusing species at any point

Subscripts o and s denote bulk and surface respectively.

As the specimen surfaces were flat and depths of diffusion field were very small compared to the thickness of samples, the problem may be treated as unsteady diffusion through a semi-infinite flat specimen. Assuming that (i) diffusion occurred through a single phase, (ii) no internal oxidation in the diffusion field, (iii) the diffusion coefficient (D in m^2/sec) was constant in the entire diffusion zone, and (iv) the surface concentration (C_s) was constant and not a function of time, equation (1) can be combined with the standard diffusion equation to obtain

$$\frac{MHv - MHv_b}{MHv_s - MHv_b} = \frac{C - C_b}{C_s - C_b} = 1 - \text{erf}\left(\frac{z}{2\sqrt{Dt}}\right) = \text{erfc}\left(\frac{z}{2\sqrt{Dt}}\right) \qquad (2)$$

where z is the distance from scale alloy interface (in m) and t is the known exposure time (in sec).

Smooth curves were drawn from data points in this case and diffusivity was determined using equation (2). The assumption of constant surface concentration (C_s) in equation (2) may not be strictly valid as C_s may vary due to variation in the nature of growing oxide scales on the surface with time and equation (2) is not expected to be obeyed well. Therefore, the technique consisted of picking up various pairs of points on the smoothed microhardness vs distance curve and employing the following procedures. For two given points 1 and 2, the parameter Y_{12} could be obtained on the basis of equation (2) as follows

$$Y_{12} = \frac{(C_1-C_b)/(C_s-C_b)}{(C_2-C_b)/(C_s-C_b)} = \frac{C_1-C_b}{C_2-C_b} = \frac{\text{erfc}(z_1/2\sqrt{Dt})}{\text{erfc}(z_2/2\sqrt{Dt})} = \frac{(MHv)_1 - (MHv)_b}{(MHv)_2 - (MHv)_b} \qquad (3)$$

where MH_1 is the microhardness value at location z_1, MH_2 at location z_2, and MH_b the bulk microhardness value. Since Y_{12} is a

ratio, errors in the estimated value of D would be partly eliminated due to cancellation effect. This also eliminates C_s which is an unknown. This is the rationale behind the procedure based on equation (3) [70]. The diffusivity (D) is the only unknown parameter in the above equation as the exposure time for each experiment is known. By using an error function and by trial and error solution, values of D were obtained. Several pairs of data points were chosen from each curve for the analysis. Then the average of these D values (D_{av}) for a particular set was obtained as this procedure is expected to reduce estimation errors further.

Table 8 presents the diffusivities and average D of oxygen and nitrogen at 1273 K obtained by the above procedure. The values of average D may be taken as diffusivity values obtained in the present study. Diffusivities of oxygen and nitrogen in Ti alloys have been compiled from literature sources in Table 9 for the sake of comparison.

It should be realized that assumption (i) is simple and this may not be applicable to the case of intermetallic A. Intermetallic A can not be strictly considered as single phase material as the microstructure of the sub-surface regions indicates that it is primarily a two phase structure of α_2/O phase in β matrix. Therefore, the calculated diffusivity of oxygen would not be for a diffusion through a single phase but rather through a mixture of phases, in which case the diffusivity of oxygen would be lower due to the discontinuous nature of distribution of the phases. The subsurface microstructure of intermetallic A taken by the BSE mode on the SEM is provided in Figure 37b. It can be seen that the black phase (α_2 in this case) is enveloped by the O phase (which is also twinned) and the β phase is present as isolated regions in the microstructure. The presence of O phase at the interphase between the α_2 and β phases is well documented [10-12]. Moreover, oxygen does not significantly alter the sub-surface microstructure like noticed in the case of intermetallic B. In view of these points, it can be reasonably concluded that the measured diffusivity does not represent diffusion through a single phase and hence cannot be relied upon. It was earlier noted that oxygen diffuses predominantly through α_2 phase in Ti-24Al-15Nb the

assumption of single phase diffusion is reasonable for titanium aluminides of lower Nb content alloys [70]. However, this may not be applicable to the high Nb containing Ti-24Al-20Nb alloy used in the present study.

On the other hand, this assumption may be applicable to the higher Nb containing Ti-24Al-27Nb as the presence of oxygen stabilizes the microstructure such that a single phase structure is obtained in the near-surface regions (Figures 38b and 39). The measured value of diffusivity in this study resembles closely to the diffusivity of oxygen in Nb containing titanium aluminides [56,62] and also to that of nitrogen in α-Ti [61]. As the environment used for the oxidation experiment was air, it is not possible to differentiate whether it is oxygen or nitrogen that causes microhardness increases in the near surface regions. However, on comparison with the literature data, it is seen that the diffusing species could be either oxygen or nitrogen or both in intermetallic B and the measured diffusivity is similar to the reported diffusivities of oxygen and nitrogen in titanium aluminides and titanium at this temperature (Table 9).

Table 8

Diffusivities of oxygen and nitrogen in intermetallics A and B at 1273 K.

System	Time (hrs)	Estimated D (m^2/sec)	Average D (m^2/sec)
Sample A	10	4.94×10^{-15} 5.36×10^{-15} 4.22×10^{-15} 3.59×10^{-15}	4.53×10^{-15}
	46	3.77×10^{-15} 2.62×10^{-15} 2.44×10^{-15} 0.78×10^{-15}	2.40×10^{-15}
Sample B	10	1.74×10^{-14} 2.95×10^{-14} 0.85×10^{-14} 0.60×10^{-14}	1.54×10^{-14}
	46	1.86×10^{-14} 0.31×10^{-14} 0.65×10^{-14} 0.23×10^{-14}	0.64×10^{-14}

Table 9

Diffusivity of oxygen and nitrogen in Ti and Ti alloys.

System	Diffusing Species	D (m^2/sec)	Temperature (K)	References
α-Ti	oxygen	1.29×10^{-12}	1300	66
α-Ti	nitrogen	3.21×10^{-14}	1273	73
Ti-25Al	oxygen	3.40×10^{-13}	1373	68
Ti-25Al	nitrogen	1.97×10^{-14}	1300	70
Ti-25Al -11Nb	oxygen	3.00×10^{-14}	1300	67
Ti-24Al -15Nb	oxygen	2.56×10^{-14}	1300	70
Ti-24Al -15Nb	nitrogen	2.86×10^{-14}	1300	70

CHAPTER 5

SUMMARY

5.1 CONCLUSIONS

The behaviour of hydrogen in two titanium aluminides (containing high Nb) of composition Ti-24Al-20Nb and Ti-24Al-27Nb were studied. Hydrogen was introduced into the intermetallics by cathodic hydrogen charging at room temperature. The hydrogen behaviour in the intermetallics was followed by microhardness profiling of the specimens. The microstructures were characterized by optical and scanning electron microscopy. The presence of hydrides in the specimens were studied by baking experiments on the hydrogen charged specimens. The following are the significant conclusions of the present study.

1. The microstrcutures of the intermetallics could not be altered by heat treatments because the solutionizing temperature used in the present study was not above the $\alpha_2(O)/\beta$ transus temperature. Therefore, the as-received microstructures were utilized for studying the behaviour of hydrogen. The as-received microstructures of intermetallic A contained distribution of the α_2 and O phases in the β matrix, while that of B contained distribution of the O phase in the β matrix. The precipitate size in intermetallic B was finer than in intermetallic A.

2. The hardness of both the intermetallics increases with increasing hydrogen charging time. The hardness profiles obtained after hydrogen charging exhibits two distinct regions: a surface hardened layer and a central region showing a lower hardness than the surface. The surface hardened layer obeys the parabolic rate law as regards its extent as a function of hydrogen charging time. The hardness increase at the surface is attributed to hydrogen in solution, hydriding of the α_2/O phase and to the stabilization of part of the α_2 phase to an orthorhombic phase in the presence of hydrogen.

3. The hardness increase is higher in the case of intermetallic B

ompared to intermetallic A after for all hydrogen charging times ndicating hydriding from the O phase, which is harder than the α_2 nd β phases. The parabolic growth of the surface hardened layer s slower in intermetallic A which is due to the larger volume raction of the precipitates in this intermetallic which act as locking sites and also are hydride formers. The growth of the urface hardened layer has similarities to the growth of internal xidation zone in internal oxidation.

. Baking of the hydrogen charged specimens at 800°C for 10 inutes resulted in a decrease in the surface and bulk hardness, lthough the nature of the profile remained similar to that btained after hydrogen charging. The depth of the surface ardened layer also did not exhibit a change. However, the elative hardness changed after baking at 800°C for 24 hours was ery small for the surface and bulk regions of both the intermetallics indicating the outgassing of hydrogen from the samples. The depth of the surface hardened layer also showed a decrease with increasing baking time. The nature of presence of hydrogen (i.e. whether in solid solution or as hydrides) could not be unambiguously determined from the 800°C baking experiments.

5. Baking the hydrogen charged specimens at 400°C for 90 minutes resulted in a decrease in both the surface and bulk hardness with the depth of the surface hardened layer remaining constant. This has been attributed to outgassing of hydrogen present in solid solution in the surface and bulk regions of the charged intermetallics. Baking for 24 hours at 400°C resulted in further decrease in hardness. However, the relative change in hardness was still significant after the long baking time indicating that a part of hydrogen was present in the form of hydrides in the hydrogen charged specimens, with a major part being in solid solution in the matrix, most likely the β phase. The depth of the surface hardened layer also showed a decrease with increasing baking time at 400°C indicating that hydrogen in solid solution is a major component of the surface hardened layer.

6. The microstructures of the intermetallics do not show variations after hydrogen charging and baking experiment compared to the as-received microstructures on observation with scanning

electron and optical microscopy. The hydrides that form are therefore finely distributed the α_2/O phases.

7. XRD studies of the intermetallics after different stages of experimentation (i.e. charging and baking) did not reveal the presence of TiH_2 or TiH hydrides. The hydrides that form in these intermteallics on room temperature hydrogenation is expected to be ternary hydrides with lattice parameters very close to that of the α_2/O phase which make identification of the hydrides difficult due to overlap of diffraction peaks from the hydrides with that of the α_2/O phase. The presence of hydride is indicated by the baking experiments.

8. The scaling behaviour of both the intermetallics was studied at 1000^{o}C. It was observed that the scale was adherent on sample A while it exhibited considerable spallation on sample B. The scales in both the cases were composed primarily of TiO_2 and Al_2O_3 with minor amounts of Nb_2O_5 andTiN (only in A). The sample A exhibited good oxidation resistance (i.e. lower parabolic rate constant) compared to other titanium aluminides and this has been attributed to the doping effect of Nb in TiO_2 (which lowers the defect concentration leading to lower ionic diffusion) and to the formation of the TiN, most likely in the form of a layer at the metal oxide/substrate interface. The poor adherence of the scale on intermetallic B is due to the formation of Nb_2O_5 . The poor oxidation behaviour of sample B is also due to the absence of TiN.

9. The microstructures of intermetallic A was not affected by the presence of oxygen whereas the microstructure of intermetallic B was drastically affected by the presence of oxygen. The presence of oxygen stabilized the O phase in intermetallic B and pores resulted during the stabilization process, which is not well understood.

10. The diffusivity of oxygen/nitrogen was determined from the subscale microhardness profiling of the intermetallics. The diffusivity of oxygen/nitrogen in intermetallic B is comparable to that reported for oxygen and nitrogen in the literature for titanium aluminides. The diffusivity of oxygen/nitrogen in intermetallic A could be in error due to the presence of a two-phase microstructure.

5.2 SUGGESTIONS FOR FUTURE WORK

Based on the present study, the following are the suggestions that are proposed and that could be undertaken in the future:

1. The microstructures obtained after several treatments should be characterized by transmission electron microscopy inorder to obtain further insights into hydride formation and effect of hydrogen on the microstuctures.
2. The hydrogen contents at various stages of the experimentation should be determined. The possible use of weight change method and vacuumm hydrogen extraction techniques can be explored. The latter is expected to provide accurate results.
3. The as-received microstructure was used for the experimentation in the thesis. The effect of several microstructures on hydrogen behaviour should be explored. The heat treatments to produce the different microstrctures should necessarily involve a high solutionizing temperature (1140^{o}C for intermetallic A and 1120^{o}C for intermetallic B). Moreover, the cooling rate after the heat treatment could be controlled in order to obtain the α_2/O phase in different shapes and sizes. There would be a large variation in interfacial area between the α_2/O and β phases going from the equiaxed to accicular structure and this should also affect hydriding behaviour.
4. Hydrogenation at high temperatures could also be done in order to evaluate the hydride formation characteristics. The hydrides that form after high temperature hydrogenation are different from that formed after room temperature hydrogenation.
5. The conditions used in the cathodic hydrogen charging experiment (i.e. electrolyte type, cathodic charging current density, temperature and time) could also be varied to study their effect of hydrogen uptake behaviour of the intermetallics.
6. The baking experiments could be performed at different temperatures (with well characterized hydrogen contents) and coupled with characterization techniques, the terminal solid solubility of hydrogen in these intermetallics could be determined.
7. The high Nb containing alloy could be heat treated at high temperature for very long times (500 hours) in order to obtain as

much conversion to the O phase as possible and hydriding of this phase can be studied. Similarly, a Ti_3Al sample heat treated to obtain only the α_2 phase can be used to study its hydriding behaiour. In this way, the subtle differences between the hydriding of the α_2 phase and the O phase can be elucidated, although the present study has shown that their hydriding and hydrogen solution behaviour should be similar.

8. Continuous weight gain oxidation experiments should be conducted at different temperatures to elucidate the oxidation of these intermetallics in greater detail. Different oxidizing environments (pure oxygen, pure nitrogen, oxygen-nitrogen, oxygen-argon mixtures) could be also used to understand the mechanism of oxidation.

9. The stabilization of the O phase by oxygen at high temperature is one of the interesting results of the present thesis. This aspect needs to be studied in greater detail in order to understand the stabilization process and the pore formation mechanism. The embrittling effect due to oxygen solution needs to be also addressed in this regard.

REFERENCES

1. D. Swarup and M.N. Saxena, *Elements Of Metallurgy*, Rastogi Publications, Meerut (1984) 170.
2. T.K. Roy, *Ph. D. Thesis*, Indian Institute of Technology, Kanpur, India (1995).
3. D.A. Lukasak and D.A. Koss, "The Flow and Fracture of a Ti_3Al-Nb Alloy", *Metall. Trans.*, **21A** (1990) 135-143.
4. N.J. Kim, J.Y. Kim and W.S. Cho, "Morphological Effect on the Mechanical Behaviour of a Two-Phase Ti_3Al-Nb Alloy", *Metall. Trans.* **24A** (1993) 1785-1793.
5. K.S. Chan, "Fracture and Toughening Mechanism in α_2 Titanium Aluminide Alloy", *Metall. Trans.*, **21A** (1990) 2687-2699.
6. K.S. Chan, "Developing Hydrogen Tolerant Microstructure for an α_2-Titanium Aluminide Alloy", *Metal. Trans.* **23A** (1992) 497-507.
7. H.T. Kestener-Weycamp, C.H. Word, T.F. Broderik and M.J. Kaufman,"Microstructures and Phase Relationship in the Ti_3Al+Nb system", *Scripta Metall.* **23** (1989) 1697-1702.
8. S.M.L. Sastry and H.A. Lipsitt, "Ordering Transformations and Mechanical Properties of Ti_3Al and Ti_3Al-Nb Alloys", *Metall. Trans.* **8A** (1977) 1543-1552.
9. J.A. Peters and C. Bassi, "Isothermal Transformation in β-Stablised Ti_3Al Intermetallics", *Scripta Metall.* **24** (1990) 915-920.
10. K. Muraleedharan, S.V. Nagerder Naidu and D. Banerjee, "Orthorhombic Distortions of the α_2 Phase in Ti_3Al+Nb Alloys : Artifacts and facts", *Scripta Metall.* **24** (1990) 27-32.
11. A.K. Gogia, D. Banerjee and T.K. Nandy, "Structure, Tensile Deformation and Fracture of Ti_3Al+Nb Alloy", *Metall. Trans.* **21A** (1990) 609-625.
12. D. Banerjee, A.K. Gogia, T.K. Nandy and V.A. Joshi, "A New Ordered Orthorhombic Phase in Ti_3Al-Nb Alloy", *Acta Metall.* **36** (1988) 871-882.
13. R. Strychor, J.C. Williams and W.A. Soffa, "Phase Transformations and Modulated Microstructure in Ti-Al-Nb Alloys", *Metall. Trans.* **19A** (1988) 225.

14. D.M. Dimiduk, D.B. Miracle, Y.W. Kim and M.G. Mendiratta, *ISIJ. Intl.* vol. **31** (1991) 1223-34.
15. C.T. Liu, J.O. Stiegler, and F.H. Froes, *Metals Handbook, ASM Intl.*, 10th edition vol. **2** (1990) 913-42.
16. H.A. Lipsitt,"*High Temperature Ordered Intermetallic alloys*" (MRS Symp. 39)(edited by C. C. Koch et al.) 351-364. *Mater. Res. Soc.* Pittsburgh, Pa (1985).
17. H. G. Nelson, SAMPE Q, **20** (1988) 20.
18. L. Kirschfeld and A. Sieverts, *J. Phys. Chem.* **145A**, (1929), 227.
19. H. Numakura and M. Koiwa, "Hydride Precipitation in Titanium", *Acta Metall.* **32** (1984) 1799-1807.
20. H. Numakura, M. Koiwa, H. Asaho, H. Murata and F. Izumi,"X-ray Diffraction Study on the Formation of γ-Titanium Hydride", *Scripta Metall.* **20** (1986) 213-216.
21. W.Y. Chu, A.W. Thompson and J.C. Williams, "Hydrogen Solubility in a Titanium Aluminide Alloy", *Acta Metall.* **40** (1992) 455-462.
22. P.S. Rudman, J.J. Reilly and R.H. Wiswall, "The Formation of Metastable Hydrides $Ti_{0.75}Al_{0.25}H_x$ with x less than 1.5.", *J. Less-common Metals* **58** (1978) 231.
23. P.S. Rudman, J.J. Reilly and R.H. Wiswall, "Hydrogen absorption in Ti_3Al", *Ber Bunsenges, Phys Chem* **81** (1977) 76-80.
24. W.R. Kerr, "The Effect of Hydrogen as a Temporary Alloying Element on the Microstructure and Tensile Properties of Ti-6Al-4V", *Metall.Trans.* **16A** (1985) 1077-86.
25. K. Yang and D.V. Edmonds, "Effect of Hydrogen as a Temporary Alloying Element on the Microstructure of Ti_3Al Intermetallics", *Scripta Metall.* **28**, (1993) 71-76.
26. K. Yang, Z. X. Guo and D.V. Edmonds, "Study of the Effect of Hydrogen on Titanium Alloys Foils to be used as Potential Composite Matrices", *Scripta Metall.* **27** (1992) 1021-26.
27. F.H. Fores and D. Eylon, "Thermochemical processing (TCP) of Titanium Alloys by Temporary alloying with Hydrogen", ***Hydrogen Effects On Materials Behaviour***, eds., N. R. Moddy and A. W. Thompson, TMS, Warrendale (1990) 261.

28. W.M. Mueller, J P. Blackledge and G.G. Libowitz, *Metal Hydrides*, Academic Press, New York, (1968).
29. G. G. Libowitz, *J. Nucl. Mater.* **2** (1960) 3.
30. G. A. Lenning, C. M. Craighead and R.J. Jaffee, "Constitution and Mechanical Properties Of Ti-H Alloys", *Trans. Met. Soc. AIME*, **200** (1954) 370.
31. H.J. Goldschmidt, *Interestitial Alloys*, Butterworths, (1967).
32. H.L. Yakel, *Acta. Crystallograph.* **11** (1958) 46.
33. S.S. Sidhu, L. Heaton and D.D. Zauberis, *Acta. Crystallograph.* **9** (1956) 607.
34. J. Brauer and H. Hermann, *Mater. Trans.* JIM **4** (1963).
35. R. Balasubramaniam, "Accommodation Effects due to Room Temperature Hydrogen Transformations in the Niobium Hydrogen System", *Acta. Metall. Mater.* **41** (1993) 3341-3347.
36. S.W. Ciaraldi, J.L. Nelson, R.A. Yeske and E.N. Pugh, *Hydrogen Effect in Metals*, I.M. Berstein and A.W. Thompson, Eds., AIME,New York (1981) 437.
37. D.S. Shih, G.K. Scarr and G.E. Wasielewski, "On Hydrogen Behaviour in Ti_3Al", *Scripta Metall.* **23** (1989) 973-978.
38. M. Blank-Bewersdroff and J.A. Peters, "Effect of Different Atmospheres on the Microstructure of Super α_2 Titanium Foils", *Scripta Metall. Mater.* **31** (1994) 945-950.
39. E. Manor and D. Eliezer, "Hydrogen Effects on Ti_3Al -Nb Alloy", *Scripta Metall.* **23** (1989) 1313-1318.
40. D. Eliezer, F.H. Fores and C. Suryanarayana, "The Effects of Hydrogen on Titanium aluminides", *J. Metals,* (1991) 59-62.
41. G.S. Upadhyaya and A.D. Mcquillan, "Crystal Structure of Saturated Mixed Hydrides of Titanium and Niobium", *Trans. Met.Soc.AIME* **224** (1962) 1290.
42. M. Gao, J. Bart Boodey and R.P. Wei, "Hydrides in Thermally Charged in α_2 Titanium Aluminides", *Scripta Metall.* **24** (1990) 2135-2138.
43. R. Jaffe, *J. Metals*, **8** (1956) 861.
44. M. Gao, J.B. Boodey and R.P. Wei, "Misfit Strains and Mechanisms for the Precipitation of Hydrides in Thermally Charged α_2 Titanium Aluminides", *Environmental Effects on Advance Materials*, R. H. Jones and R. E. Ricker, TMS,

Warrendale (1991) 47.

45. Y.W. Chu and A.W. Thompson, "Effect of Microstructure and Hydrogen as a Temporary β Stablizer on Cleavage Fracture Behaviour in Titanium Aluminide" *Hydrogen Effects On Materials Behaviour* , eds., N. R. Moddy and A. W. Thompson, TMS, Warrendale (1990) 285.

46. W.Y. Chu and A. W. Thompson, "Effect of Hydrogen as a Temporary β Stabliser on Microstructure and Brittle Fracture Behaviour in a Titanium Aluminide Alloy", *Metall. Trans.* **22A** (1991) 71-81.

47. H.T. Weykamp, D.R. Baker, D.M. Paseton and M.J. Kaufman, "Continuous Cooling Transformation in Ti_3Al+Nb Alloys", *Scripta Metall.* **24** (1990) 445.

48. L.W. Quattodrochi, D. A. Koss and G. Scarr, "Precipitation Hardening of a β-Titanium Alloy by the α_2 phase", *Scripta Metall. Mater.* **26** (1992) 267-272.

49. A.D. McQuillan, *J. Inst. Metals* **79** (1951) 371-378.

50. P. Kofstad, P.B. Anderson and O.J. Krudtaa, *J. Less Common Metals* **3** (1961) 89-97.

51. P. Kofstad, *High Temperature Corrosion*, Elsevier Applied Science Publishers Ltd. (1988).

52. Y. Umakoshi, M Yamaguchi, T. Sakagami and T. Yamane, "Oxidation Resistance of Intermetallic Compounds Al_3Ti and TiAl", J. *Mater. Sc.* **24** (1989) 1599-1603.

53. R. Prescott and M.J. Graham, *Oxid. Of Metals* **38** (1992) 233-53.

54. G. Welsch and A.I. Kavechi, *Oxidation of High Temperature InterMetallics*, T. Grobstein and J. Doychak, eds., TMS, Warrendale, PA (1988) 207-18.

55. S.N. Sankaran, R.K. Clark, J. Unnam, and K.E. Wiedemann, *NASA Tech. Paper* **TP3012** (1990) 22.

56. T.A. Wallace, R.K. Clark, S. N. Sankaran, and K.E. Wiedemann, "Oxidation Characteristics of Ti-33Al-6Nb-1.4Ta" *Environmental Effects on Advanced Materials*, R. H. Jones and R. E. Ricker, eds., TMS, Warrendale, PA (1991) 79-89.

57. N.S. Choudhury, H.C. Graham, and J.W. Hinze, *Proc. Of Symp. On Prop. Of High Temperature Alloys*, Z.A. Foroulis and F.S. Pettit, eds., *Electrochem. Soc. Proc.* **77-1**

(1976) 668-80.
58. M. Hoch, Unpublish Research (see ref.57).
59. T.K. Roy, R. Balasubramaniam and A. Ghosh, *Metall. Mater. Trans.* (1997) in press.
60. J. Subramanyam, "Cyclic Oxidation of Aluminized Ti-14Al-24Nb Alloy", *J. Mat. Sci* **23** (1988) 1906-1910.
61. S. Becker, A. Rahmel, M. Schorr, and M. Schutze, *Oxidation of Metals* **38** (1992) 425-64.
62. L. Singheiser, H.W. Grunling, and K. Schneider, *High Temp. Materials For Power Engg.*, II Proc. Conf., Liege, Belgium (1990) 1687-1702.
63. G. Chen, Z. Sun, and Z. Zhou, *Corrosion* **48** (1992) 939-46.
64. S.J. Balsone,"The Effect of Elevated Temperature Exposure on the Tensile and Creep Properties of Ti-24Al-11Nb", *Oxidation of High Temperature Intermetallics* (edited by T. Grobstein and J. Doychak), TMS,Warrendale (1988) 219-234.
65. Y. Saitoh and K. Mino, *Mater. Trans*, JIM **34** (1993) 393.
66. Z. Liu and G. Welsch, "Literature Survey on Diffusivities of Oxygen, Aluminium and Vanadium in Alpha Titanium, Beta Titanium and Rutile", *Metall. Trans.* **19A** (1988) 1121-1125.
67. K.E. Wiedemann, S.N. Sankaran, R.K. Clark and T.A. Wallace, "Static and Dynamic Oxidation of Ti-14Al-21Nb", *Oxidation of High Temperature InterMetallics* (edited. by T. Grobstein and J. Doychak), TMS, Warrandale, (1988) 195-206.
68. Y. Shida and H. Anada, *Mater. Trans*, JIM **34** (1993) 236.
69. T.A. Wallace, R.K. Clark, K. E. Wiedemann and S. N. Sankaran, *Oxidation of Met.* **37** (1992) 111.
70. T.K. Ray, R. Balasubramaniam and A Ghosh, "Determination of Oxygen and Nitrogen Diffusivities in Titanium Aluminides by Subscale Microhardness Profiling", *Scripta Mater.* **34** (1996) 1425-1430.
71. A.K. Gogia, Private communication.
72. J.L. Meijéring, "Internal Oxidation", *Advances in Materials Research*, H. Herman, ed, Wiley, New York, (1971) 1.
73. K.N. Strafford and J.M. Towell, *Oxidation of Met.* **10** (1976) 41.
74. R.L. Rowe and C.J. Rosa, *Oxidation of Met.* **14** (1980) 549.